NASA TECHNICAL NOTE

NASA TN D-8524

NASA TN D-8524

AERODYNAMIC CHARACTERISTICS OF WING-BODY CONFIGURATION WITH TWO ADVANCED GENERAL AVIATION AIRFOIL SECTIONS AND SIMPLE FLAP SYSTEMS

Harry L. Morgan, Jr., and John W. Paulson, Jr.

Langley Research Center
Hampton, Va. 23665

NATIONAL AERONAUTICS AND SPACE ADMINISTRATION • WASHINGTON D. C. • AUGUST 1977

1. Report No.	2. Government Accession No.	3. Recipient's Catalog No.
NASA TN D-8524		

4. Title and Subtitle	5. Report Date
AERODYNAMIC CHARACTERISTICS OF WING-BODY CONFIGURATION WITH TWO ADVANCED GENERAL AVIATION AIRFOIL SECTIONS AND SIMPLE FLAP SYSTEMS	August 1977
	6. Performing Organization Code
7. Author(s)	8. Performing Organization Report No.
Harry L. Morgan, Jr., and John W. Paulson, Jr.	L-11305
	10. Work Unit No. 505-10-11-10
9. Performing Organization Name and Address	11. Contract or Grant No.
NASA Langley Research Center Hampton, VA 23665	
	13. Type of Report and Period Covered
12. Sponsoring Agency Name and Address	Technical Note
National Aeronautics and Space Administration Washington, DC 20546	14. Sponsoring Agency Code

15. Supplementary Notes

16. Abstract

An investigation was conducted in the Langley V/STOL tunnel to determine the aerodynamic characteristics of a general aviation wing equipped with NACA 65_2-415, NASA GA(W)-1, and NASA GA(PC)-1 airfoil sections. The NASA GA(W)-1 wing was equipped with plain, split, and slotted partial- and full-span flaps and ailerons. The NASA GA(PC)-1 wing was equipped with plain, partial- and full-span flaps. Experimental chordwise static-pressure distribution and wake drag measurements were obtained for the NASA GA(PC)-1 wing at the 22.5-percent spanwise station. Comparisons were made between the three wing configurations to evaluate the wing performance, stall, and maximum lift capabilities. The tests were conducted over an angle-of-attack range of -4° to 22° and a Reynolds number range of 1.21×10^6 to 1.92×10^6 based on wing chord.

The results of this investigation indicated that the NASA GA(W)-1 wing had a higher maximum lift capability and almost equivalent drag values compared with both the NACA 65_2-415 and NASA GA(PC)-1 wings. The NASA GA(W)-1 had a maximum lift coefficient of 1.32 with 0° flap deflection, and 1.78 with 41.6° deflection of the partial-span slotted flap. The effectiveness of the NASA GA(W)-1 plain and slotted ailerons with differential deflections were equivalent. The NASA GA(PC)-1 wing with full-span flaps deflected 0° for the design climb configuration showed improved lift and drag performance over the cruise flap setting of -10°.

17. Key Words (Suggested by Author(s))	18. Distribution Statement
General aviation Airfoils Wings	Unclassified - Unlimited Subject Category 02

19. Security Classif. (of this report)	20. Security Classif. (of this page)	21. No. of Pages	22. Price*
Unclassified	Unclassified	69	$4.50

* For sale by the National Technical Information Service, Springfield, Virginia 22161

AERODYNAMIC CHARACTERISTICS OF WING-BODY CONFIGURATION WITH TWO ADVANCED GENERAL AVIATION AIRFOIL SECTIONS AND SIMPLE FLAP SYSTEMS

Harry L. Morgan, Jr., and John W. Paulson, Jr.
Langley Research Center

SUMMARY

An investigation was conducted in the Langley V/STOL tunnel to determine the aerodynamic characteristics of a general aviation wing equipped with NACA 65_2-415, NASA GA(W)-1, and NASA GA(PC)-1 airfoil sections. The NASA GA(W)-1 wing was equipped with plain, split, and slotted partial- and full-span flaps and ailerons. The NASA GA(PC)-1 wing was equipped with plain, partial- and full-span flaps. Experimental chordwise static-pressure distribution and wake drag measurements were obtained for the NASA GA(PC)-1 wing at the 22.5-percent spanwise station. Comparisons were made between the three wing configurations to evaluate the wing performance, stall, and maximum lift capabilities. The tests were conducted over an angle-of-attack range of -4° to 22° and a Reynolds number range of 1.21×10^6 to 1.92×10^6 based on wing chord.

The results of this investigation indicated that the NASA GA(W)-1 wing had a higher maximum lift capability and almost equivalent drag values compared with both the NACA 65_2-415 and NASA GA(PC)-1 wings. The NASA GA(W)-1 wing had a maximum lift coefficient of 1.32 with 0° flap deflection, and 1.78 with 41.6° deflection of the partial-span slotted flap. The effectiveness of the NASA GA(W)-1 plain and slotted ailerons with differential deflections were equivalent. The NASA GA(PC)-1 wing with full-span flaps deflected 0° for the design climb configuration showed improved lift and drag performance over the cruise flap setting of -10°.

INTRODUCTION

Research on advanced aerodynamic technology airfoils for general aviation applications has been conducted over the last several years at the Langley Research Center and reported in references 1 to 4. The first of these airfoils was developed from a 17-percent-thick supercritical airfoil to provide an airfoil with improved low-speed characteristics. This airfoil designated NASA GA(W)-1 in reference 1 showed a 30-percent increase in maximum lift coefficient and more gradual stall characteristics than a typical older NACA 65 series airfoil used for comparison.

Wings using this improved low-speed section would be suitable for application to light general aviation aircraft. These aircraft usually have limited payload weights because of low-powered engines and generally have poor ride quality because of large wing areas. Application of the improved airfoil section should increase payload capability because of the lighter wing weight

attainable with thicker sections and should improve ride quality because of the smaller wing areas possible with an increase in lift capability.

This investigation was conducted to determine the longitudinal aerodynamic characteristics of an aspect-ratio-9 wing with the NASA GA(W)-1 airfoil section equipped with typical simple flaps and ailerons. This wing was attached to a representative fuselage shape with a fineness ratio of approximately 8. An additional airfoil section, designated NASA GA(PC)-1, which was designed for optimum drag coefficient at a climb lift coefficient of 0.9 was also tested during this investigation. This additional wing was equipped with a plain flap and was intended for particular application to single-engine aircraft which, in general, have poor lift-drag ratios in climb. A wing with a NACA 65-415 airfoil section was also tested to provide baseline comparison data for the other wings. The tests were conducted in the Langley V/STOL wind tunnel through an angle-of-attack range of -4° to 22° and a sideslip range of -5° to 5°. Reynolds number based on wing chord was also varied from 1.21×10^6 to 1.92×10^6. The chordwise pressure distribution and corresponding wake velocity profile were measured at the $\frac{y}{b/2} = 0.225$ spanwise station on the NASA GA(PC)-1 wing.

SYMBOLS

Values are given in both SI and U.S. Customary Units. The measurements and calculations were made in the U.S. Customary Units. The model force and moment data are referred to the stability axis system shown in figure 1. The model moment reference center was located at the quarter-chord location of the wing root chord as shown in figure 2.

b	wing span, 4.013 m (13.17 ft)
C_D	drag coefficient, Drag/$q_\infty S$
C_h	aileron hinge-moment coefficient, Hinge moment/$q_\infty c_a^2 b_a$
C_L	lift coefficient, Lift/$q_\infty S$
C_{L_α}	lift-curve slope per degree
C_l	rolling-moment coefficient, Rolling moment/$q_\infty Sb$
C_m	pitching-moment coefficient, Pitching moment/$q_\infty Sc$
C_n	yawing-moment coefficient, Yawing moment/$q_\infty Sb$
C_p	pressure coefficient, $(p_s - p_\infty)/q_\infty$
C_Y	side-force coefficient, Side force/$q_\infty S$
c	wing chord, 44.7 cm (17.6 in.)

c_d section profile drag coefficient determined from wake measurements,

$$2\int_0^1 \frac{\sqrt{p_t - p_s}}{q_\infty}\left(1 - \frac{\sqrt{p_t - p_\infty}}{q_\infty}\right)d\left(\frac{y}{\ell}\right)$$ (see eq. 24.16, ref. 9)

c_n section normal-force coefficient, $\int_l C_p\, d\left(\frac{x}{c}\right) - \int_u C_p\, d\left(\frac{x}{c}\right)$

L/D lift-drag ratio

ℓ wake rake height, 16.76 cm (6.60 in.)

p_s local static pressure, Pa (lbf/ft^2)

p_t total pressure, Pa (lbf/ft^2)

p_∞ free-stream static pressure, Pa (lbf/ft^2)

q_∞ free-stream dynamic pressure, kPa (lbf/ft^2)

R Reynolds number based on free-stream conditions and airfoil chord

S wing area, 1.795 m^2 (19.307 ft^2)

V_∞ free-stream velocity

x airfoil abscissa, cm (in.)

y vertical distance in wake profile, cm (in.)

z airfoil ordinate, cm (in.)

α angle of attack, measured vertically between free stream and fuselage center line (positive direction, nose up), deg

β angle of sideslip, measured laterally between free stream and fuselage center line (positive direction, nose left), deg

δ control surface deflection, measured vertically between wing chordline and control surface chordline (positive direction, control surface down), deg

Subscripts:

a aileron

f flap

max maximum

s static

t total

∞ free-stream conditions

Notation:

l lower surface

u upper surface

GA(I)-I airfoil designation, General Aviation (Initial of designer's name) - Identification number of particular airfoil design

MODELS

The configurations tested during this investigation consisted of three aspect-ratio-9 rectangular wings mounted on a fineness-ratio-8 tailless fuselage. The planform details of the wing and fuselage are presented in figure 2 and photographs of the model installed in the Langley V/STOL tunnel, in figure 3. All the wings had a span of 4.013 m (13.17 ft), a wing chord of 44.7 cm (17.6 in.), and a wing area of 1.795 m^2 (19.307 ft^2). The first wing had a NACA 65_2-415 airfoil section; the second, a NASA GA(W)-1 [General Aviation (Whitcomb) - Number One]; and the third, a NASA GA(PC)-1 [General Aviation (Peterson and Chen) - Number One] airfoil section. Plots of these airfoil shapes are presented in figure 4 and their tabulated coordinates, in tables I, II, and III. The NACA 65_2-415 and NASA GA(W)-1 wings had a positive 2° incidence at the root with 2° washout at the wing tips. The NASA GA(PC)-1 wing had 0° incidence of the root with 2° washout at the wing tip.

The NACA 65_2-415 airfoil section is a member of the family of low-drag airfoils developed by the NACA and are often referred to as the "laminar flow" airfoils. (See ref. 5.) These airfoils have been used successfully on sailplanes; however, on general aviation wings laminar boundary-layer conditions are difficult to maintain because of surface roughness near the leading edge caused either by wing fabrication techniques or by insect remains gathered during flight. The NACA 65_2-415 airfoil section has leading-edge flow separation characteristics at high angles of attack in two dimensions which results in unfavorable wing stall characteristics. This airfoil, nevertheless, is used on many current general aviation aircraft and was tested during this investigation to obtain baseline comparison data. This wing was not equipped with flaps or ailerons.

The NASA GA(W)-1 was designed by Richard T. Whitcomb specifically for low-speed application. (See ref. 1.) This airfoil section was designed for a cruise lift coefficient of 0.4, for a good lift-drag ratio at a climb lift coefficient of 1.0, and for a maximum lift coefficient of 2.0. The key design features of this airfoil are (1) a large upper surface leading-edge radius; (2) an approximate uniform loading at the cruise lift coefficient; and (3) a blunt

trailing edge. The large upper surface leading-edge radius was used to attenuate the peak negative pressure coefficients and thereby to delay airfoil stall to a high angle of attack. A blunt trailing edge provided the airfoil with approximately equal upper and lower surface slopes to moderate the upper surface-pressure recovery and thus further delay stall. A 17-percent-thick NASA supercritical airfoil was used as a starting geometry for the low-speed airfoil design because the highly aft-cambered supercritical airfoils had indicated good low-speed characteristics. The final low-speed airfoil geometry was obtained by tailoring the supercritical airfoil geometry until the desired cruise, climb, and maximum lift conditions were satisfied. The computer program of reference 6 was used to predict the design and off-design characteristics of the airfoil during the tailoring process.

The NASA GA(W)-1 wing was equipped with full-span plain, slotted, and split flap systems as shown in figure 5. The chord of both the plain and slotted flap was 18 percent of the wing chord, and the chord of the split flap was 24.6 percent of the wing chord. Each flap system was divided at the mid-semispan location to allow for independent movement of the inboard and outboard sections. The inboard section had a range of deflection from 0° to 40° down, and the outboard, a range of deflection from 0° to 10° down. The outboard section of the left wing panel of the plain and slotted flap systems could be deflected from 30° up to 20° down and was used as a representative aileron. These aileron sections were equipped with a push-rod type hinge-moment gage as shown in figure 6 to determine aileron control forces.

The NASA GA(PC)-1 was designed by John B. Peterson, Jr., of Langley Research Center and Allen W. Chen, NRC-NASA Resident Research Associate, for optimum drag at a climb lift coefficient of 0.9. Details of the design procedure used for this airfoil are given in the appendix. A suitable airfoil shape for cruise flight was obtained by deflecting a 19-percent-chord simple flap 10° upward ($\delta_f = -10^\circ$) with the center of rotation on the lower surface at the 80.8-percent-chord location. A representative landing shape was obtained by deflecting the simple flap down 10° ($\delta_f = 10^\circ$) as shown in figure 7. This flap system, like those on the NASA GA(W)-1 wing, was divided at the mid-semispan location to allow for independent movement of the inboard and outboard sections. Partial- and full-span flap combinations with flap deflections from -10° to 10° were tested.

The left wing panel was equipped with a chordwise row of surface-pressure orifices at a spanwise location equal to 22.5 percent of the span to determine the sectional characteristics of the NASA GA(PC)-1 airfoil. The pressure orifice locations are given in table IV. The pressure data were integrated to obtain the section normal-force coefficients. A wake rake was positioned 5.08 cm (2.0 in.) downstream of the wing trailing edge at the same spanwise location as that of the pressure orifices to measure profile drag. The rake consisted of 41 total and 4 static-pressure probes as shown in figure 8. This rake was supported by a horizontal strut which was mounted to the model fuselage. A photograph of the rake and horizontal strut are shown in figure 9. The rake was positioned to keep its center line approximately 5.08 cm (2.0 in.) downstream of the wing trailing edge when the flap was deflected.

INSTRUMENTATION AND TEST CONDITIONS

Aerodynamic forces and moments were measured with a six-component, electrical strain-gage balance mounted inside the fuselage as shown in figure 2. Angle of attack was set by the pitch drive of the model support system and measured by an electronic sensor mounted inside the fuselage. Sideslip angle was set by the yaw drive of the model support system and measured by an electronic counter mounted to the yaw drive gearing system. The surface pressures of the NASA GA(PC)-1 wing were obtained through pressure orifices set normal to the local surface and were measured by using two 15.44 kPa (2.5 psi) differential pressure transducers and two 48-port scanning valves. Wake pressures were also measured using one 15.44 kPa (2.5 psi) differential pressure transducer and one 48-port scanning valve. Fuselage chamber pressure was measured by using a 6.17 kPa (1.0 psi) differential pressure transducer.

This investigation was conducted in the Langley V/STOL tunnel at dynamic pressures of 0.8576 kPa (20 lb/ft^2), 1.4364 kPa (30 lb/ft^2), 1.7152 kPa (40 lb/ft^2), and 2.3940 kPa (50 lb/ft^2) which correspond to Reynolds numbers based on the chord of 1.21, 1.49, 1.72, and 1.92×10^6, respectively. The Mach number ranged from 0.12 to 0.18. The model was tested through an angle-of-attack range of -4° to 22° and a sideslip angle range of -5° to 5°. The NASA GA(W)-1 and NASA GA(PC)-1 wings were tested with partial- and full-span flap deflections. The NASA GA(W)-1 wing was tested with single and differential aileron deflections. The fuselage was also tested without a wing and the NASA GA(W)-1 wing was tested without a fuselage.

Boundary-layer transition strips 0.25 cm (0.1 in.) wide were placed on the upper and lower surface of each wing leading edge. The strips were located 2.3 cm (0.9 in.) or $x/c = 0.051$ on the upper surface and 4.3 cm (1.7 in.) or $x/c = 0.097$ on the lower surface. The roughness was sized according to reference 7 and required a commercial number 60 grit sparsely applied.

Wind-tunnel boundary corrections were determined according to reference 8 and applied to the data. Drag corrections due to model chamber pressure were also applied to the data.

PRESENTATION OF RESULTS

The results are presented in the following figures:

RESULTS AND DISCUSSION

Fuselage Alone

The effect of Reynolds number on the longitudinal characteristics of the body alone are presented in figure 10. There are no measurable effects over this limited Reynolds number range of this investigation.

The aerodynamic characteristics of the body at various sideslip angles are presented in figure 11. There are no significant effects on C_L, C_D, C_n, or C_l due to sideslip. Yawing moment is destabilizing over the angle-of-attack range below 18° and is stabilizing above 18°. Side force steadily increases with sideslip angle as would be expected.

NASA GA(W)-1 Wing Alone

As shown in figure 12, the effect of Reynolds numbers is rather small for the NASA GA(W)-1 wing alone; only small increases in C_L are obtained at the higher angles of attack. Drag values are almost unchanged until the wing nears stall. The lift-curve slope is about 0.077/deg and is quite linear up to an angle of attack of about 5° and then becomes nonlinear as flow separation begins on the aft portion of the wing. The $C_{L,max}$ is about 1.31 for the wing alone.

NACA 65_2-415 Configuration

The baseline comparison data for the NACA 65_2-415 wing are presented in figure 13. The variations of the longitudinal aerodynamic characteristics with Reynolds number are not large and show the expected trend of increasing C_L, especially in the range near $C_{L,max}$, as Reynolds number increases. The increased Reynolds number also tends to reduce trailing-edge flow separation as indicated by the reduction in C_D and C_m associated with the increases in C_L. This NACA 65_2-415 wing-body has a lift-curve slope of 0.090/deg with a $C_{L,max}$ of 1.08 to 1.16 depending on the Reynolds number. At a cruise C_L of 0.4, this wing has a C_D of 0.028 and a C_m of -0.042; whereas, at a climb C_L of 0.9, it has a C_D of 0.060 and a C_m of 0.035. These values are compared with the NASA GA(W)-1 and NASA GA(PC)-1 configurations to evaluate the performance of each wing.

The aerodynamic characteristics of the model at various sideslip angles are presented in figure 14. As the model is yawed, there is very little effect on the aerodynamic characteristics until the downwind wing stalls or is blanketed by the wake of the body at an angle of attack of about 9°. The large rolloff indicated in the C_l data corresponds to stall breaks in the lift and drag data. As expected for a tailless configuration, the yawing and pitching moments generated are destabilizing.

NASA GA(W)-1 Configuration

Effect of Reynolds number.- The effects of Reynolds number on the longitudinal characteristic of the wing body are presented in figure 15. Again the effects are rather small and are limited to the higher angles of attack. It is interesting to note that the stall characteristics for the lowest Reynolds number are somewhat different than those at the higher numbers with a rather pronounced peak in the data at stall. Also the angle of attack at stall is only 13° at the lowest Reynolds number and 17° at the higher Reynolds number. The addition of the body changes the lift-curve slope to 0.086/deg in the linear part of the data but the nonlinearities still occur at an angle of attack of 5°. In addition, $C_{L,max}$ varies from 1.30 to 1.41, depending on Reynolds number.

These values show a slight reduction in C_{L_α} over the NACA 65_2-415 airfoil but $C_{L,max}$ is increased about 0.22 to 0.25. At the cruise C_L the drag is nearly identical to that of the NACA 65_2-415 and the pitching moment is -0.080 and shows the increased nose-down moment due to the aft loading on the NASA GA(W)-1. At the climb C_L of 0.90, the C_D is about 0.060 which is the same as that for the NACA 65_2-415, and C_m is -0.015 as compared with 0.035 for the NACA 65_2-415. This result would indicate that for trimmed conditions the NACA 65_2-415 would have a slightly better L/D at cruise and in climb.

The aerodynamic characteristics of the model at various sideslip angles are presented in figure 16. Although the magnitudes differ somewhat, these data show the same trends as the NACA 65_2-415 configuration.

Effect of flap deflections.- The effect of the deflection of an inboard plain flap is presented in figure 17. The maximum lift coefficient is increased to 1.63 whereas the stall angle of attack is reduced to 10° at a flap deflection of 41.5°. At maximum flap deflection, drag is increased by 0.04 at the low angle of attack, to 0.05 at the higher angles. The pitching moment becomes more nose down as the flaps are deflected.

The slotted flap data are presented in figure 18 for both partial- and full-span cases. The partial-span flap increases $C_{L,max}$ to 1.78 at a stall angle of attack of 10.5°. There is very little difference in lift between the 30° and 40° flap settings; therefore, flow separation has occurred over the flap and reduced the effectiveness of the flap at the 40° deflection. Drag increments for the slotted flap are 0.005 to 0.008 higher than the plain flap over the angle-of-attack range of the tests.

Only one deflection of 10° was possible for the full-span slotted flap. The benefit of using the full-span flap can be seen over the entire angle-of-attack range as the lift is increased by 0.11 over the partial-span flap for the 10° deflection.

The split flap data are presented in figure 19 for both the partial- and full-span flaps. The lift characteristics are similar to the other flap configurations with $C_{L,max}$ equal to 1.68 at an angle of attack of 10°; however, the drag increments are higher than either of the other flap systems over the angle-of-attack range of the tests.

As for the other flaps, only the 10° flap deflection was possible for the full-span split flap. Again the benefit of using the full span was very apparent.

Effect of aileron deflections.- The effects of plain aileron deflection are presented in figure 20 and the effects of the slotted ailerons are presented in figure 21. Changes in lift, drag, and pitching-moment coefficients are about equal for both ailerons, the small differences showing up in the magnitude of the rolling moments generated with aileron deflections. For up deflections of the left aileron (figs. 20(b) and 21(b)), the plain and slotted ailerons appeared to have equal effectiveness at the lower angles of attack, the slotted aileron being more effective at the higher angles. The plain aileron rolling moments are constant with angle of attack where the slotted aileron rolling moments vary with angle of attack especially at the higher deflections. In general, the slotted aileron has lower hinge moments than does the plain aileron. When the left aileron was deflected down (figs. 20(d) and 21(d)), the slotted aileron was more effective in showing the benefit of the slot as seen before in the flap data. Figures 20(f) and 21(f) show the data for differential aileron deflections (left aileron up and right aileron down). Again it appears that the slotted aileron is slightly more effective but since the deflections are not equal for each case, the direct comparison is difficult.

NASA GA(PC)-1 Wing Body

The effects of Reynolds number on the longitudinal aerodynamic characteristics of the NASA GA(PC)-1 wing in the cruise configuration (δ_f = -10°) are presented in figure 22. The only effect of increasing Reynolds number is a slight increase in $C_{L,max}$ which is also observed on the other wings. There was a reduction in $C_{L,max}$ of 0.2 and 0.5, compared with the NACA 65_2-415 and NASA GA(W)-1 wings, respectively. The aerodynamic characteristics of this wing are presented in figure 23 and show the expected results. The effects of partial- and full-span flap deflections are presented in figure 24. These data show the expected increase in C_L with increasing flap deflection. The $C_{L,max}$ capability of this wing is considerably less than that of the NASA GA(W)-1 at equivalent flap settings. This wing does, however, exhibit a slightly smoother stall pattern than the NASA GA(W)-1 as exemplified by the gradual increase in C_L and flatness in C_m after the stall angles of attack of about 9°.

The lift/drag polars for the three wings tested are presented in figure 25 The NASA GA(PC)-1 wing is presented with both -10° and 0° full-span flap deflec-

tions. As stated in the appendix, this wing was designed for an improved L/D at the climb C_L of 0.9 which corresponds to the 0° flap deflection case. The data shown in this figure clearly demonstrate the lower performance of the NASA GA(PC)-1 wing at the cruise flap setting of -10° compared with the design climb configuration. The climb configuration resulted in an increase in L/D at a cruise C_L of 0.4 and at a climb C_L of 0.9 compared with the other wings. However, the NASA GA(PC)-1 wing for the design climb configuration is very close to stall with C_L equal to 90 percent of $C_{L,max}$.

The experimental static-pressure distributions measured at the 22.5-percent-span station are presented in figure 26 for -10°, 0°, and 10° full-span flap settings. The pressure distribution for the climb configuration (δ_f = 0°) of figure 26(b) illustrates that at C_L = 0.9, α = 11.5°, the flow is well attached. However, at $C_{L,max}$, α = 13.6°, the entire surface has separated. The section drag measured with the wake rake is presented in figure 27. The section normal-force coefficients presented in this figure were obtained by simple integration of the measured static-pressure distributions. The section characteristics of the NASA GA(W)-1 given in reference 1 are also presented in figure 27 for comparison. The drag levels of both the NASA GA(PC)-1 and NASA GA(W)-1 airfoils are approximately the same. The NASA GA(W)-1 has higher drag at the lower values of C_n and lower drag at the higher values of C_n.

CONCLUSIONS

An investigation has been conducted in the Langley V/STOL tunnel to determine the aerodynamic characteristics of three aspect-ratio-9, rectangular unswept wings with a NACA 65_2-415, a NASA GA(W)-1, and a NASA GA(PC)-1 airfoil section, respectively. The following conclusions have been made:

1. The NASA GA(W)-1 wing had a higher maximum lift coefficient capability and almost equivalent drag values compared with both the NACA 65_2-415 and NASA GA(PC)-1 wings.

2. The NASA GA(W)-1 equipped with the slotted flap showed the expected higher performance compared with the plain and split flap configurations.

3. The effectiveness of the plain and slotted ailerons for the NASA GA(W)-1 with differential deflections were almost equal.

4. The NASA GA(PC)-1 wing with the flaps deflected 0° for the design climb configuration showed improved lift and drag performance over the basic cruise, -10° flap setting configuration.

5. The NASA GA(W)-1 and NASA GA(PC)-1 configurations generally exhibit a smoother stall than the NACA 65_2-415 configuration.

Langley Research Center
National Aeronautics and Space Administration
Hampton, VA 23665
June 15, 1977

APPENDIX

DESIGN TECHNIQUE FOR THE NASA GA(PC)-1 AIRFOIL

The NASA GA(PC)-1 airfoil was designed for an optimum drag coefficient at a given lift coefficient. The design lift coefficient for this airfoil was 0.9 which is a common value for the climb lift coefficient of many current single-engine general aviation aircraft. Reducing the airfoil drag at a given climb lift means an increase in lift-drag ratio and, therefore, an improvement in the climb performance capability of the rather low-powered single-engine general aviation aircraft.

The NASA GA(PC)-1 airfoil was designed for low drag in almost fully turbulent flow, since very little laminar flow is found on general aviation airfoils due to roughness near the wing leading edge which causes transition of the boundary layer. This roughness is a result of either wing fabrication techniques or insect remains gathered during flight.

During the theoretical analysis of the NASA GA(PC)-1 airfoil, the lift coefficient was determined by integrating the pressure distribution around the airfoil surface. The drag coefficient was determined by calculating the boundary-layer development and using a modified form of the Betz's (ref. 9) profile drag formula which is

$$c_d = \frac{2\theta}{c}\left\{\left(\frac{v}{U_\infty}\right)^2 + H\left[\left(\frac{v}{U_\infty}\right)^2 - \frac{v}{U_\infty}\right]\right\}$$

where c_d is the profile drag coefficient, c is the airfoil chord, U_∞ is the free-stream velocity, θ is the boundary-layer momentum thickness at the airfoil trailing edge, v is the flow velocity at the trailing edge, and H is the boundary-layer shape factor at the trailing edge. The Truckenbrodt turbulent boundary-layer method (ref. 10) was used to compute the momentum thickness θ and the shape factor H needed in the drag formula. To determine the shape of the pressure distribution for lowest drag, a pattern or grid method of optimization was used in which all combinations of a set of variations used to define the general shape of the pressure distribution were covered. A computer program was developed by using the Truckenbrodt boundary-layer method and the Betz drag formula to rapidly calculate the drag of over 2000 combinations of these variables and present the results in an easily read form. For each successive run, the range of each variable was refined, and after a few runs, a pressure distribution that gave quite a low drag was obtained.

The airfoil geometry of NASA GA(PC)-1 was obtained by using the iterative inverse design method described in reference 11. This inverse design program calculates the pressure distribution on the surface of an initial airfoil shape and then systematically modifies the airfoil shape until the desired pressure distribution is obtained. In order to avoid both a divergent iterative process and an unrealistic airfoil geometry, a common practice in designing airfoils is

to specify the pressure distribution only on a portion of the airfoil surface. This allows the designer to select an initial airfoil shape with some desired features other than a desired pressure distribution. An airfoil geometry with the desired pressure distribution can usually be generated with acceptable accuracy in 10 iterations. This inverse design procedure generates an airfoil shape in inviscid flow. The airfoil pressure distribution in viscous flow is computed by using the method described in reference 6 and then compared with the desired pressure distributions. The inclusion of viscous effects tend, in general, to thicken an inviscid airfoil shape and uncamber its shape near the trailing edge. Appropriate changes are then made to the inviscid airfoil geometry which is cycled through the inverse program again. After a few cycles, highly dependent on user experience, an airfoil shape can be obtained that includes the viscous effects. The final shape and pressure distribution for the NASA GA(PC)-1 is presented in figure 28.

The initial input geometry for the NASA GA(PC)-1 airfoil was the NASA GA(W)-1 airfoil geometry. For a design Reynolds number of 4×10^6 based on airfoil chord and for a lift coefficient of 0.9, an optimum drag coefficient of 0.010 was predicted for the NASA GA(PC)-1 airfoil. An airfoil shape for cruise flight was obtained by deflecting a 19-percent-chord flap 10° upward with the center of rotation located on the lower surface at 80.8 percent of the chord.

REFERENCES

1. McGhee, Robert J.; and Beasley, William D.: Low-Speed Aerodynamic Characteristics of a 17-Percent-Thick Airfoil Section Designed for General Aviation Applications. NASA TN D-7428, 1973.

2. McGhee, Robert J.; Beasley, William D.; and Somers, Dan M.: Low-Speed Aerodynamic Characteristics of a 13-Percent-Thick Airfoil Section Designed for General Aviation Applications. NASA TM X-72697, 1975.

3. McGhee, Robert J.; and Beasley, William D.: Effects of Thickness on the Aerodynamic Characteristics of an Initial Low-Speed Family of Airfoils for General Aviation Applications. NASA TM X-72843, 1976.

4. McGhee, Robert J.; and Beasley, William D.: Low-Speed Wind-Tunnel Results for a Modified 13-Percent-Thick Airfoil. NASA TM X-74018, 1977.

5. Abbott, Ira H.; and Von Doenhoff, Albert E.: Theory of Wing Sections. Dover Publ., Inc., c.1959.

6. Stevens, W. A.; Goradia, S. H.; and Braden, J. A.: Mathematical Model for Two-Dimensional Multi-Component Airfoils in Viscous Flow. NASA CR-1843, 1971.

7. Braslow, Albert L.; and Knox, Eugene C.: Simplified Method for Determination of Critical Height of Distributed Roughness Particles for Boundary-Layer Transition at Mach Numbers From 0 to 5. NACA TN 4363, 1958.

8. Gillis, Clarence L.; Polhamus, Edward C.; and Gray, Joseph L., Jr.: Charts for Determining Jet-Boundary Corrections for Complete Models in 7- by 10-Foot Closed Rectangular Wind Tunnels. NACA WR L-123, 1945. (Formerly NACA ARR L5G31.)

9. Schlichting, Hermann (J. Kestin, transl.): Boundary-Layer Theory. Sixth ed., McGraw-Hill Book Co., Inc., c.1968.

10. Truckenbrodt, E.: A Method of Quadrature for Calculation of the Laminar and Turbulent Boundary Layer in Case of Plane and Rotationally Symmetrical Flow. NACA TM 1379, 1955.

11. Chen, Allen Wen-shin: The Determination of the Geometries of Multiple-Element Airfoils Optimized for Maximum Lift Coefficient. Ph.D. Thesis, Univ. of Illinois, 1971. (Also available as NASA TM X-67591.)

TABLE I.- NACA 65_2-415 AIRFOIL COORDINATES

[c = 44.7 cm (17.6 in.)]

x/c	$(z/c)_u$	x/c	$(z/c)_l$
0.0	0.0	0.0	0.0
.00313	.01208	.00687	-.01008
.00542	.01480	.00958	-.01200
.01016	.01900	.01484	-.01472
.02231	.02680	.02769	-.01936
.04697	.03863	.05303	-.02599
.07184	.04794	.07816	-.03098
.09682	.05578	.10318	-.03510
.14697	.06842	.15303	-.04150
.19726	.07809	.20274	-.04625
.24764	.08550	.25236	-.04970
.29807	.09093	.30193	-.05205
.34854	.09455	.35146	-.05335
.39903	.09639	.40097	-.05355
.44953	.09617	.45047	-.05237
.50	.09374	.50	-.04962
.55043	.08910	.54957	-.04530
.60079	.08260	.59921	-.03976
.65106	.07462	.64894	-.03342
.70124	.06542	.69876	-.02654
.75131	.05532	.74869	-.01952
.80126	.04447	.79874	-.01263
.85109	.03320	.84891	-.00628
.90080	.02175	.89920	-.00107
.95040	.01058	.94960	.00206
1.0	.0	1.0	.0
Leading-edge radius, 0.015c Slope of radius through leading edge, 0.168			

TABLE II.- NASA GA(W)-1 AIRFOIL COORDINATES

[c = 44.7 cm (17.6 in.)]

x/c	$(z/c)_u$	$(z/c)_l$
0.0	0.0	0.0
.002	.01300	-.00974
.005	.02035	-.01444
.0125	.03069	-.02052
.025	.04165	-.02691
.0375	.04974	-.03191
.05	.05600	-.03569
.075	.06561	-.04209
.100	.07309	-.04700
.125	.07909	-.05087
.150	.08413	-.05426
.175	.08848	-.05700
.20	.09209	-.05926
.25	.09778	-.06265
.30	.10169	-.06448
.35	.10409	-.06517
.40	.10500	-.06483
.45	.10456	-.06344
.50	.10269	-.06091
.55	.09917	-.05683
.575	.09674	-.05396
.60	.09374	-.05061
.625	.09013	-.04678
.65	.08604	-.04265
.675	.08144	-.03830
.700	.07639	-.03383
.725	.07096	-.02930
.750	.06517	-.02461
.775	.05913	-.02030
.800	.05291	-.01587
.825	.04644	-.01191
.850	.03983	-.00852
.875	.03313	-.00565
.900	.02639	-.00352
.925	.01965	-.00248
.950	.01287	-.00257
.975	.00604	-.00396
1.000	-.00074	-.00783

TABLE III.- NASA GA(PC)-1 AIRFOIL COORDINATES FOR

DESIGN CLIMB CONFIGURATION (δ_f = 0°)

[c = 44.7 cm (17.6 in.)]

x/c	$(z/c)_u$	$(z/c)_l$
0.0	-0.0025	-0.0025
.0025	.0098	-.0140
.005	.0160	-.0208
.01	.0245	-.0273
.02	.0360	-.0356
.03	.0448	-.0408
.04	.0521	-.0445
.05	.0583	-.0469
.08	.0726	-.0515
.10	.0796	-.0533
.125	.0863	-.0545
.15	.0909	-.0553
.175	.0947	-.0560
.20	.0970	-.0568
.25	.0993	-.0583
.30	.0998	-.0595
.35	.0983	-.0609
.40	.0953	-.0625
.45	.0915	-.0630
.50	.0861	-.0626
.55	.0797	-.0615
.60	.0721	-.0594
.625	.0683	-.0576
.65	.0644	-.0556
.675	.0606	-.0523
.70	.0564	-.0478
.725	.0521	-.0433
.75	.0471	-.0383
.775	.0420	-.0318
.808	.0355	-.0235
.828	.0312	-.0219
.848	.0269	-.0203
.868	.0226	-.0187
.888	.0183	-.0172
.908	.0141	-.0156
.928	.0098	-.0140
.948	.0055	-.0124
.968	.0012	-.0108
.988	-.0030	-.0092
1.000	-.0056	-.0083

TABLE IV.- NASA GA(PC)-1 AIRFOIL ORIFICE LOCATIONS

[c = 44.7 cm (17.6 in.)]

Upper surface	
x/c	z/c
0.0	-0.0025
.0013	.0056
.0066	.0189
.0178	.0337
.0343	.0481
.0531	.0601
.0755	.0708
.0983	.0790
.1238	.0861
.1524	.0913
.1825	.0953
.2149	.0981
.2498	.0993
.2868	.0999
.3246	.0993
.3647	.0976
.4073	.0948
.4499	.0915
.4906	.0872
.5316	.0822
.5763	.0757
.6443	.0653
.6913	.0579
.7337	.0502
.7841	.0402
.8318	.0304
.8836	.0193
.9380	.0077
.9786	-.0010

Lower surface	
x/c	z/c
0.0035	-0.0177
.0134	-.0306
.0293	-.0405
.0494	-.0468
.0695	-.0503
.0906	-.0526
.1124	-.0541
.1580	-.0556
.1826	-.0563
.2177	-.0573
.2724	-.0589
.3396	-.0606
.3947	-.0624
.4424	-.0630
.4915	-.0627
.5456	-.0616
.5891	-.0600
.6289	-.0577
.6660	-.0536
.7015	-.0475
.7370	-.0411
.7686	-.0326
.7982	-.0258
.8270	-.0218
.8698	-.0186
.9312	-.0138
.9779	-.0100

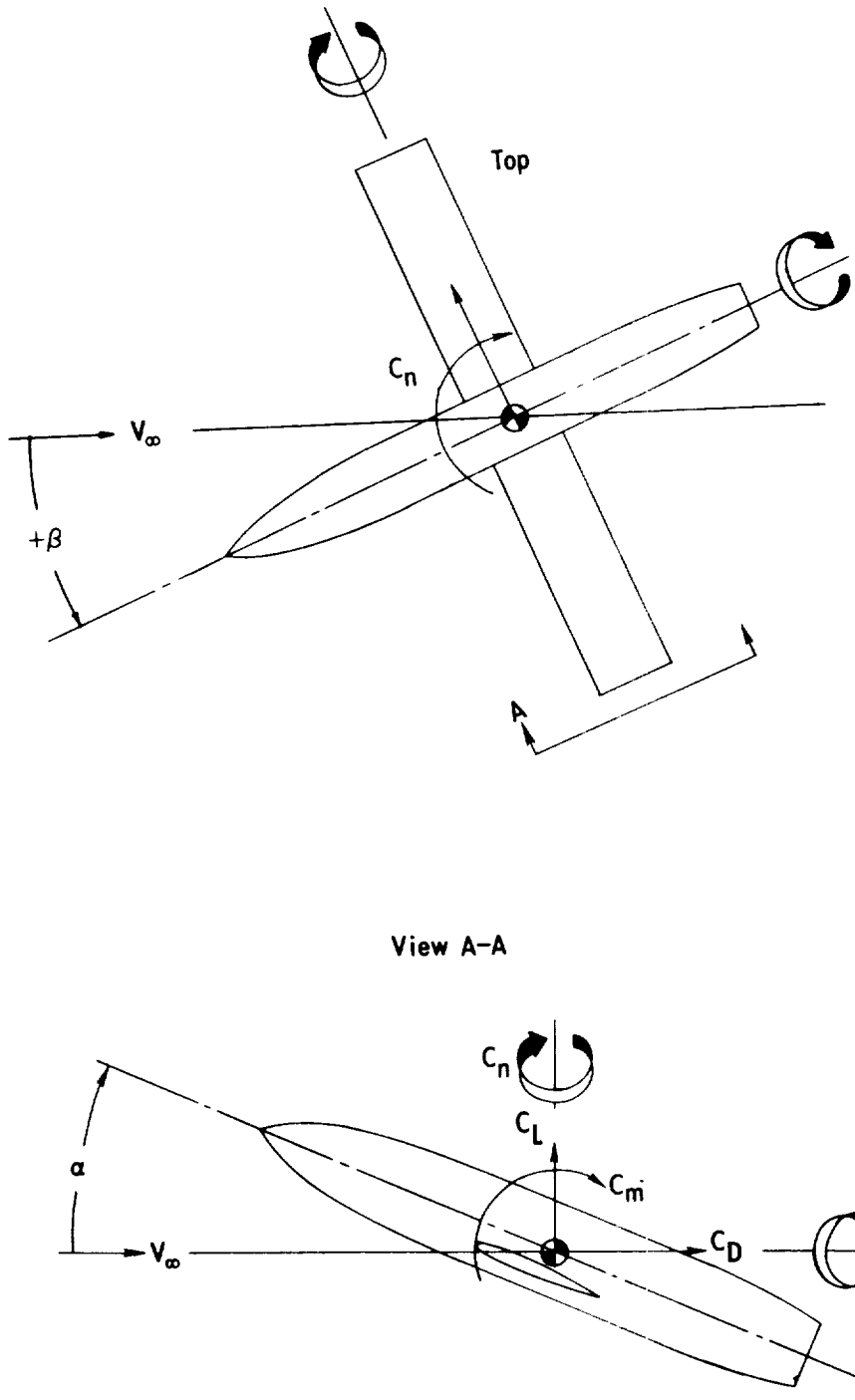

Figure 1.- Axis system used in presentation of data. Arrows indicate positive direction of moments, forces, and angles.

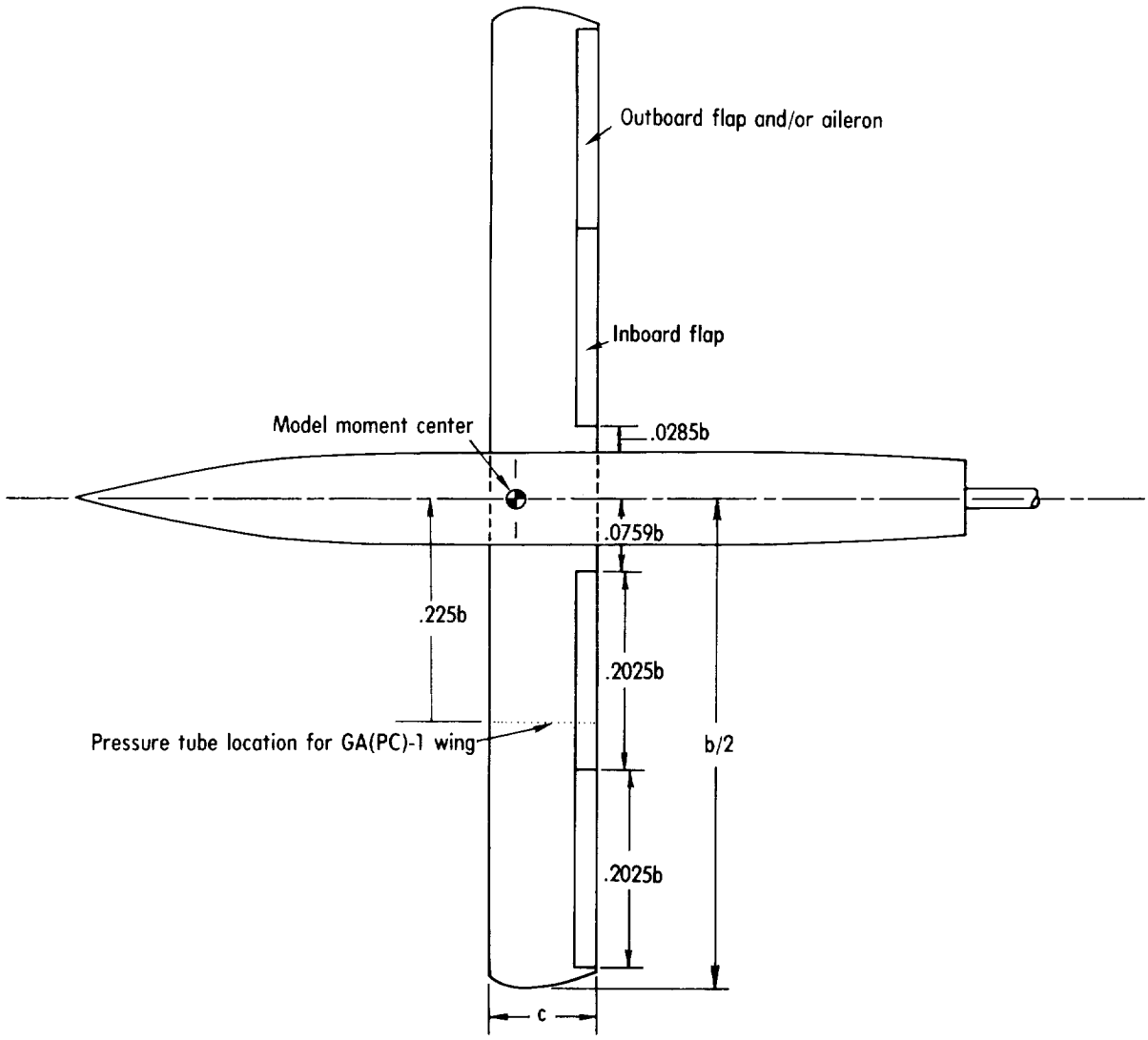

(a) Top view.

Figure 2.- Drawing of model used in investigation.

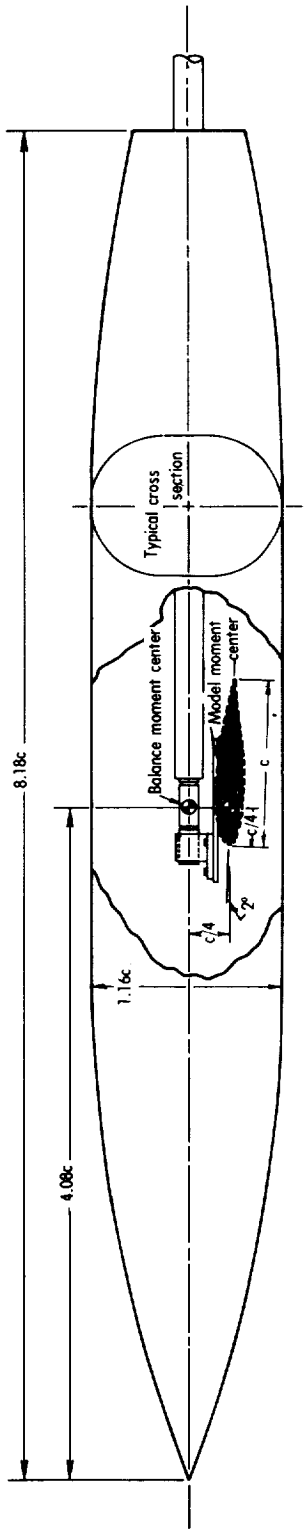

(b) Side view.

Figure 2.- Concluded.

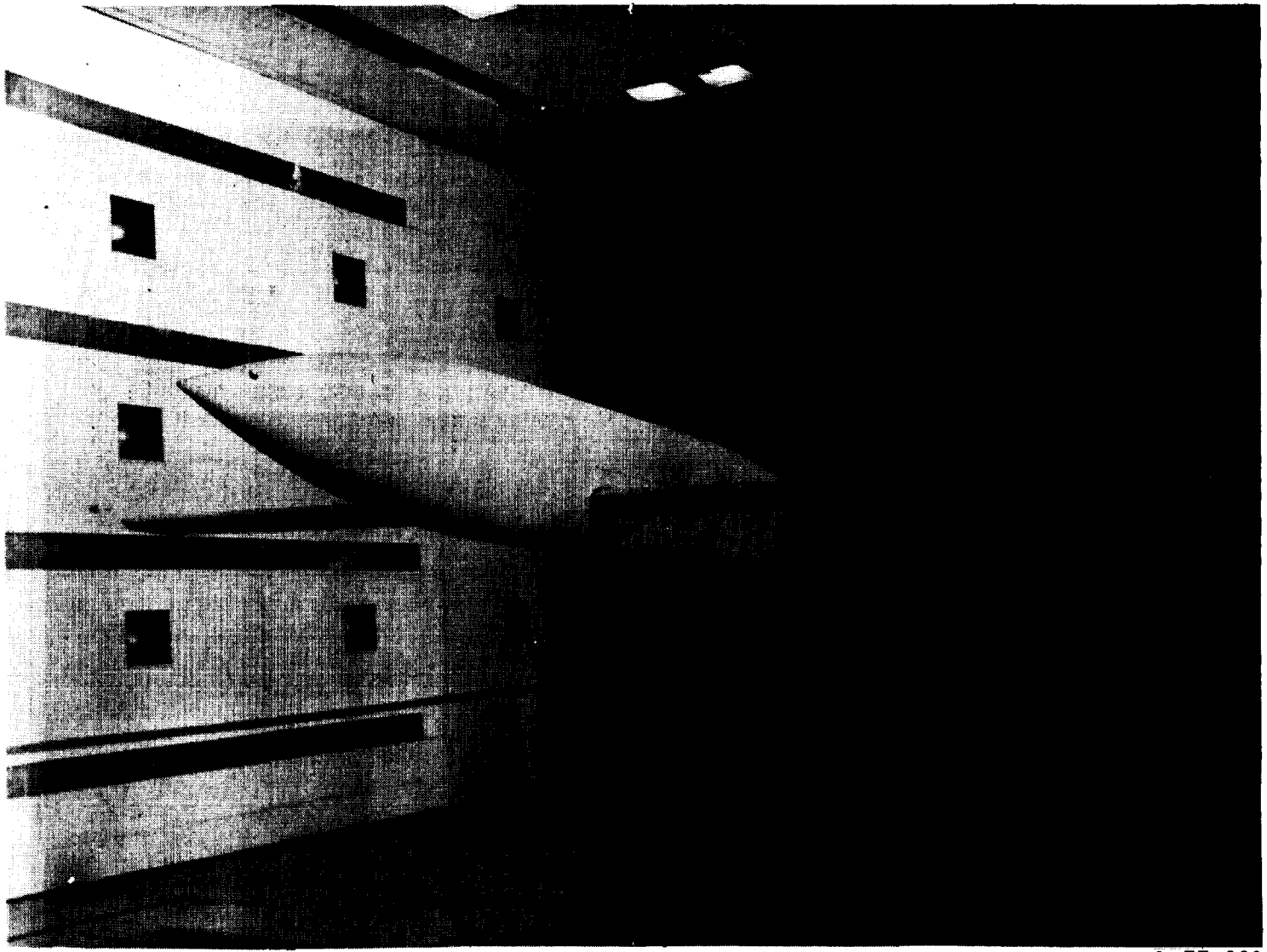

L-77-209

(a) Complete model.

Figure 3.- Photographs of model mounted in Langley V/STOL tunnel.

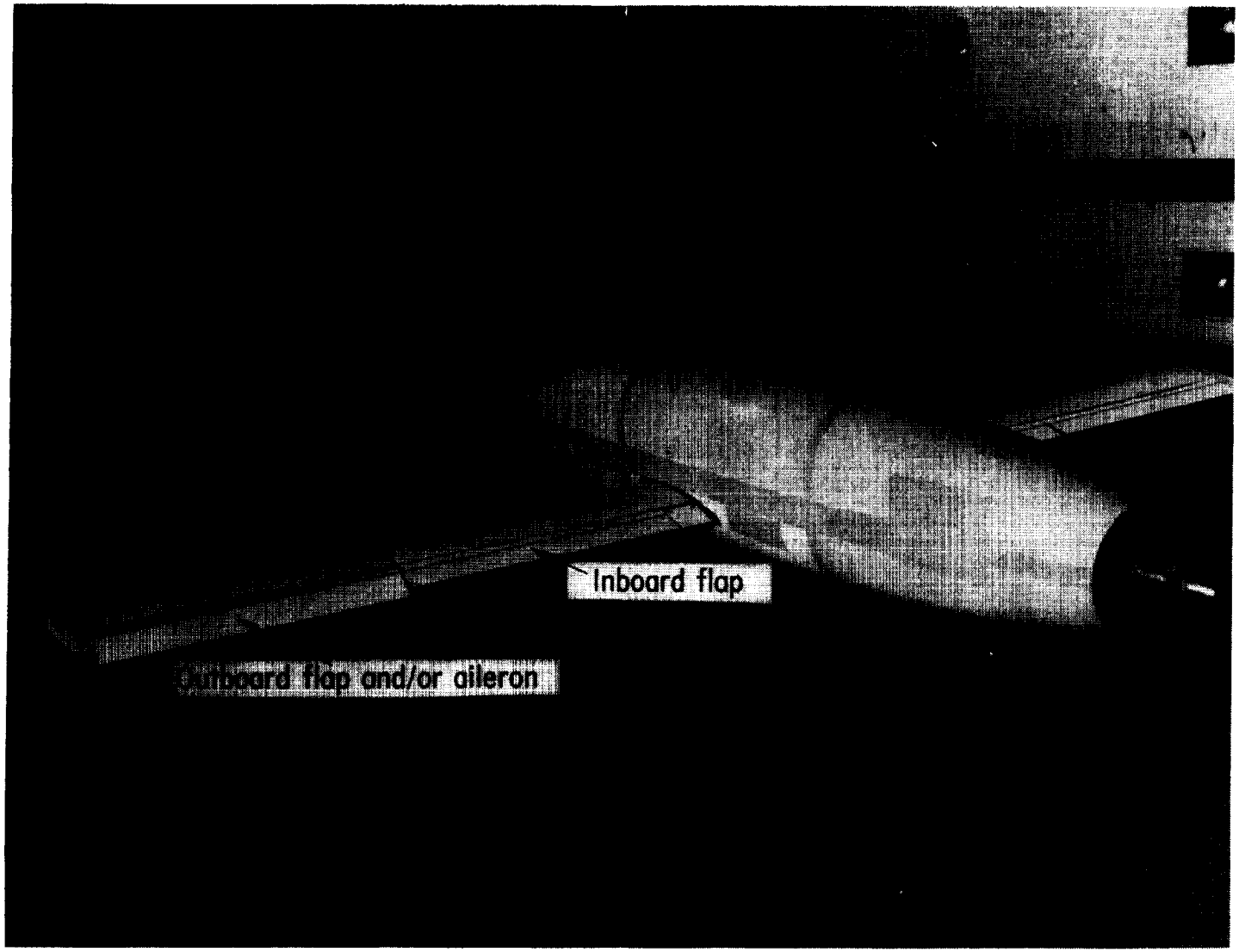

L-72-9175.1

(b) Aileron deflected.

Figure 3.- Concluded.

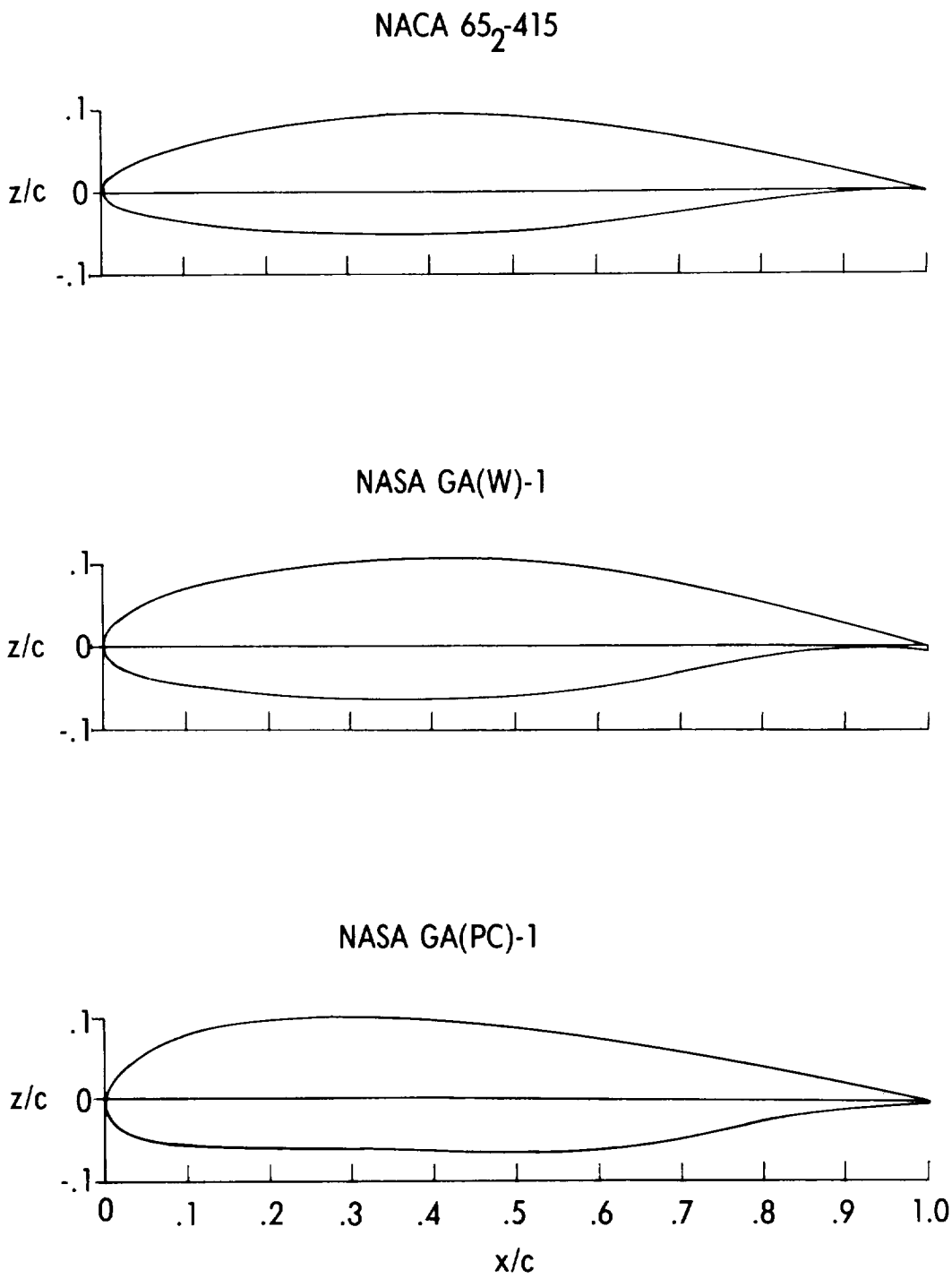

Figure 4.- Airfoil sections used in investigation.

Plain flap

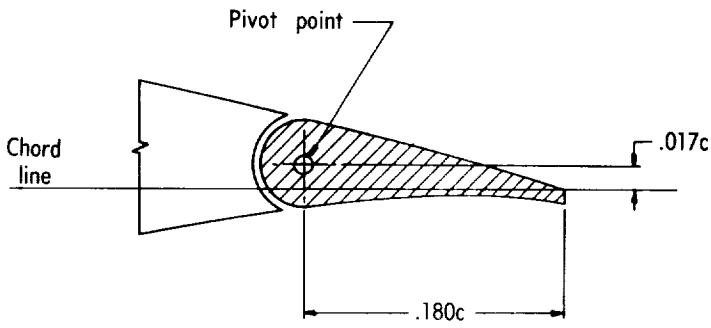

Slotted flap

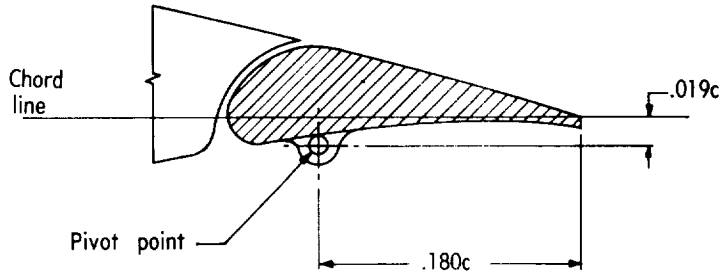

Split flap

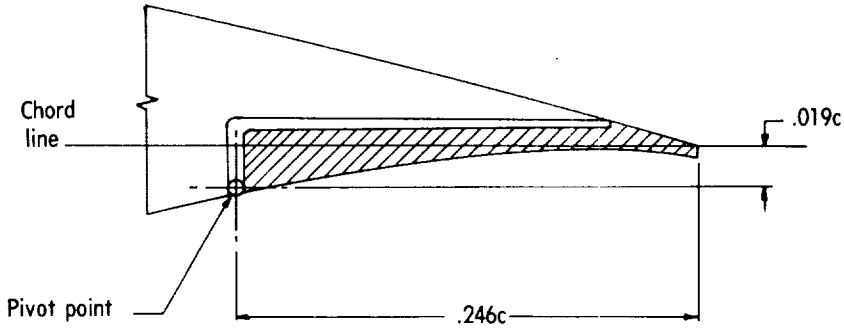

Figure 5.- Flap systems used on NASA GA(W)-1 wing.

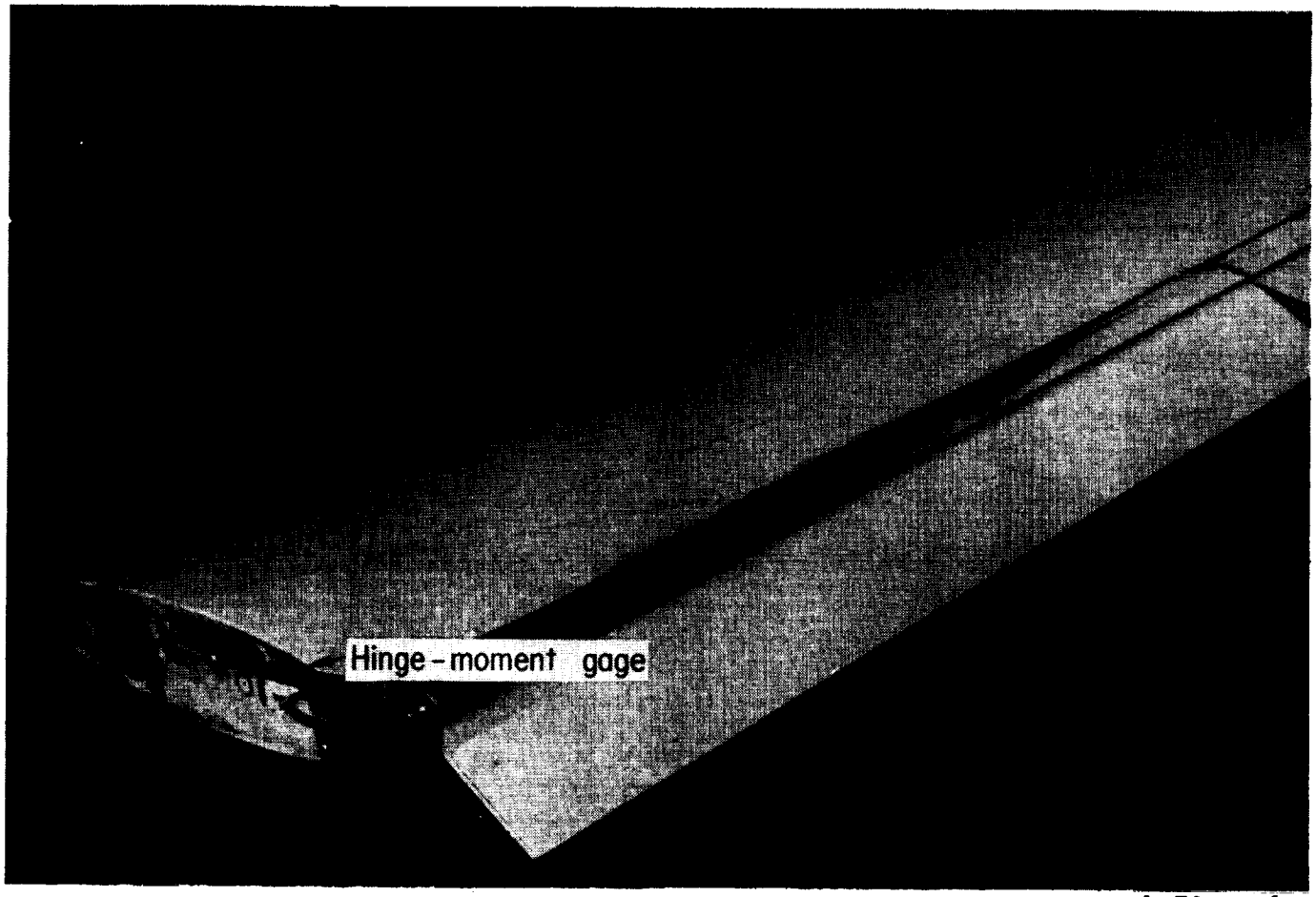

L-72-9176.1

Figure 6.- Photograph of hinge-moment gage installed on NASA GA(PC)-1 wing.

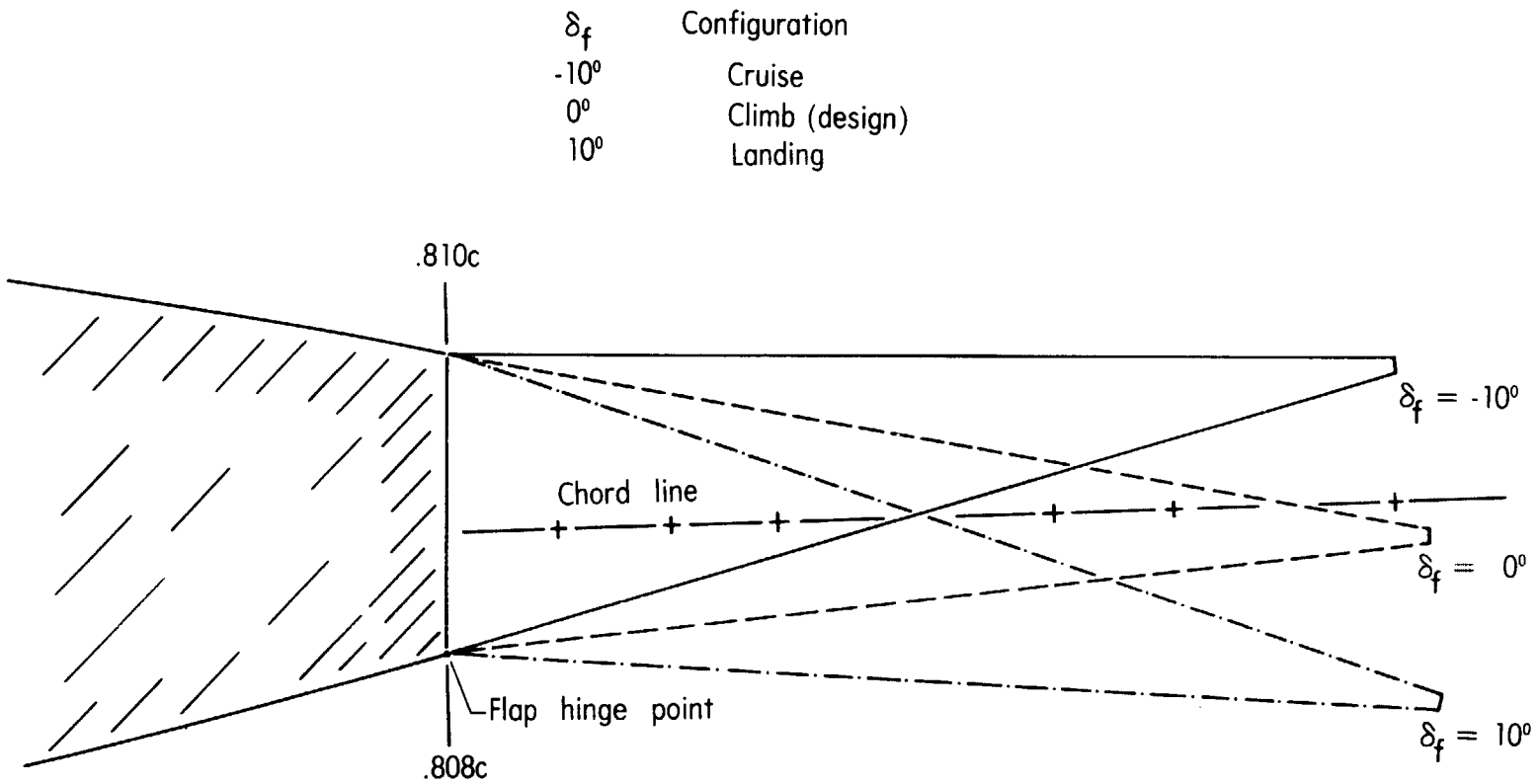

Figure 7.- Flap system used on NASA GA(PC)-1 wing.

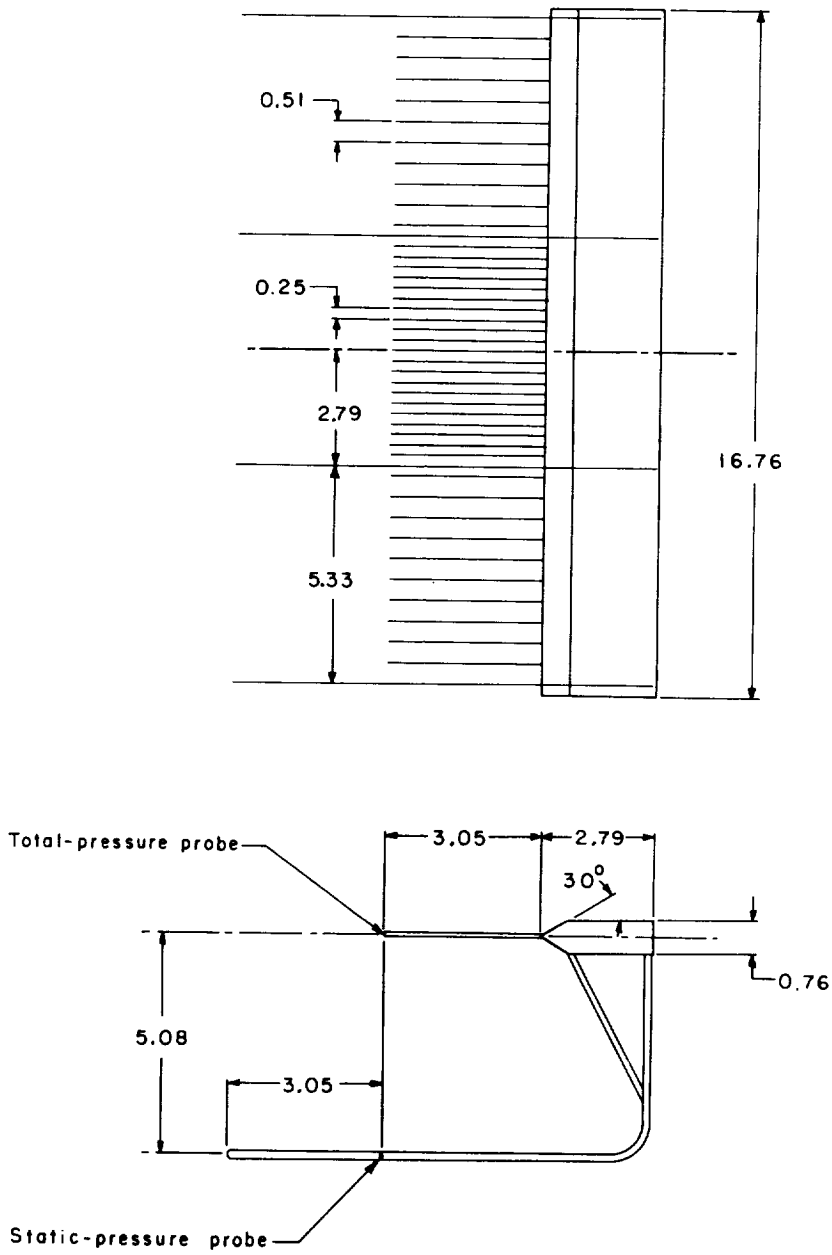

Figure 8.- Drawing of wake rake used in investigation of NASA GA(PC)-1 wing. (All dimensions are in centimeters.)

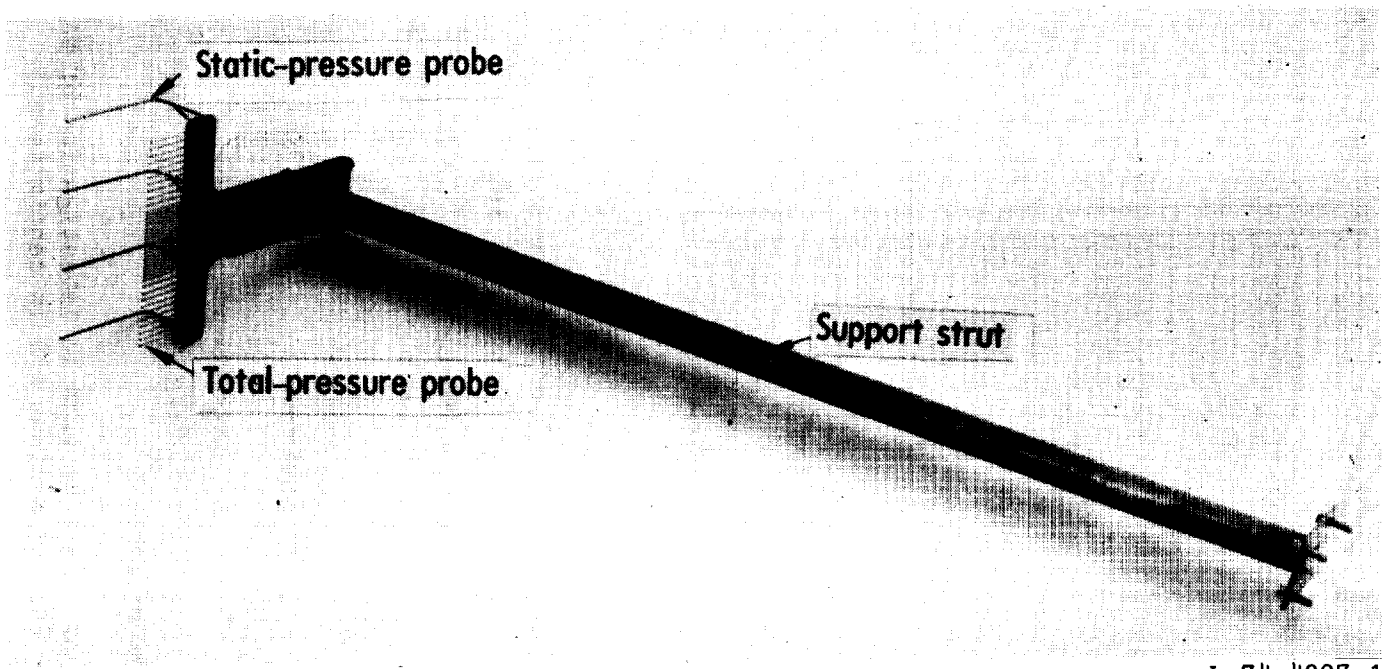

Figure 9.- Photograph of wake rake used in investigation of NASA GA(PC)-1 wing.

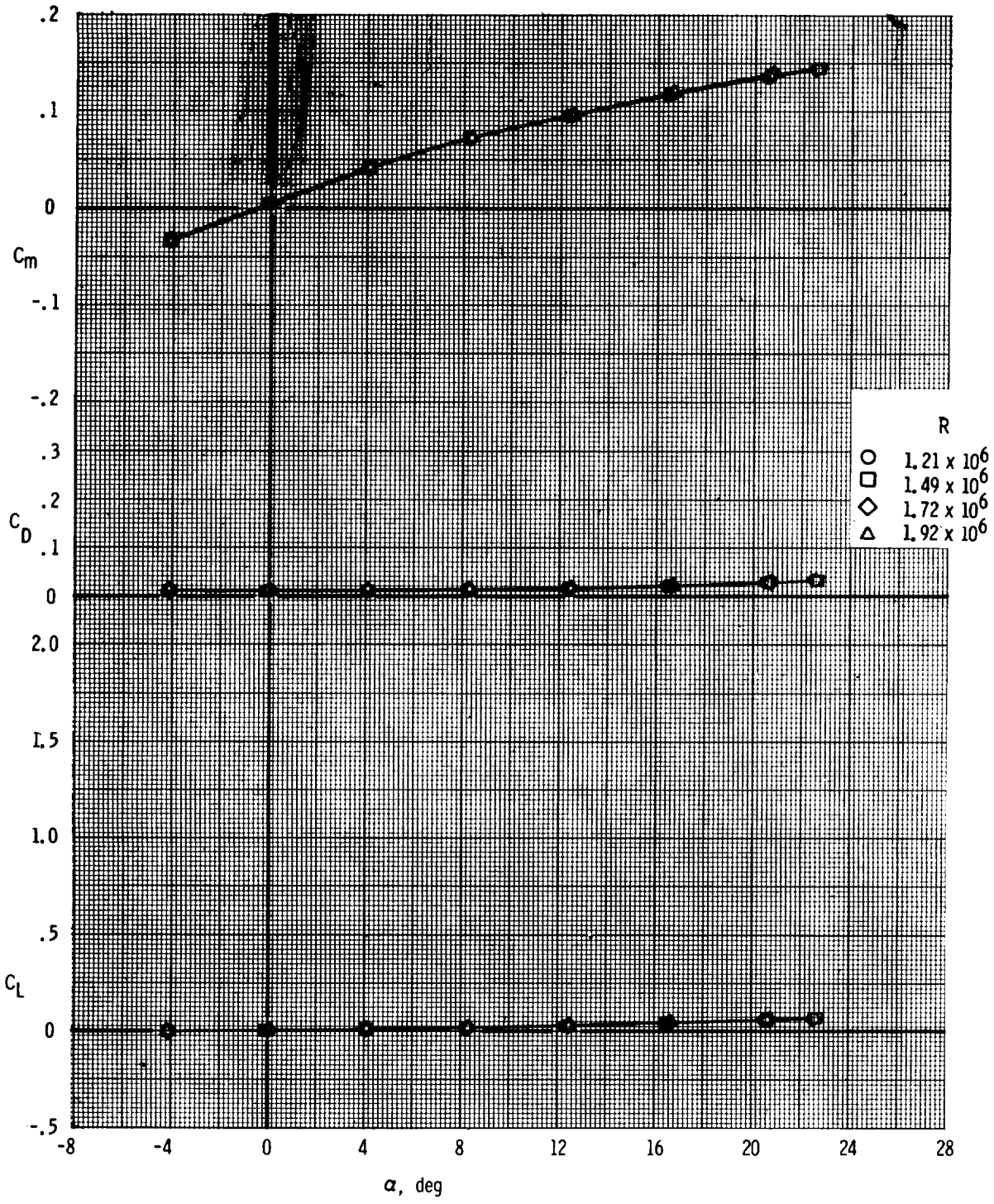

Figure 10.- Effect of Reynolds number on longitudinal aerodynamic characteristics of fuselage used in investigation.

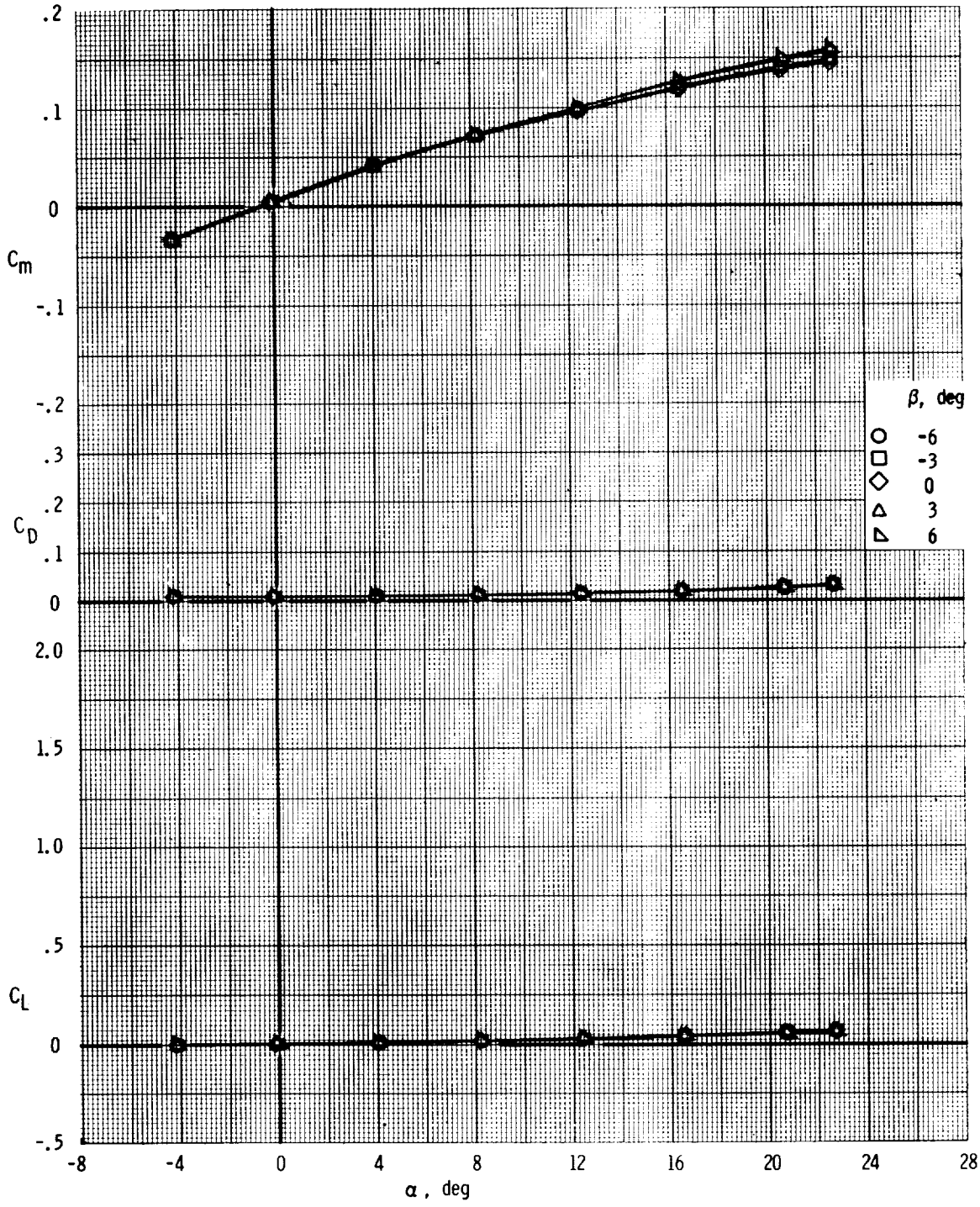

Figure 11.- Aerodynamic characteristics of fuselage used in investigation. ($R = 1.49 \times 10^6$.)

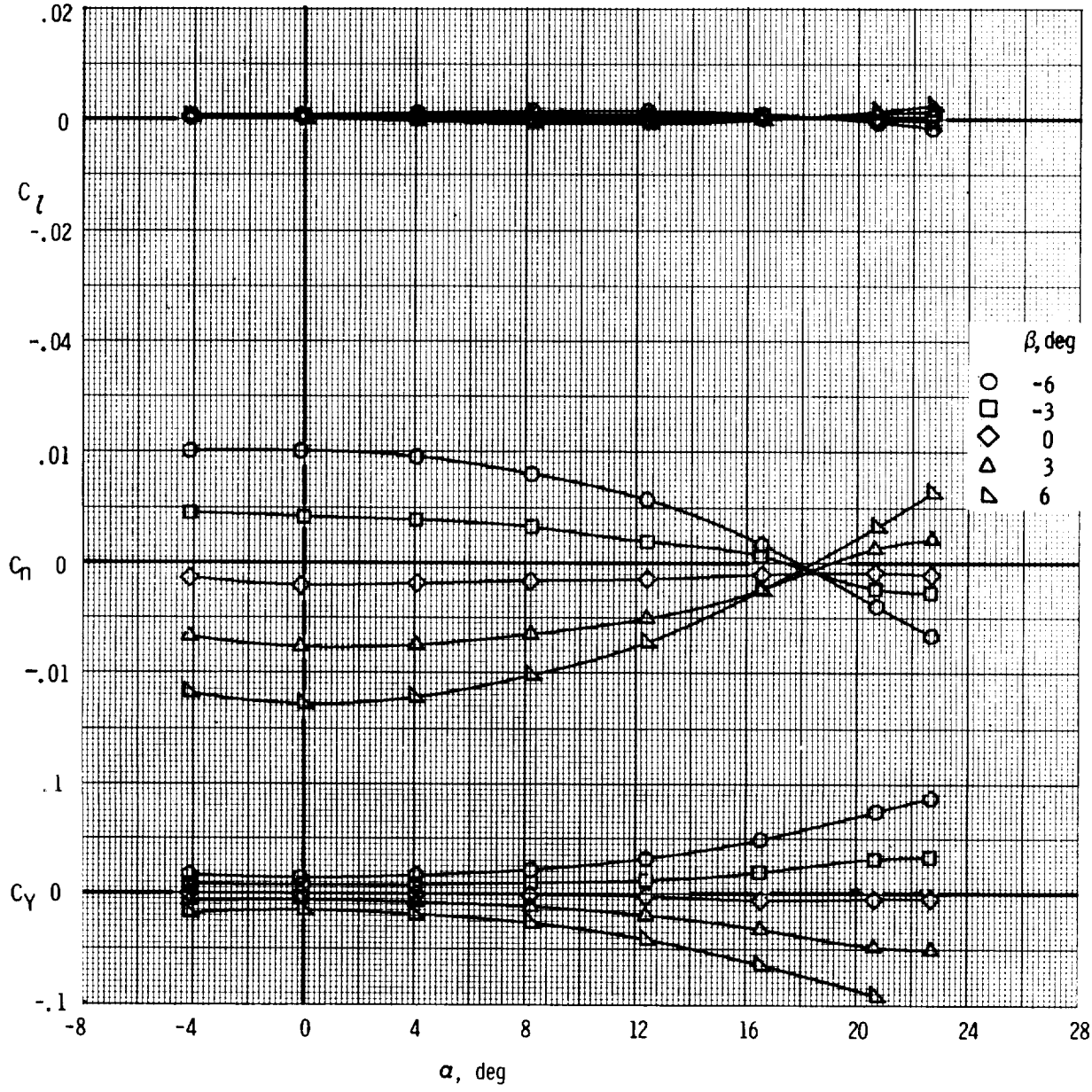

Figure 11.- Concluded.

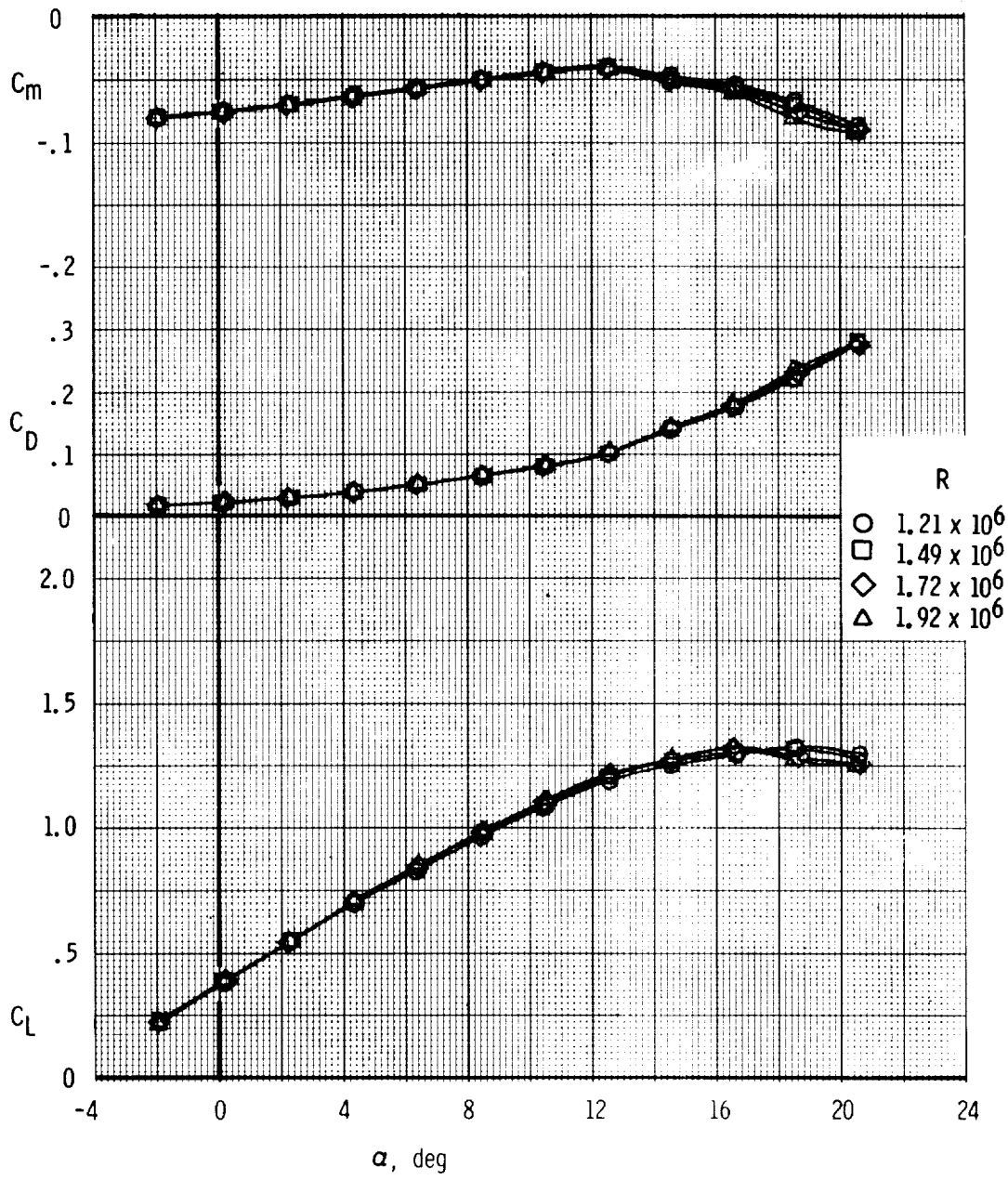

Figure 12.- Effect of Reynolds number on longitudinal aerodynamic characteristics of NASA GA(W)-1 wing alone.

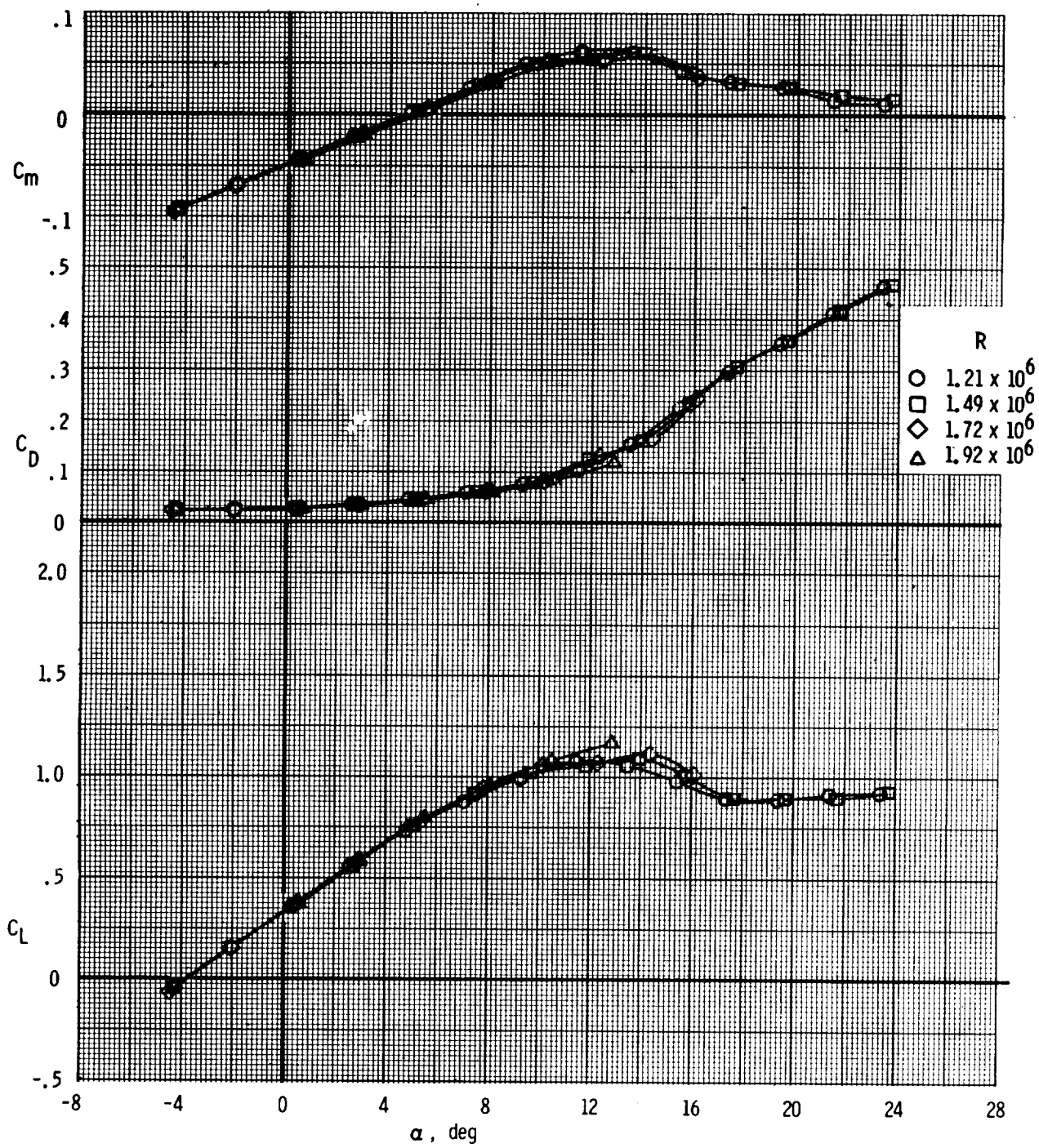

Figure 13.- Effect of Reynolds number on longitudinal aerodynamic characteristics of NACA 65_2-415 wing.

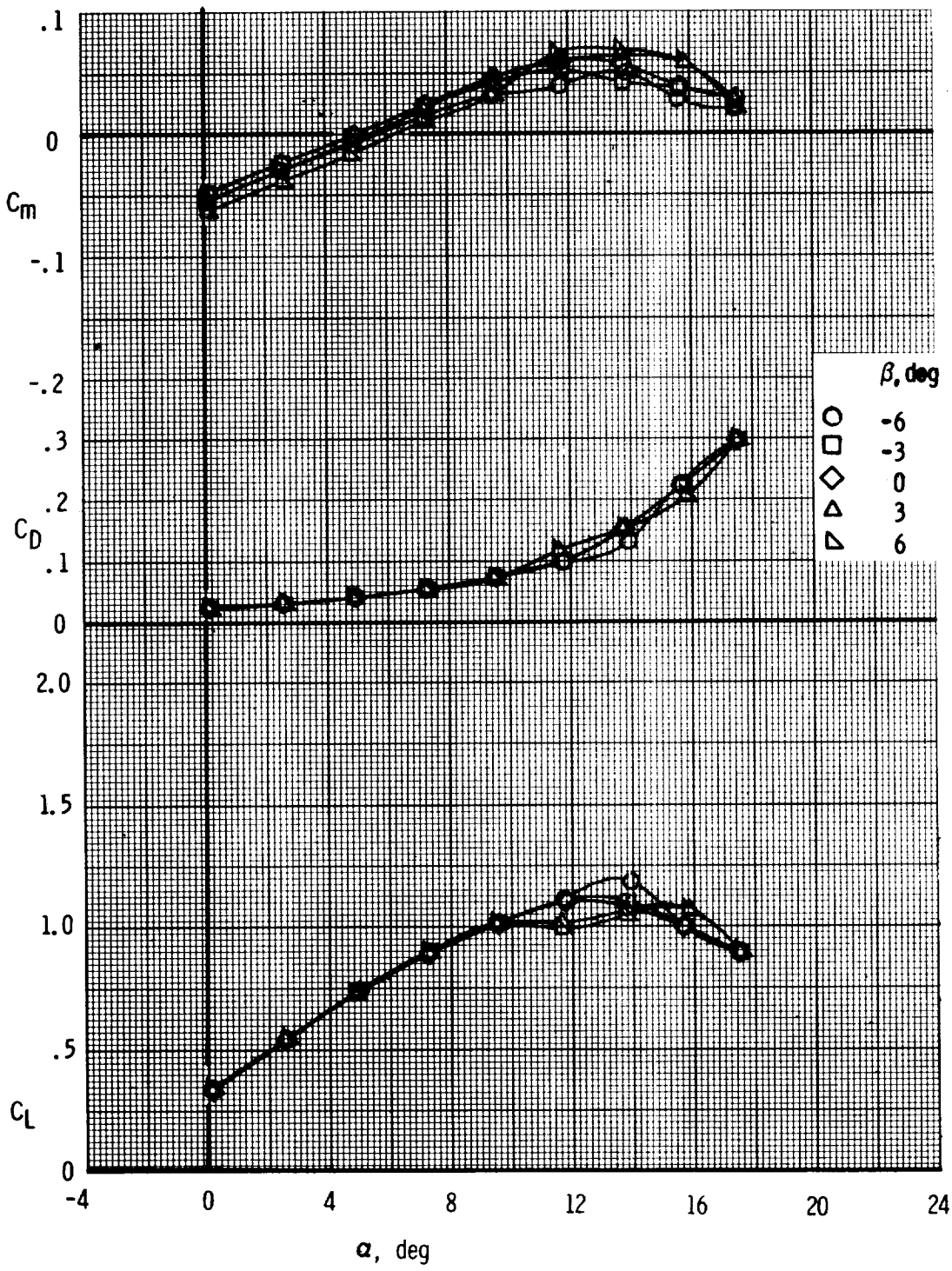

Figure 14.- Aerodynamic characteristics of NACA 65_2-415 wing. ($R = 1.49 \times 10^6$.)

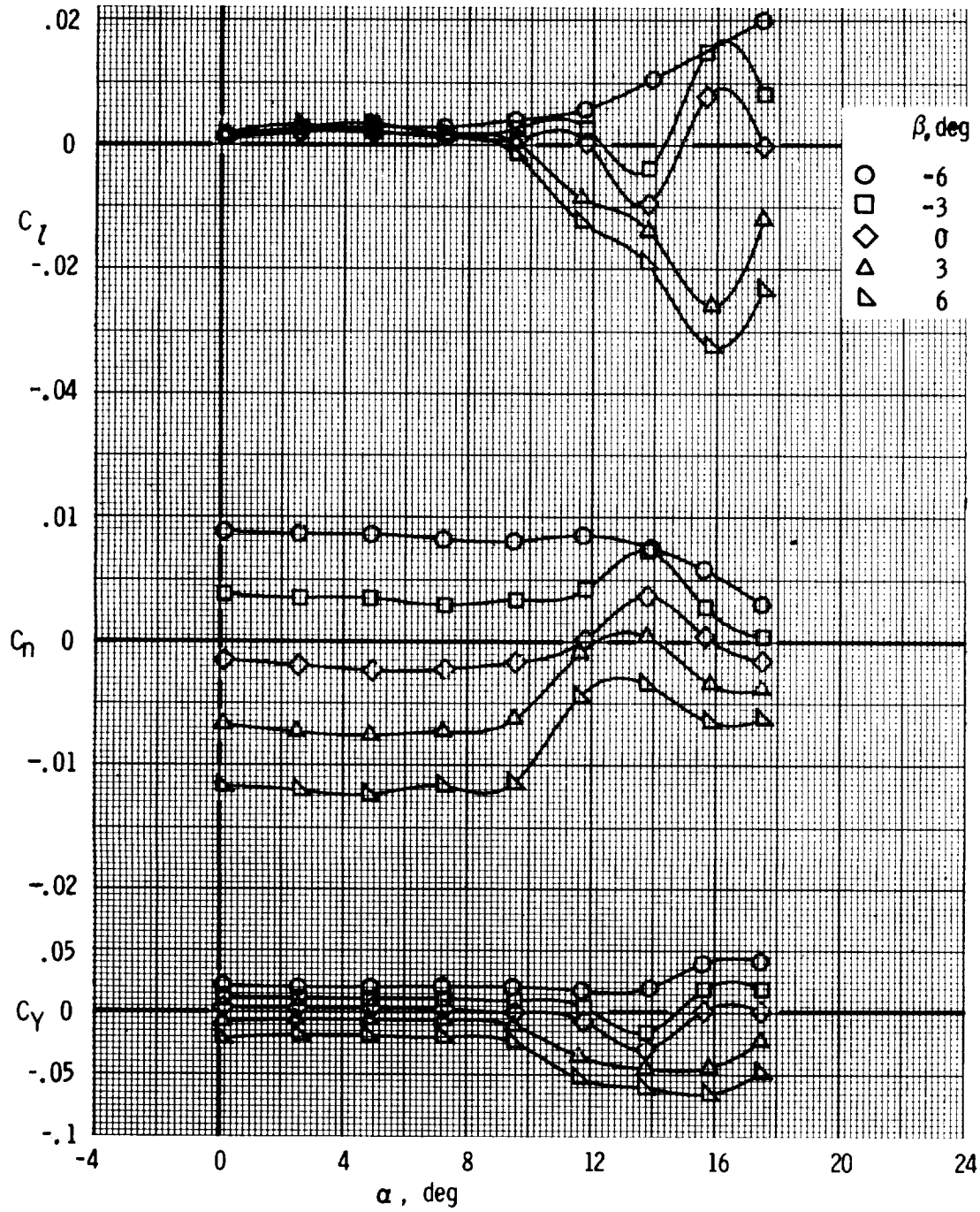

Figure 14.- Concluded.

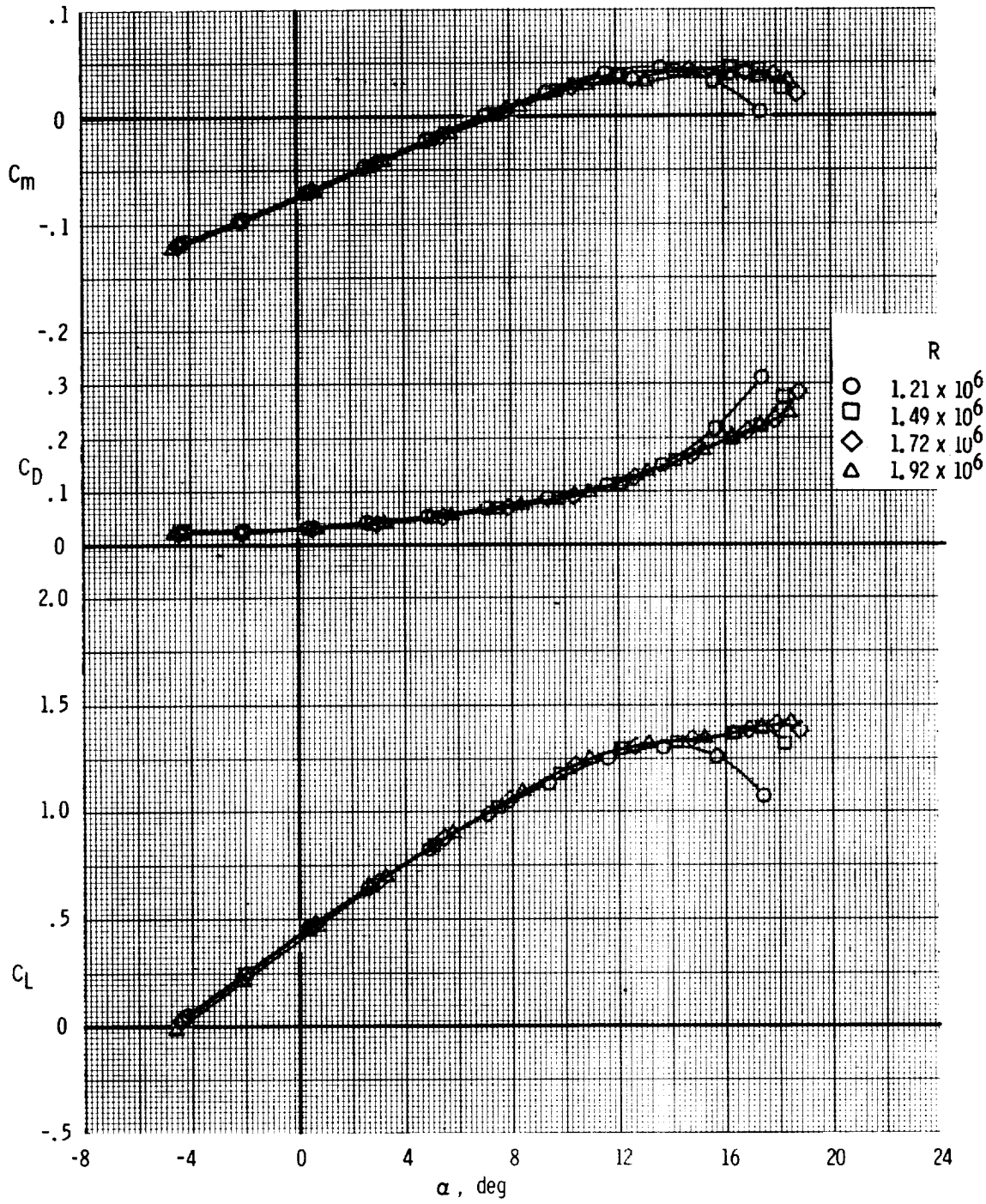

Figure 15.- Effect of Reynolds number on longitudinal aerodynamic characteristics of NASA GA(W)-1 wing.

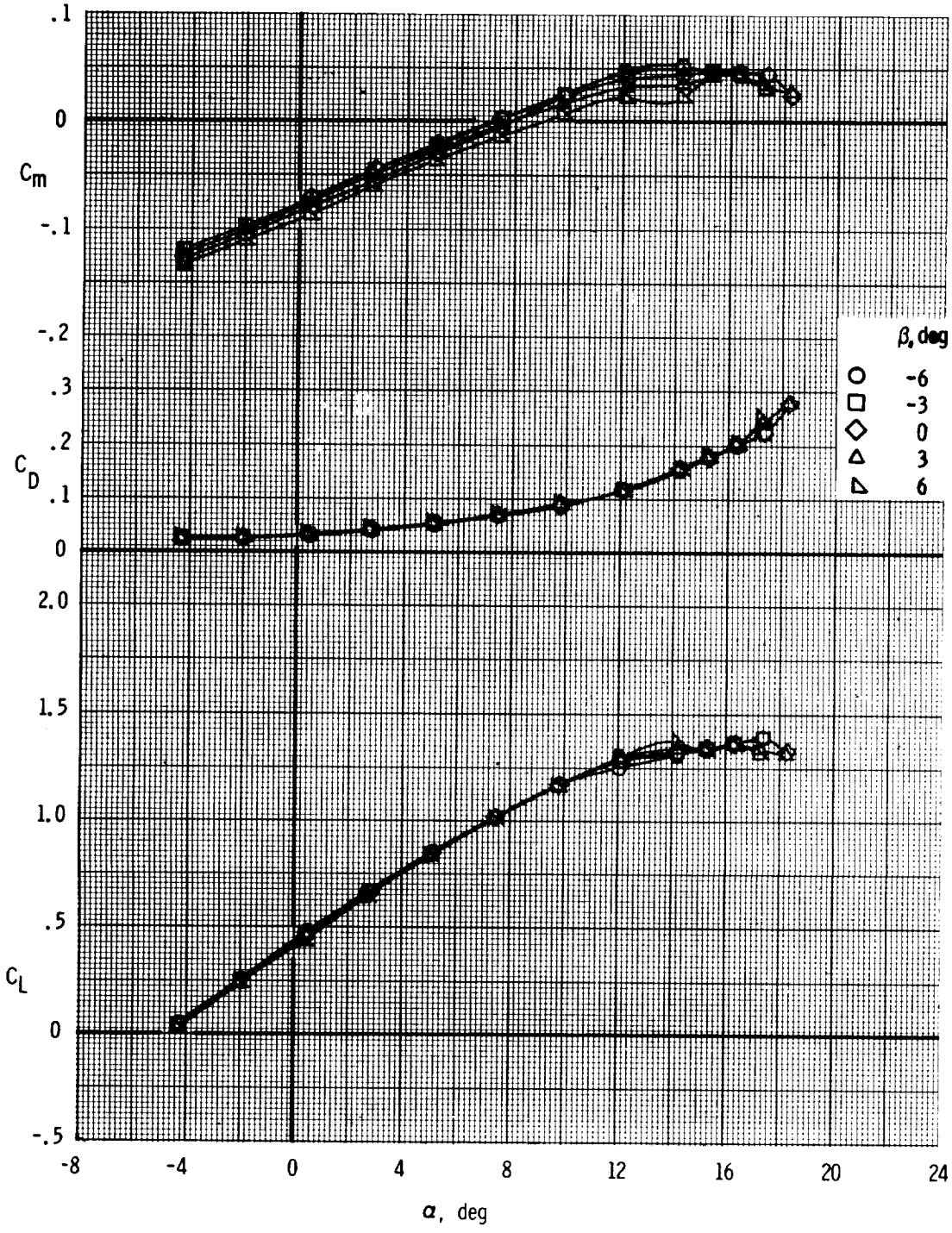

Figure 16.- Aerodynamic characteristics of NASA GA(W)-1 wing.
($R = 1.49 \times 10^6$.)

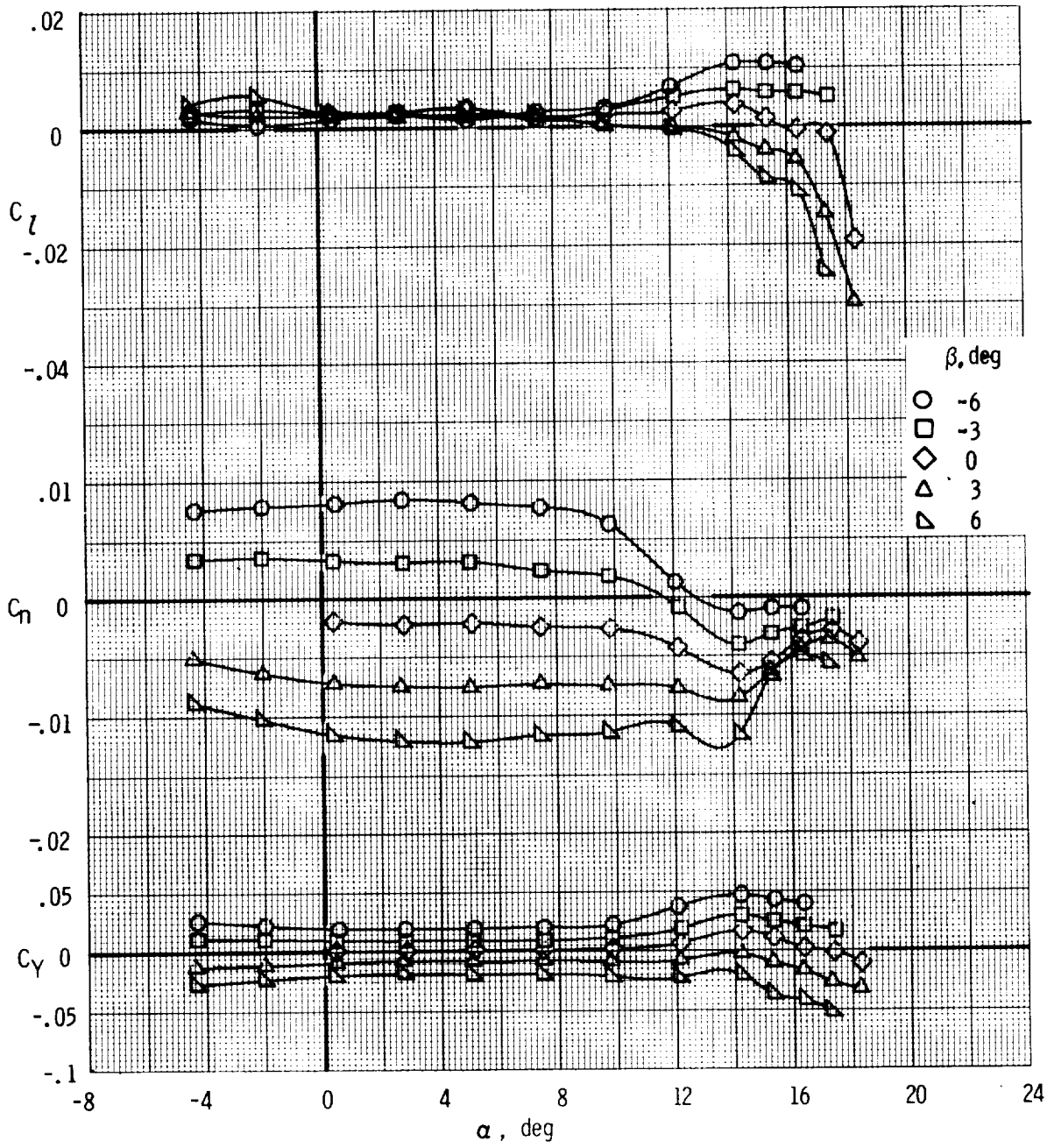

Figure 16.- Concluded.

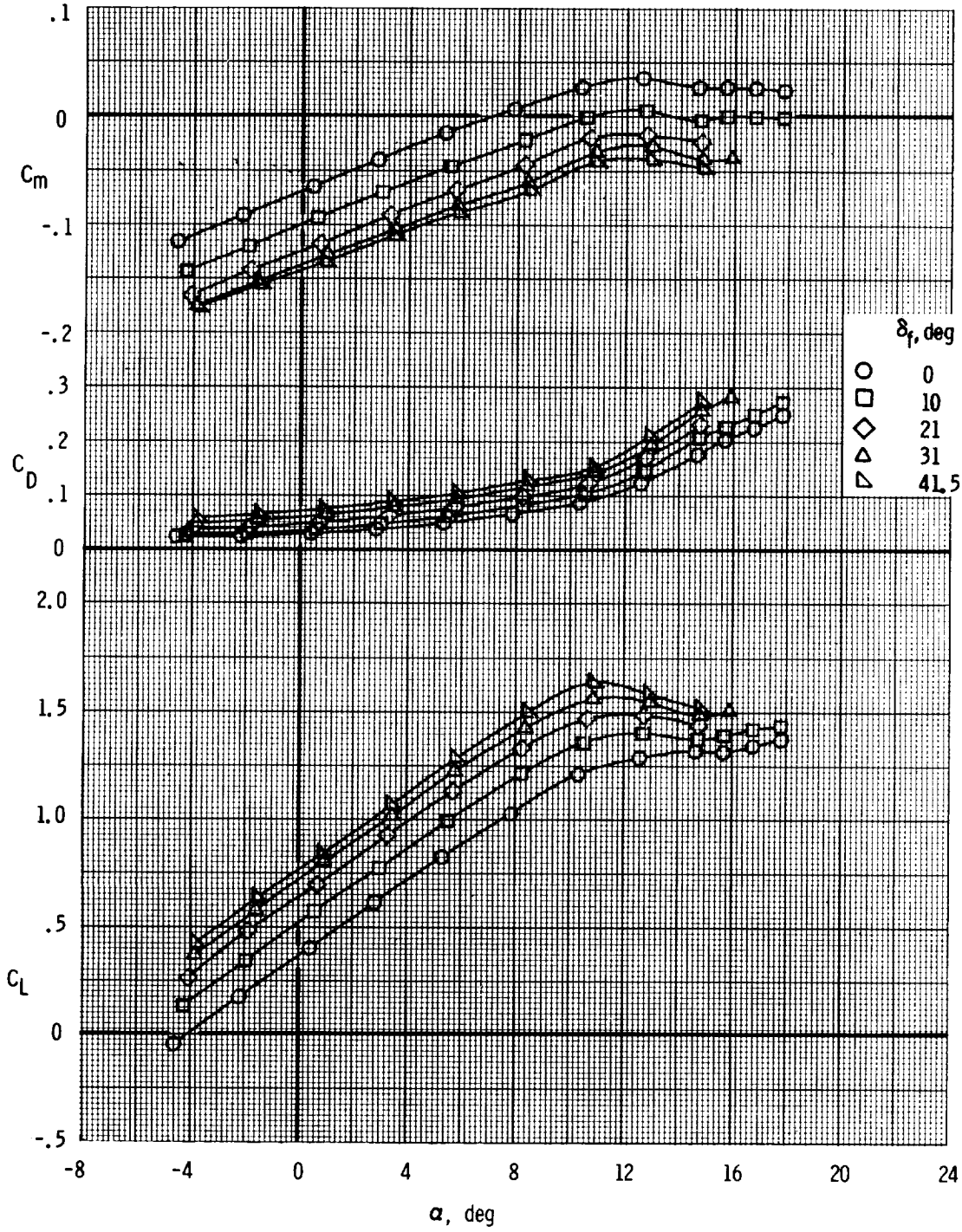

Figure 17.- Effect of deflection of inboard plain flap on longitudinal aerodynamic characteristics of NASA GA(W)-1 wing. ($R = 1.72 \times 10^6$.)

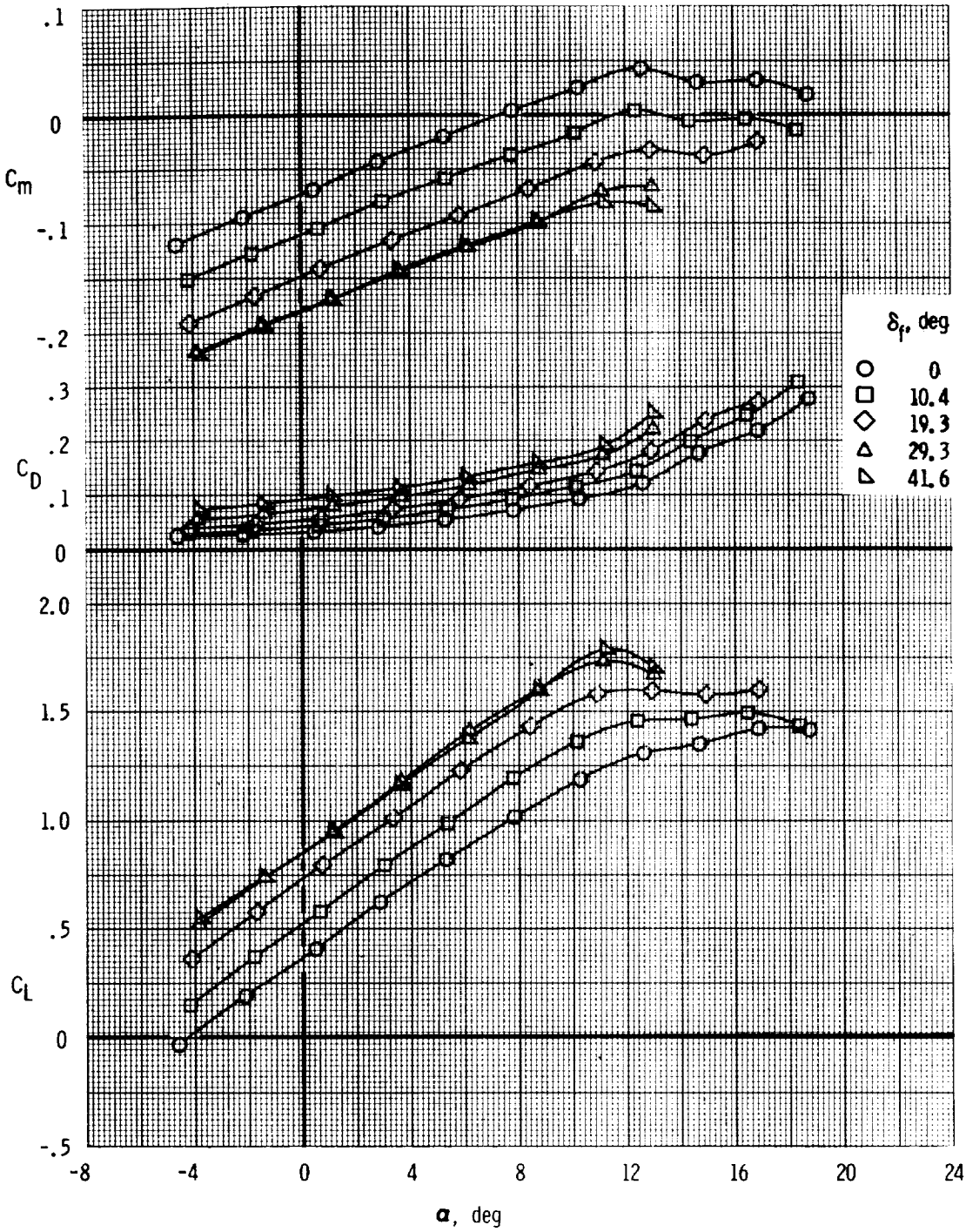

(a) Partial-span slotted flap.

Figure 18.- Effect of deflection of partial- and full-span slotted flap on longitudinal aerodynamic characteristics of NASA GA(W)-1 wing. ($R = 1.72 \times 10^6$.)

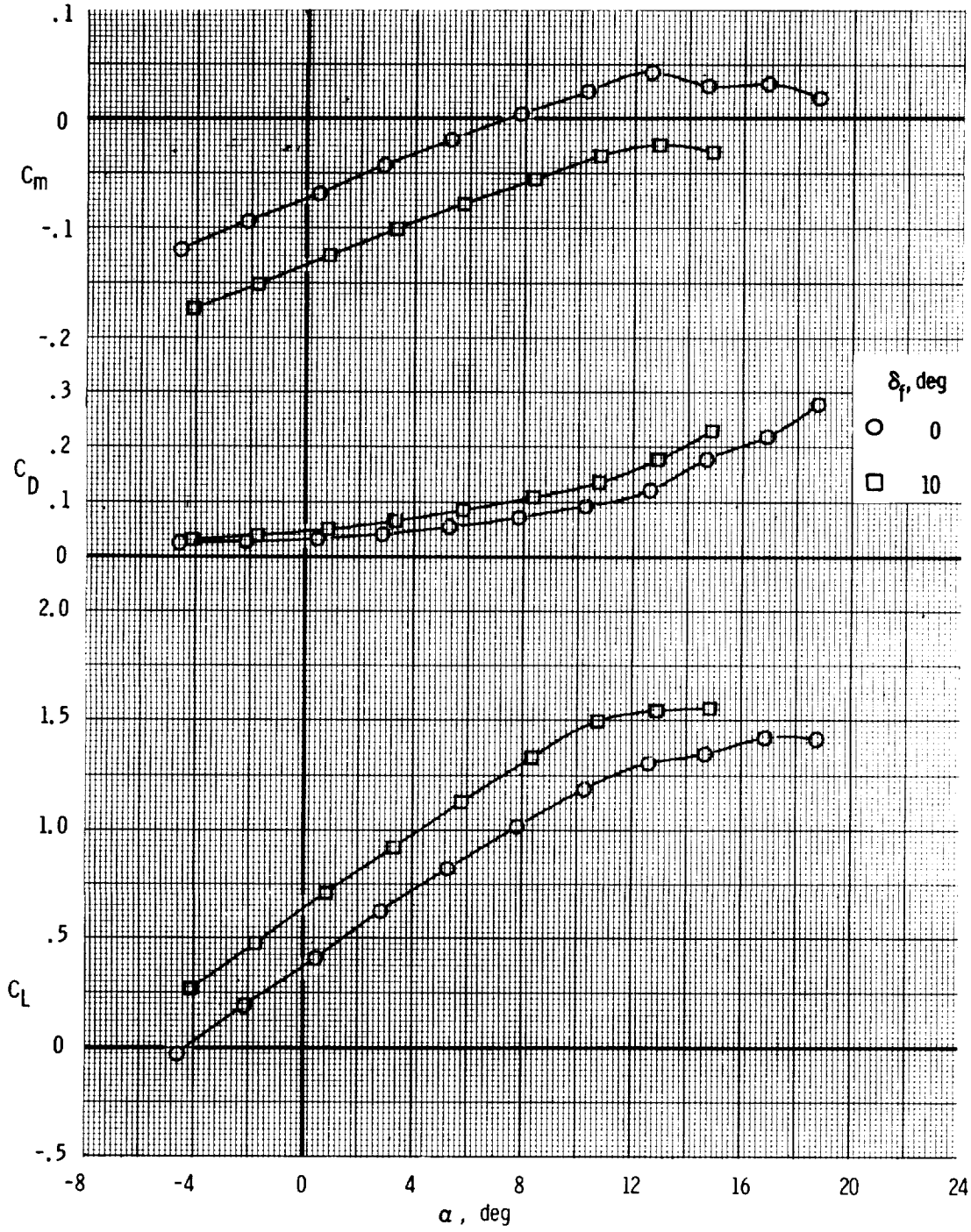

(b) Full-span slotted flap.

Figure 18.- Concluded.

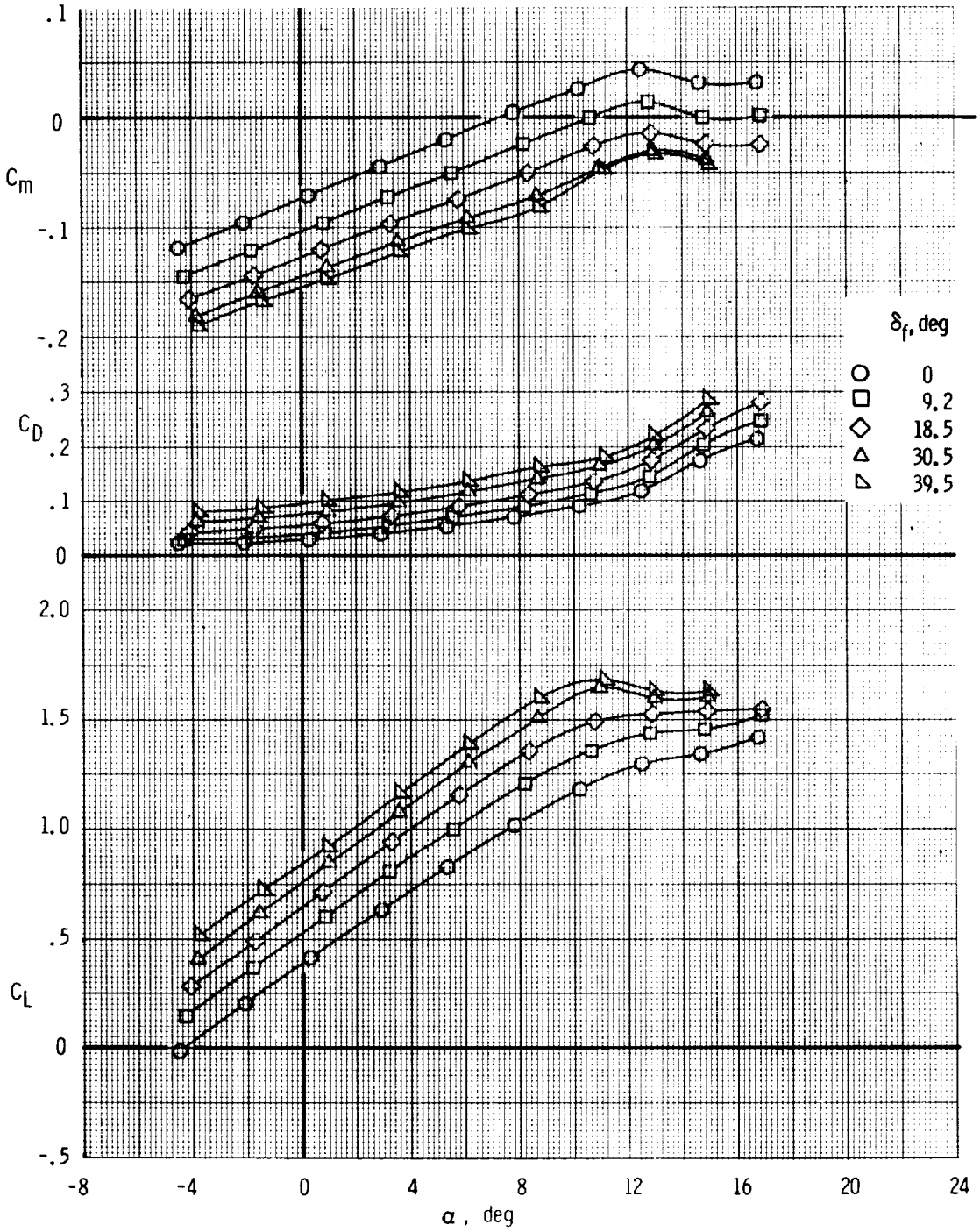

(a) Partial-span split flap.

Figure 19.- Effect of deflection of partial- and full-span split flap on longitudinal aerodynamic characteristics of NASA GA(W)-1 wing. ($R = 1.72 \times 10^6$.)

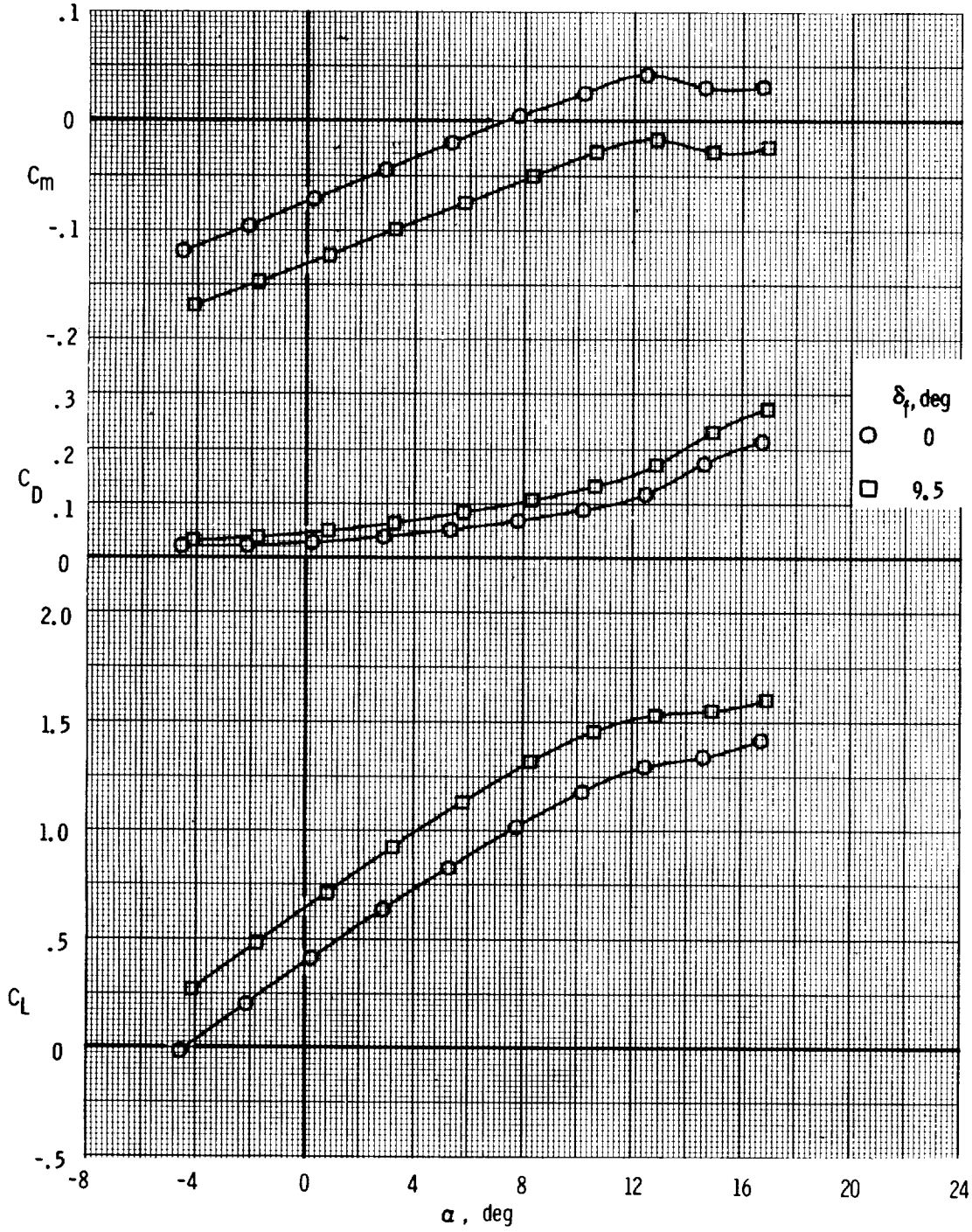

(b) Full-span split flap.

Figure 19.- Concluded.

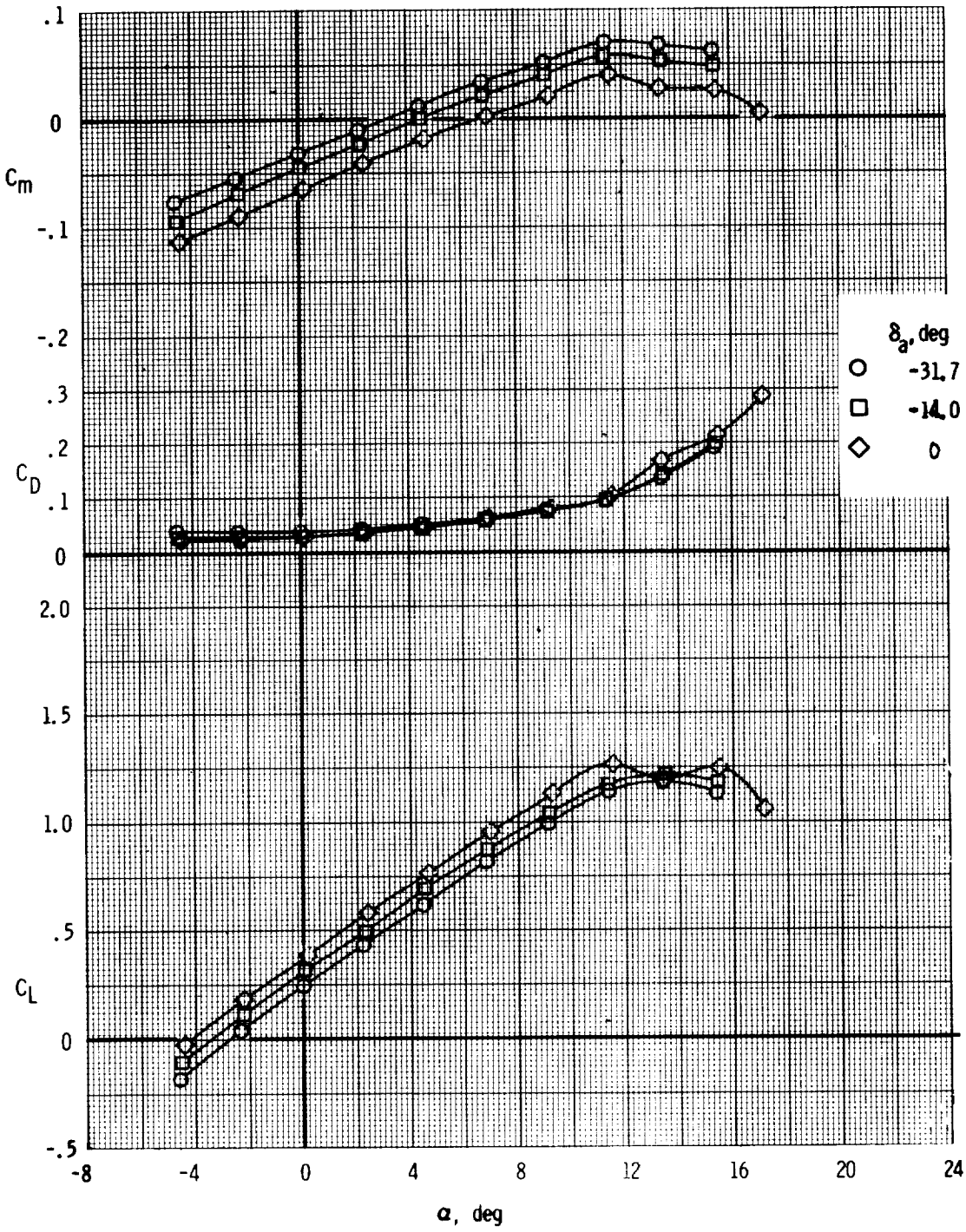

(a) Longitudinal characteristics for up deflections of left aileron.

Figure 20.- Effect of deflections of plain aileron on longitudinal and lateral aerodynamic characteristics and hinge-moment characteristics of NASA GA(W)-1 wing. ($R = 1.21 \times 10^6$.)

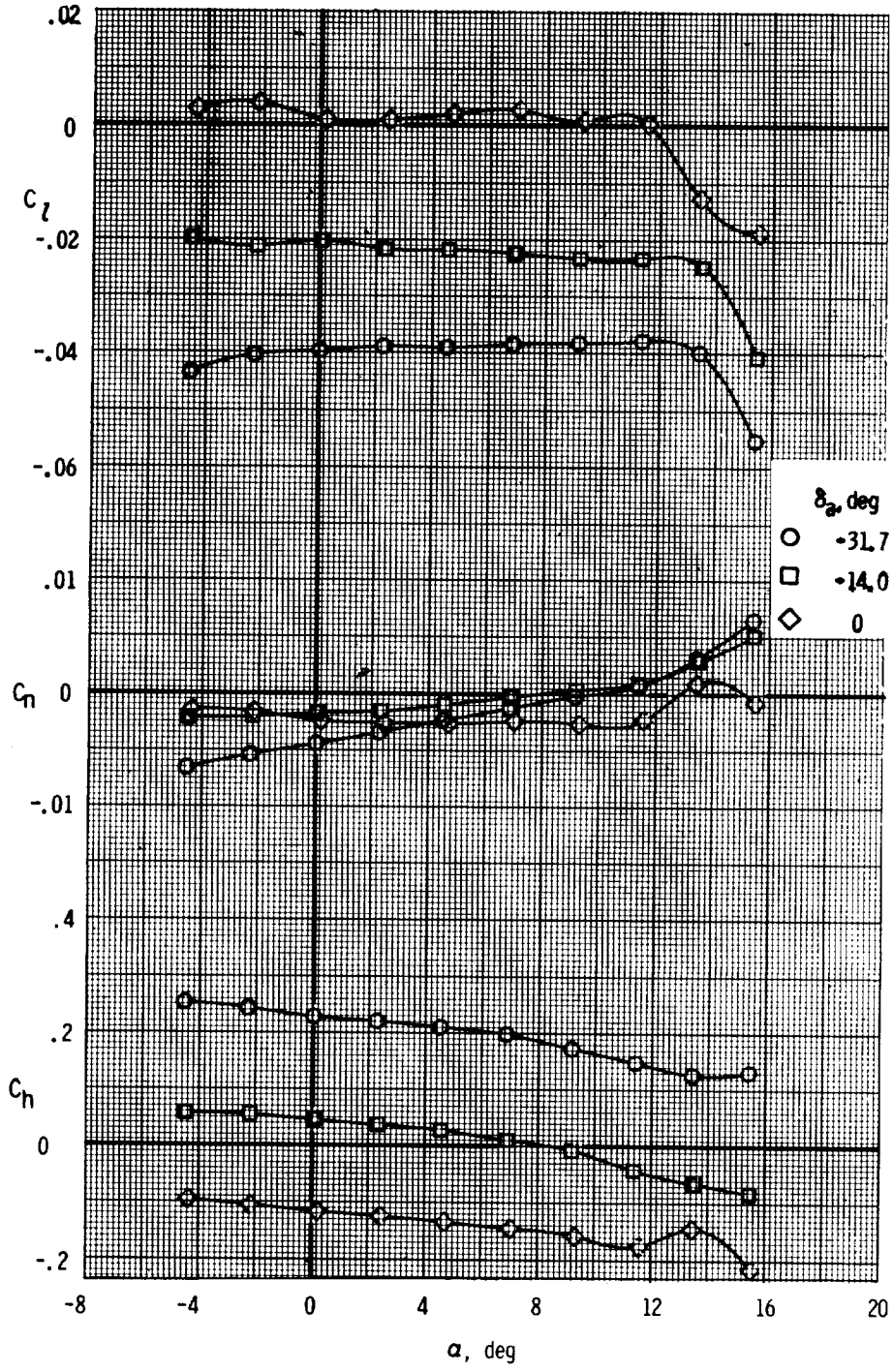

(b) Lateral and hinge-moment characteristics for up deflections of left aileron.

Figure 20.- Continued.

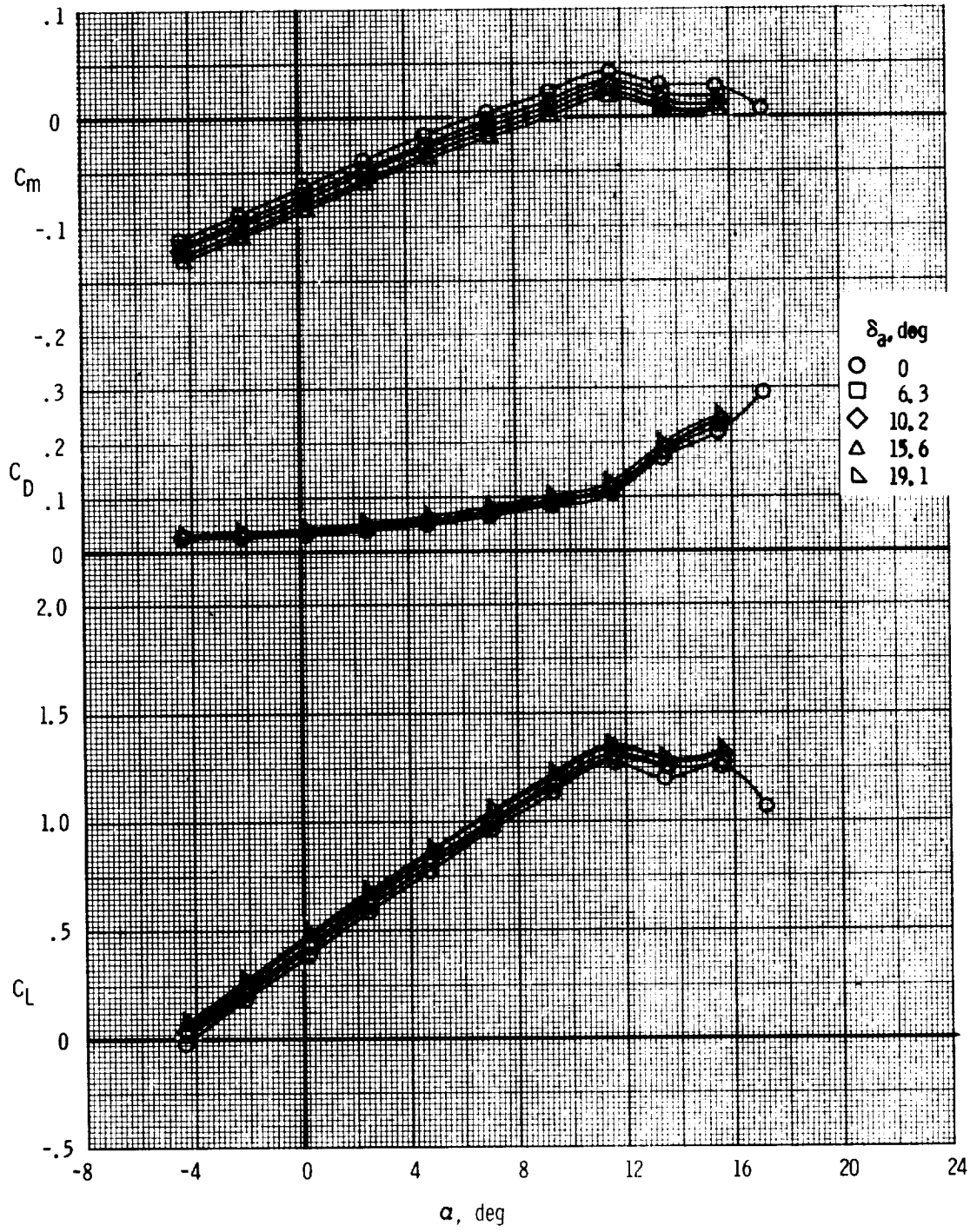

(c) Longitudinal characteristics for down deflections of left aileron.

Figure 20.- Continued.

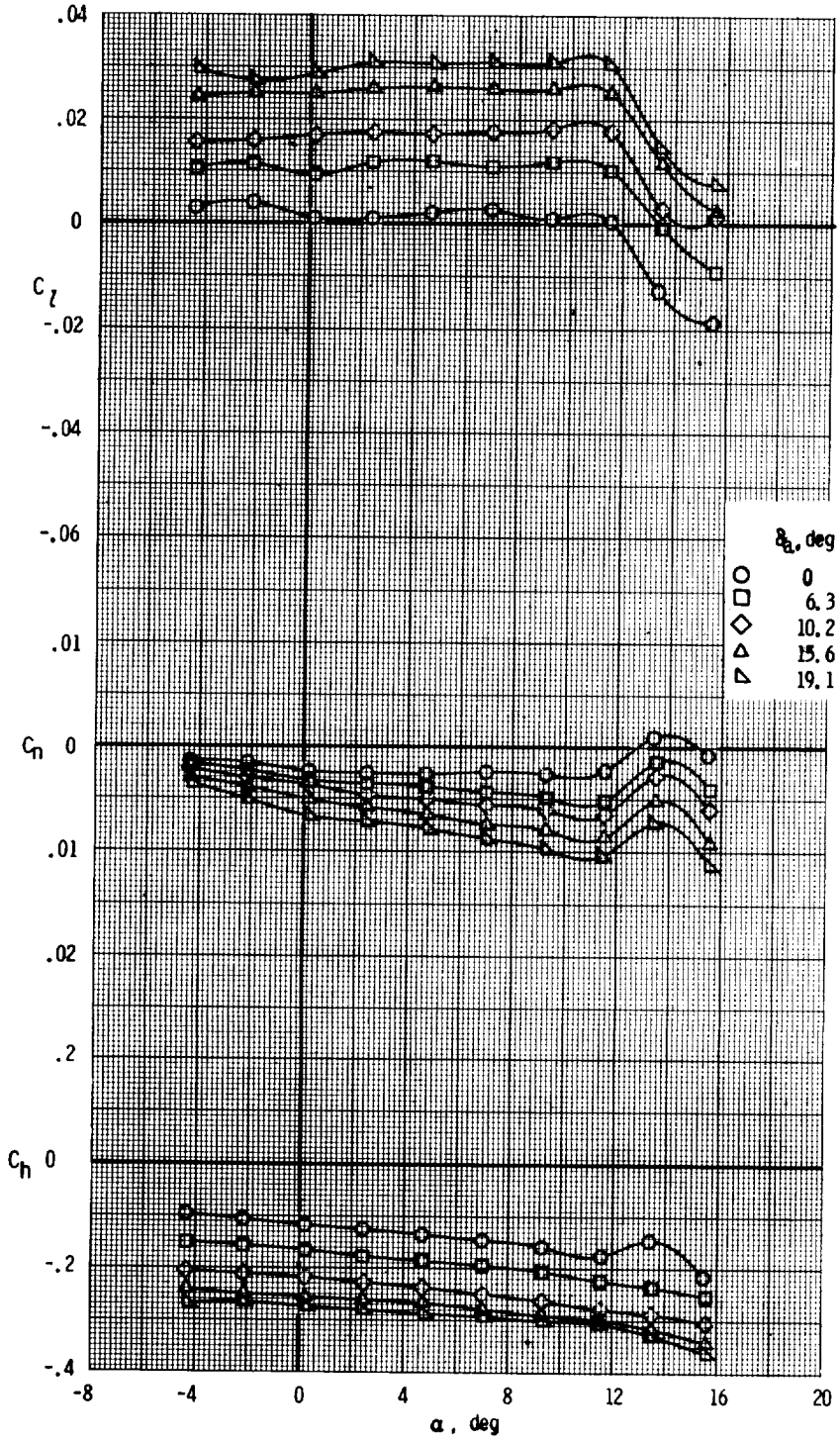

(d) Lateral and hinge-moment characteristics for down deflections of left aileron.

Figure 20.- Continued.

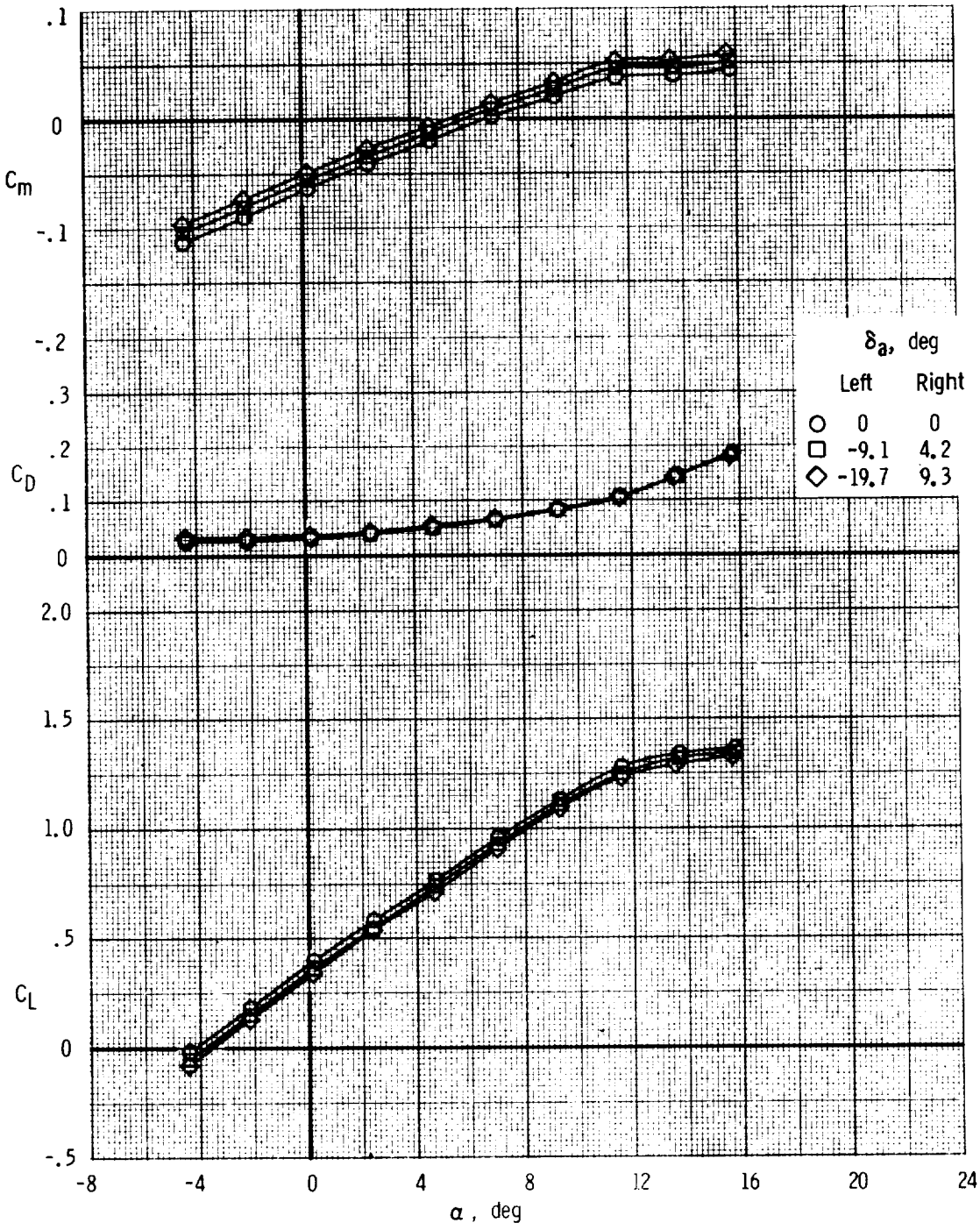

(e) Longitudinal characteristics for differential deflections of right and left ailerons.

Figure 20.- Continued.

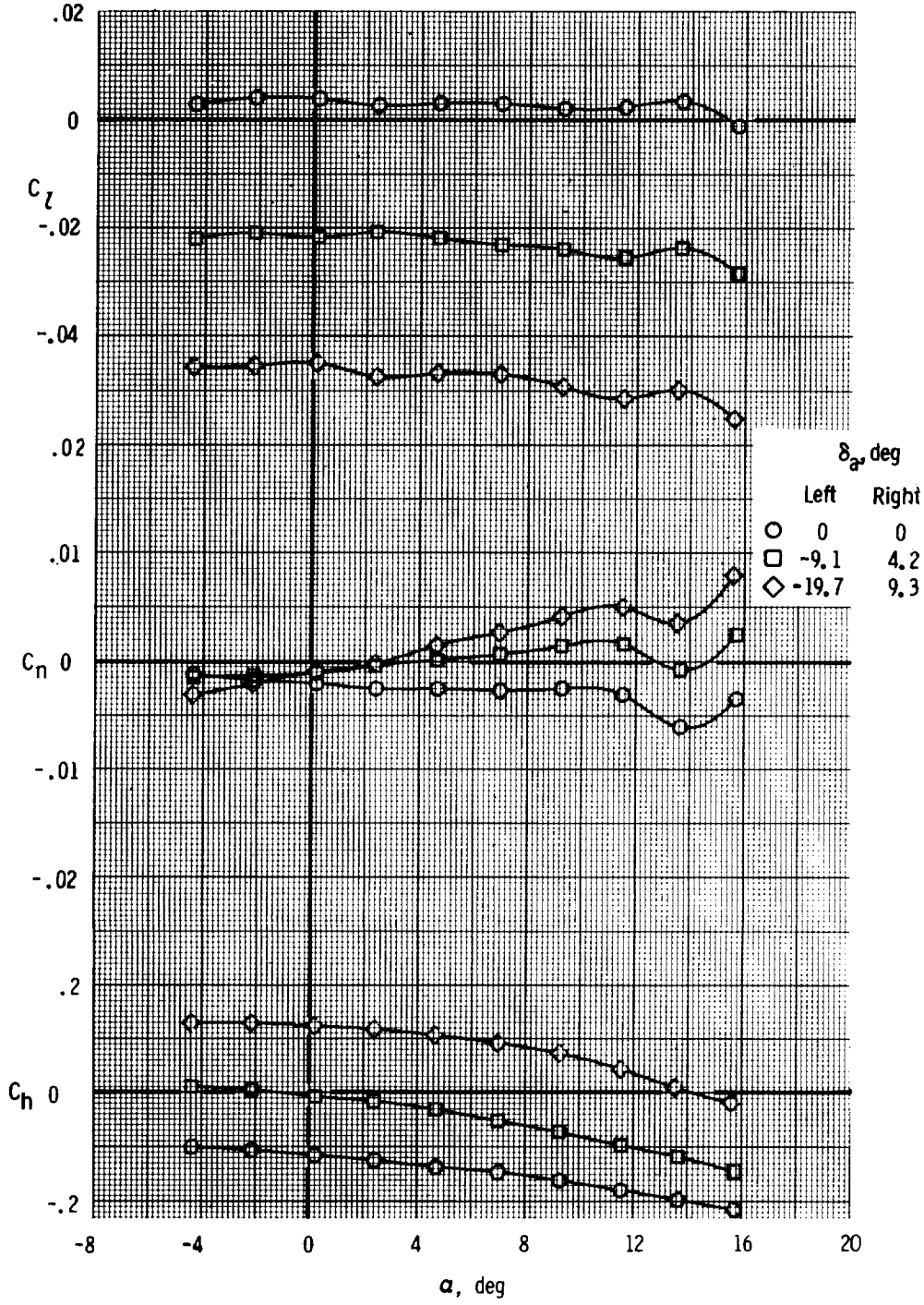

(f) Lateral and hinge-moment characteristics for differential deflections of right and left ailerons.

Figure 20.- Concluded.

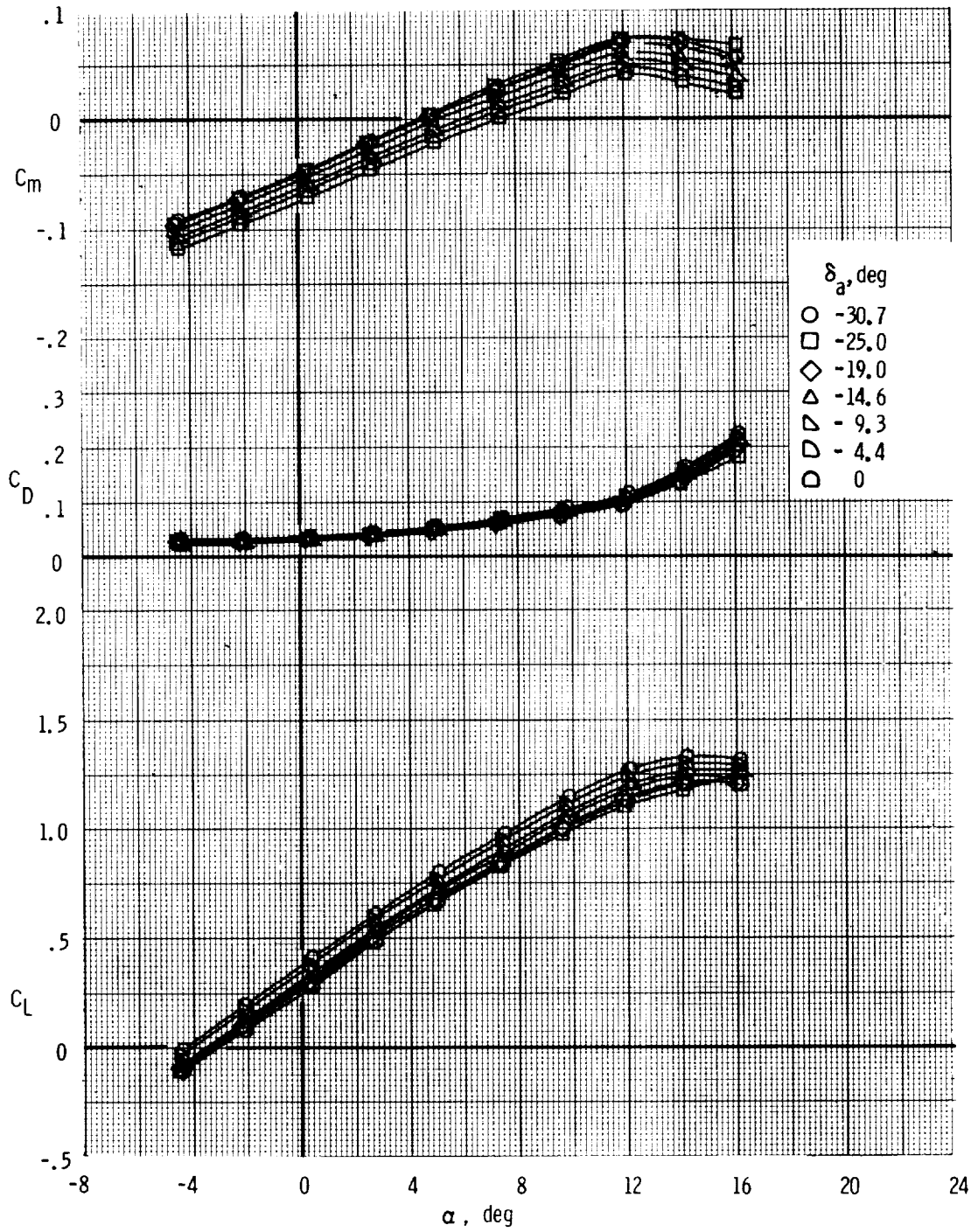

(a) Longitudinal characteristics for up deflections of left aileron.

Figure 21.- Effect of deflections of slotted ailerons on longitudinal and lateral aerodynamic characteristics and hinge-moment characteristics of NASA GA(W)-1 wing. ($R = 1.49 \times 10^6$.)

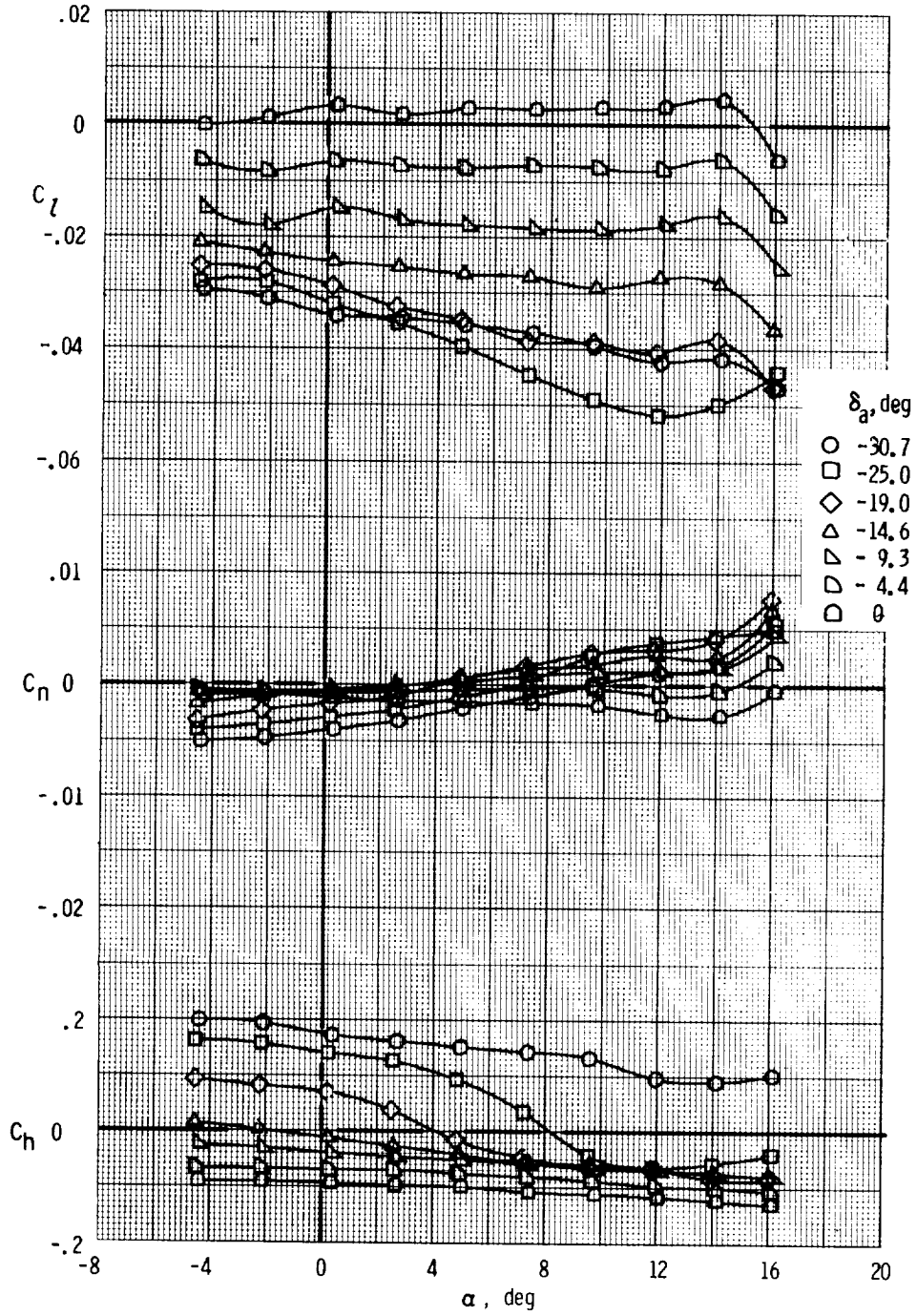

(b) Lateral and hinge-moment characteristics for up deflections of left aileron.

Figure 21.- Continued.

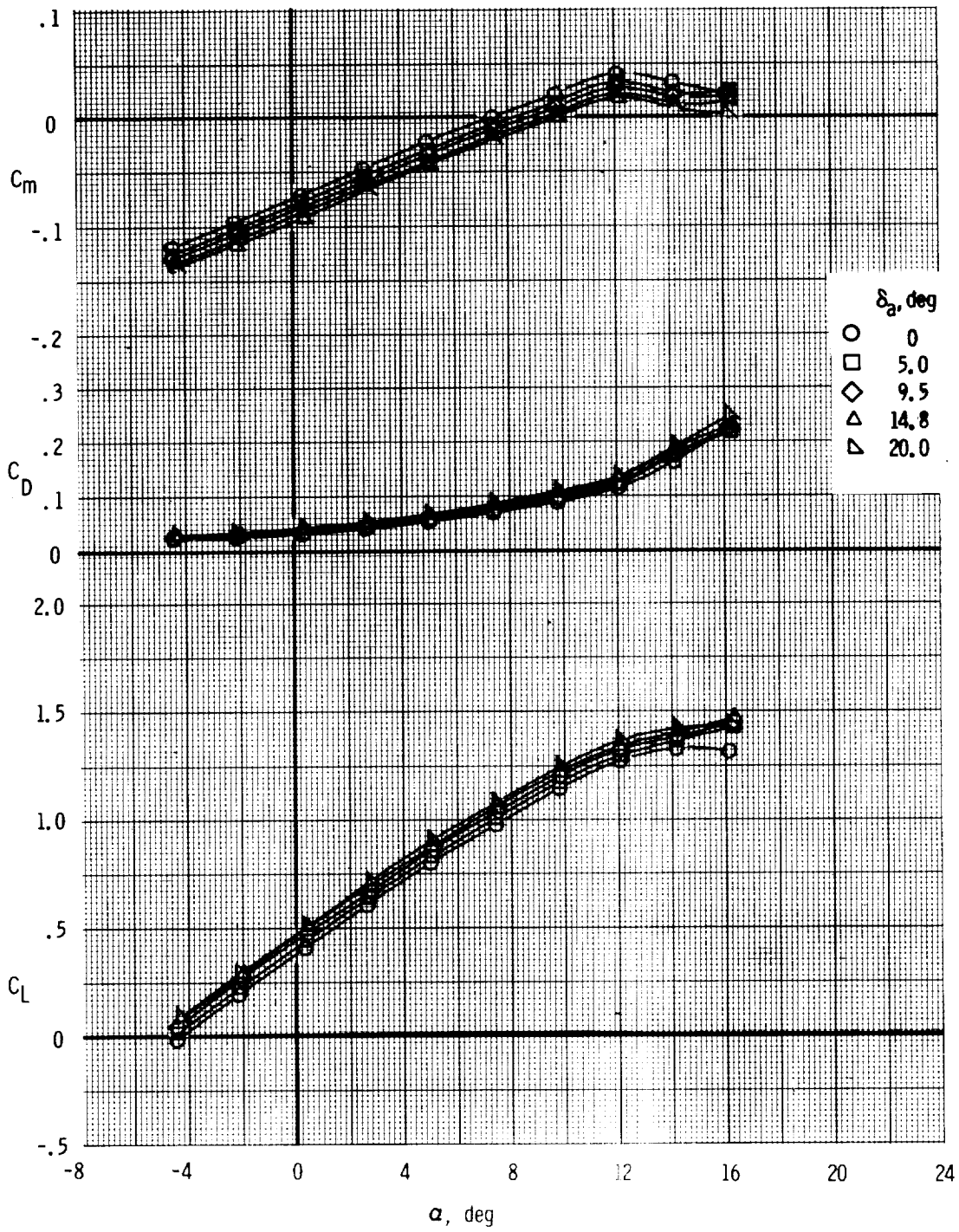

(c) Longitudinal characteristics for down deflections of left aileron.

Figure 21.- Continued.

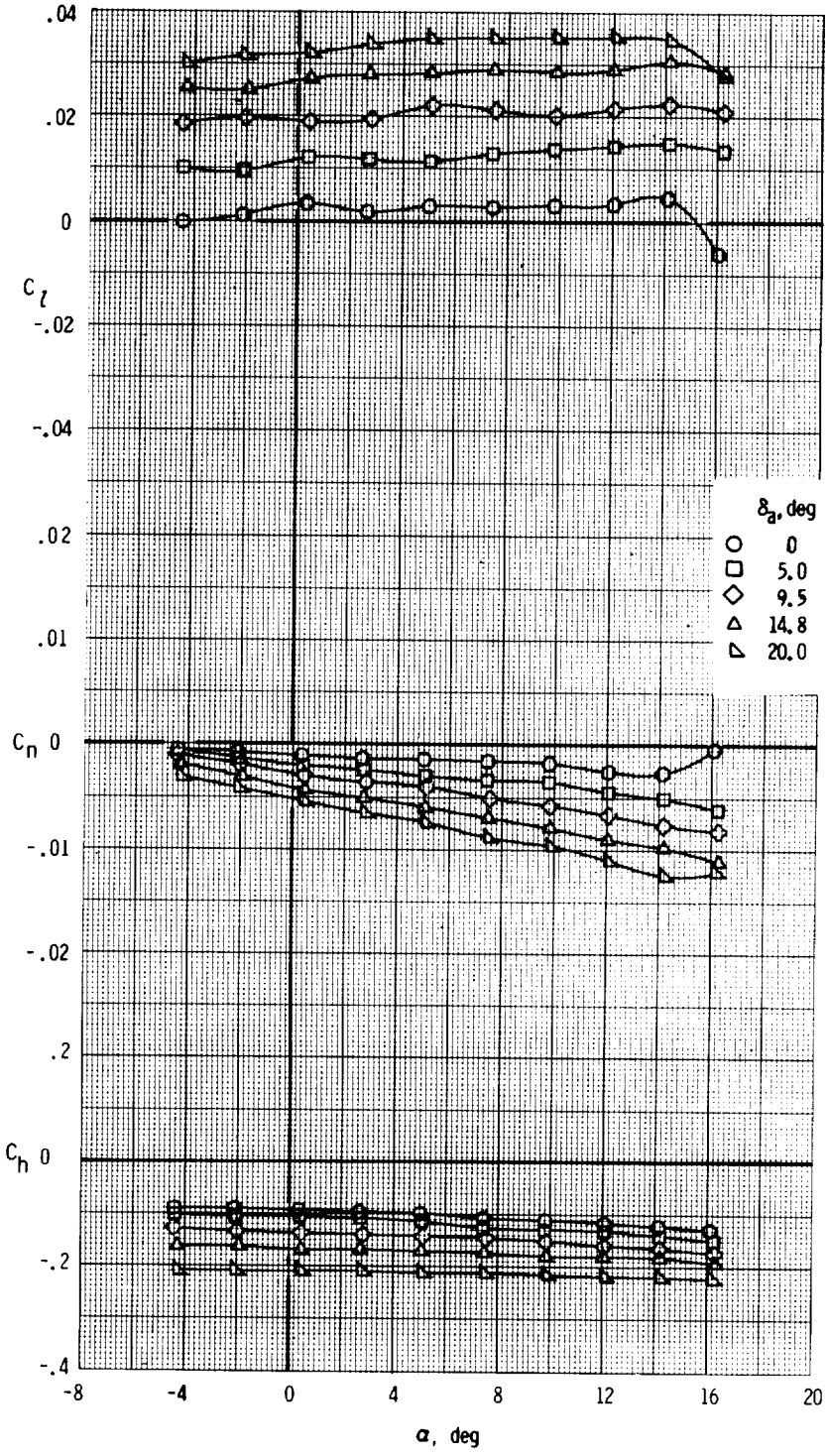

(d) Lateral and hinge-moment characteristics for differential deflections of right and left ailerons.

Figure 21.- Continued.

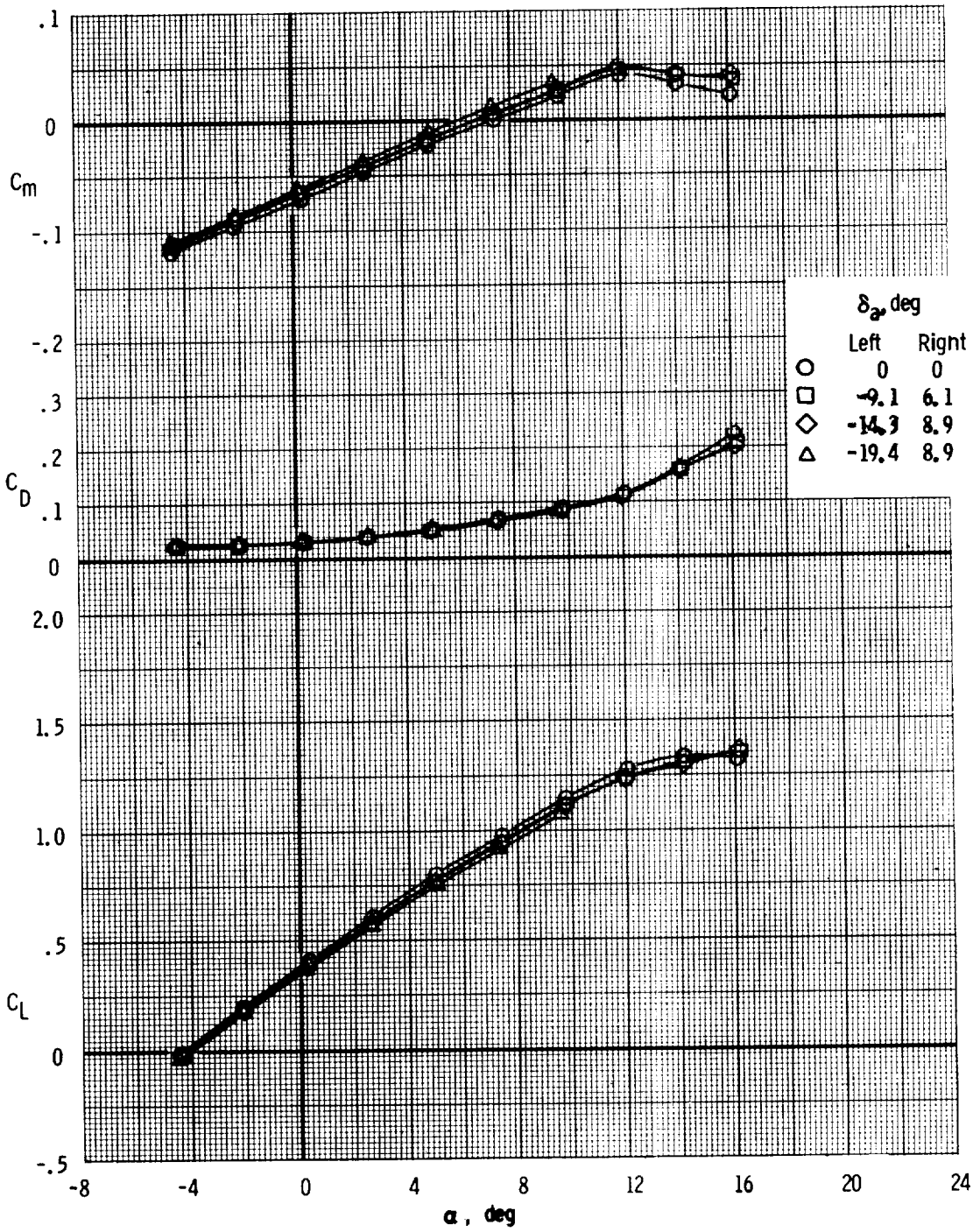

(e) Longitudinal characteristics for differential deflections of right and left ailerons.

Figure 21.- Continued.

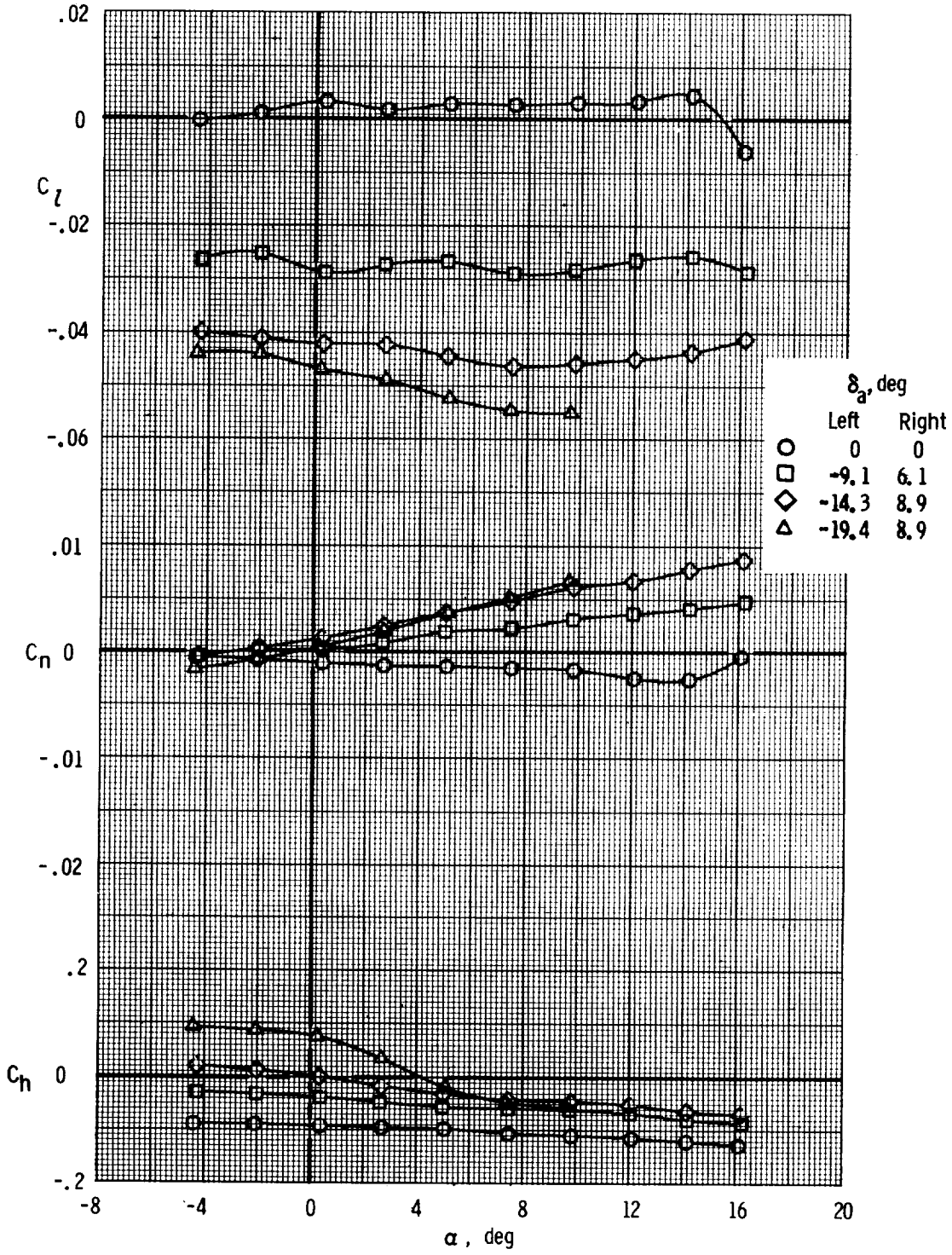

(f) Lateral and hinge-moment characteristics for differential deflections of right and left ailerons.

Figure 21.- Concluded.

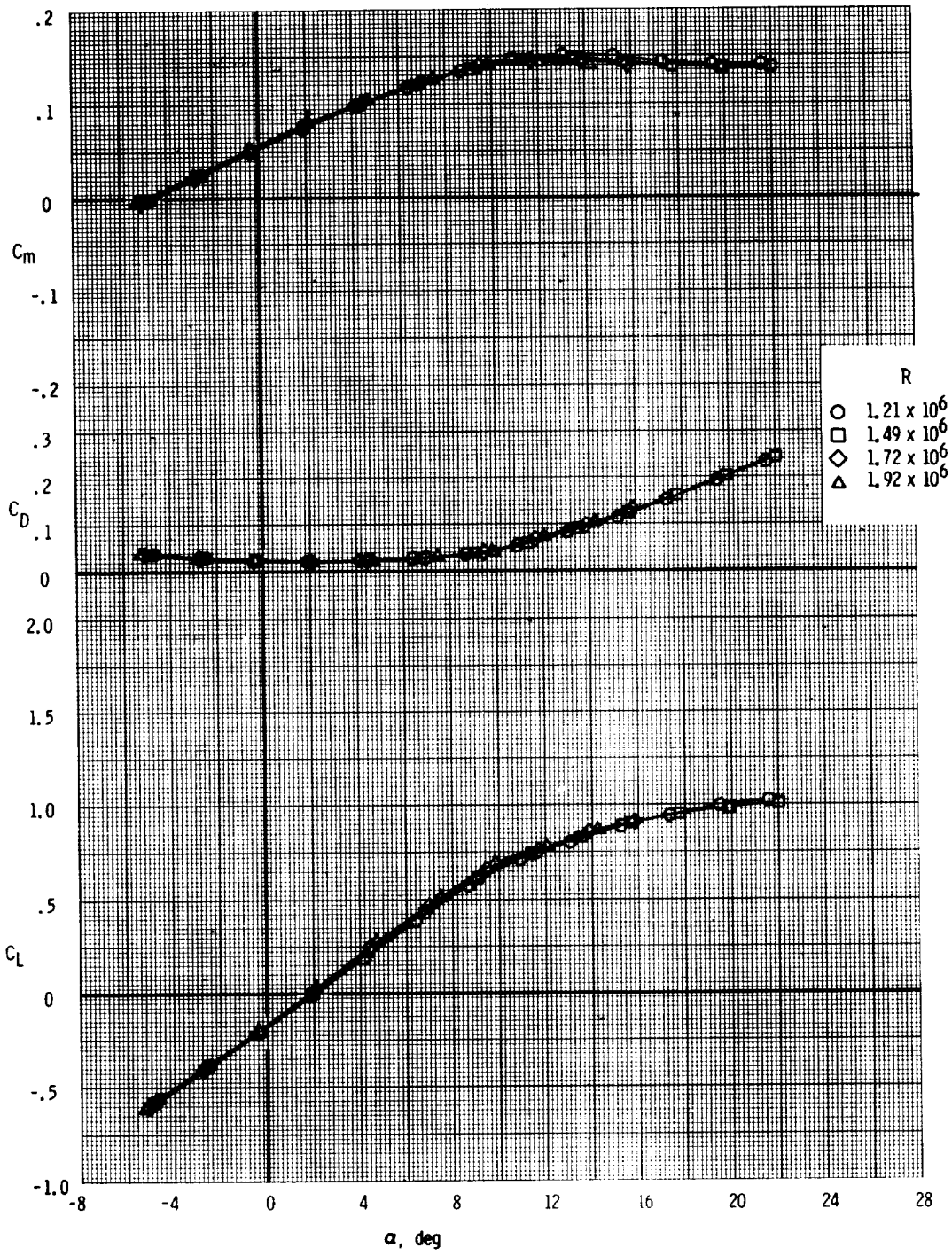

Figure 22.- Effect of Reynolds number on longitudinal aerodynamic characteristics of NASA GA(PC)-1 wing. $\delta_f = -10^o$.

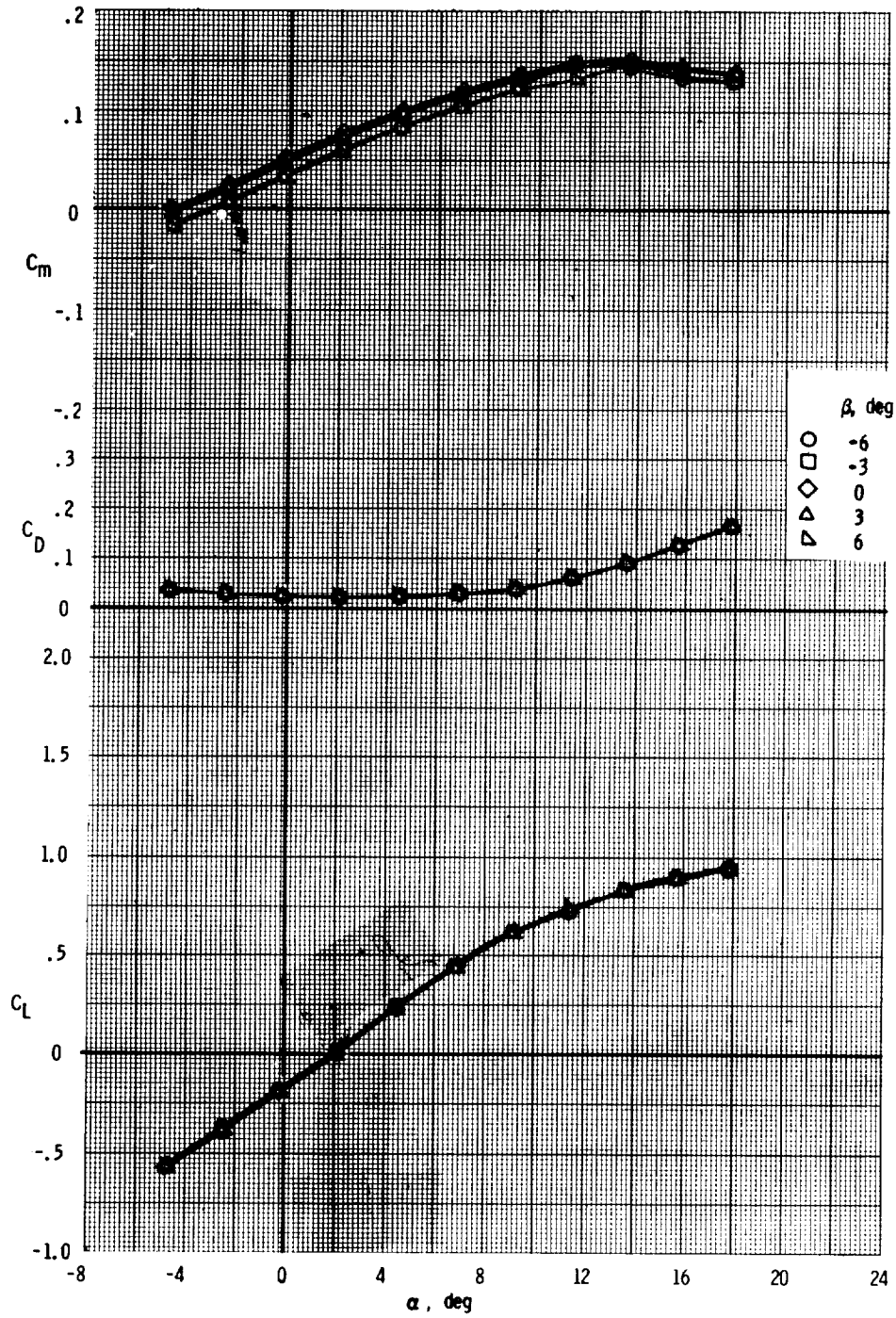

Figure 23.- Aerodynamic characteristics of NASA GA(PC)-1 wing. ($R = 1.49 \times 10^6$; $\delta_f = -10^o$.)

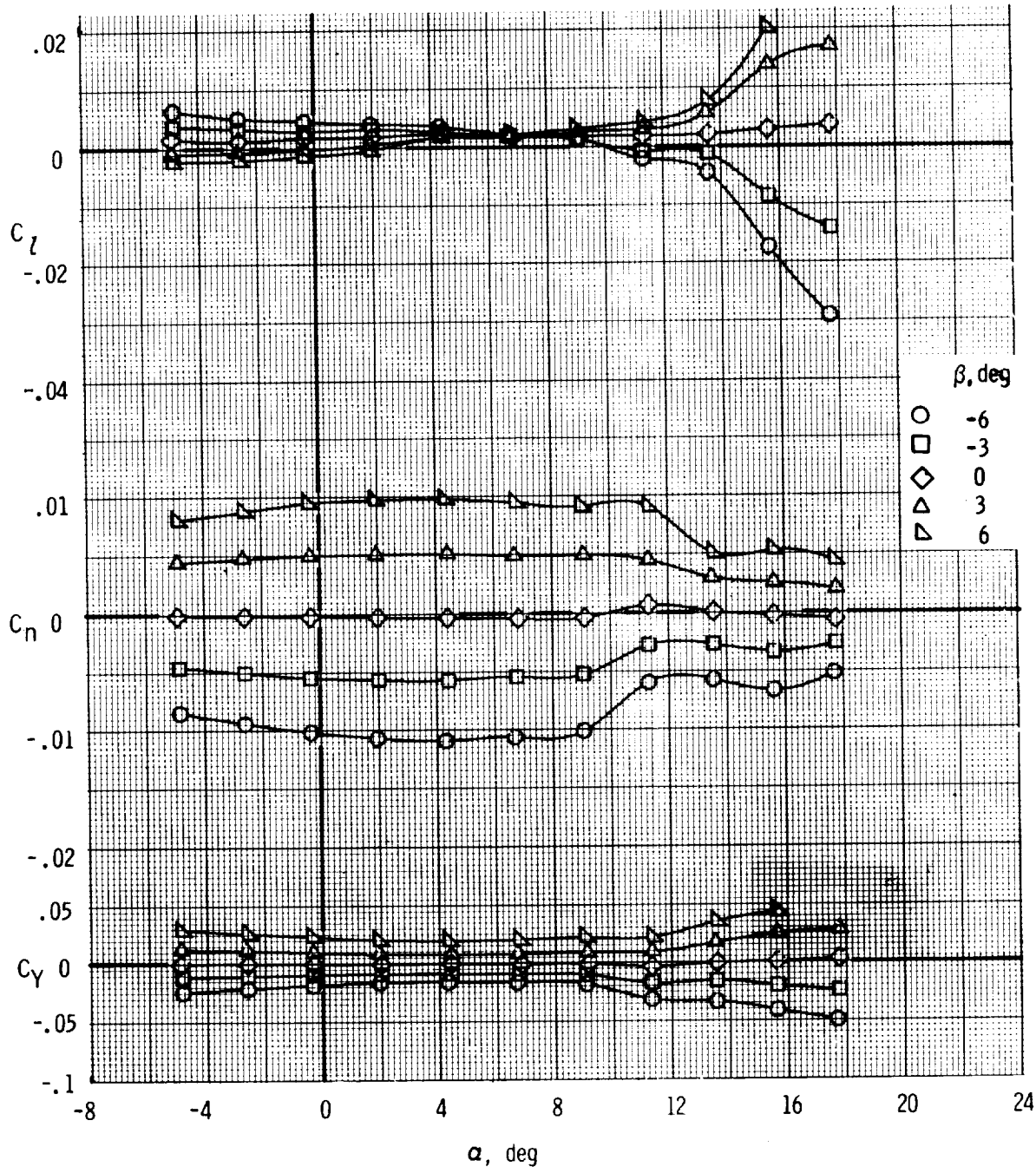

Figure 23.- Concluded.

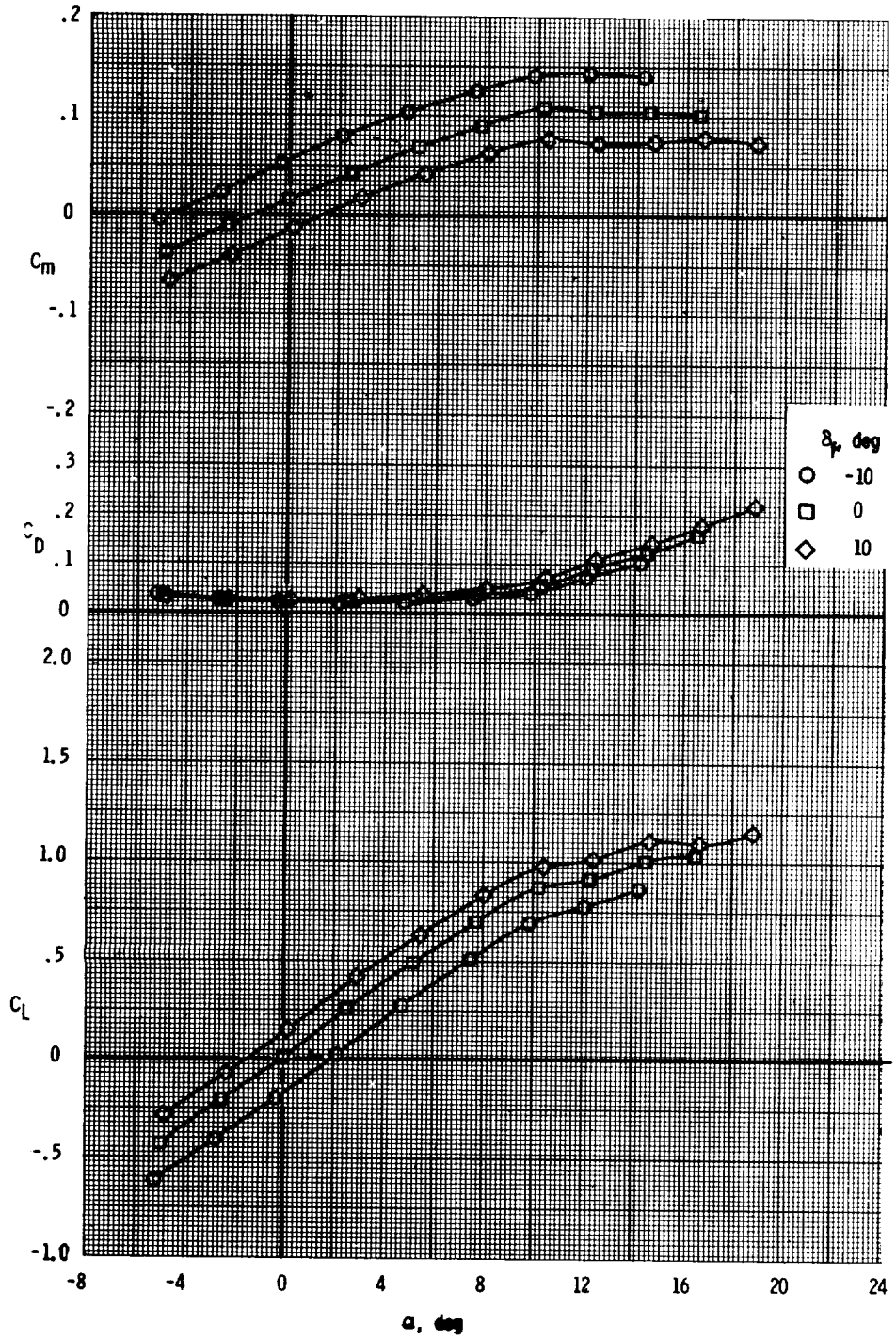

(a) Partial-span flap.

Figure 24.- Effect of deflection of partial- and full-span flap on longitudinal aerodynamic characteristics of NASA GA(PC)-1 wing. ($R = 1.92 \times 10^6$.)

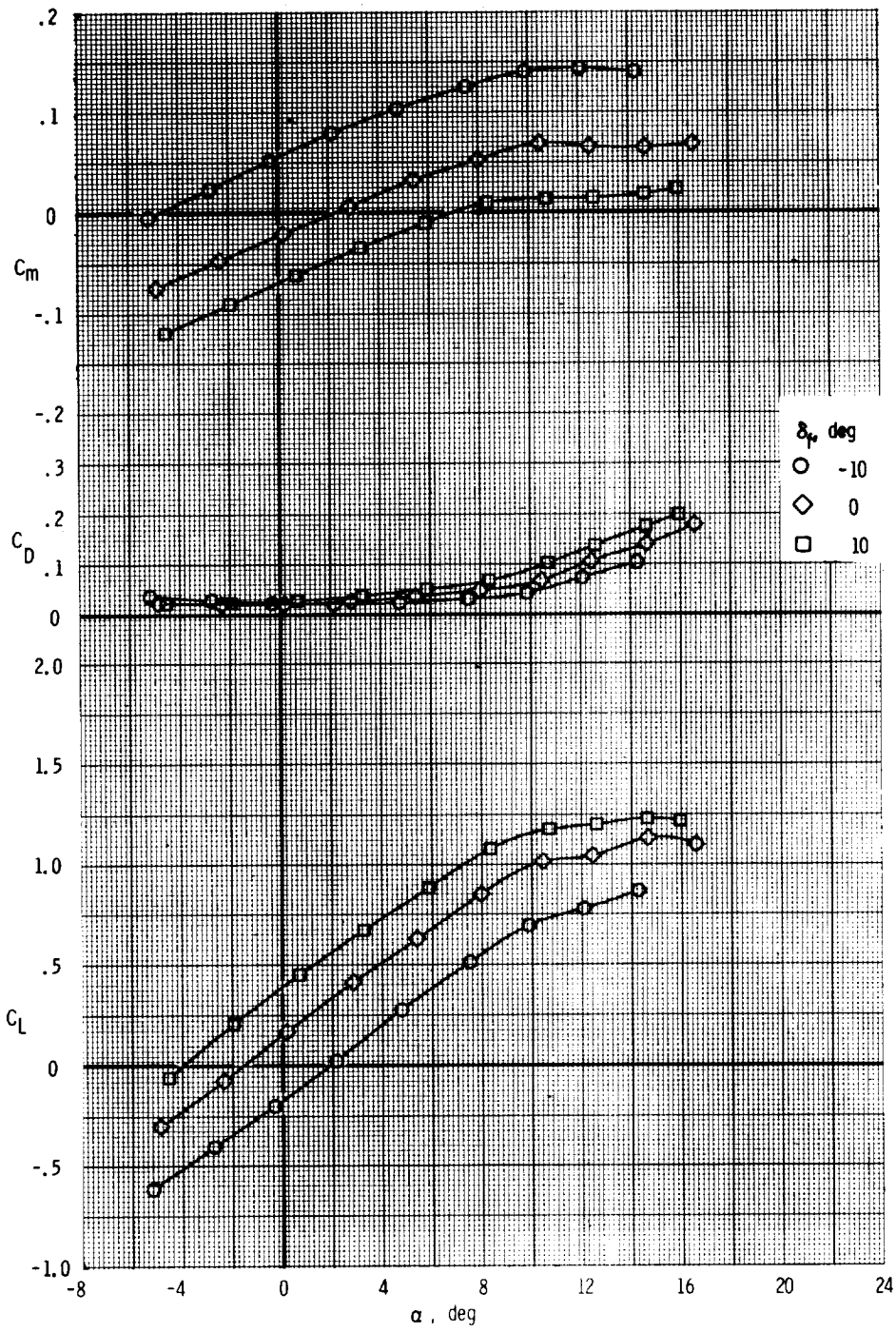

(b) Full-span flap.

Figure 24.- Concluded.

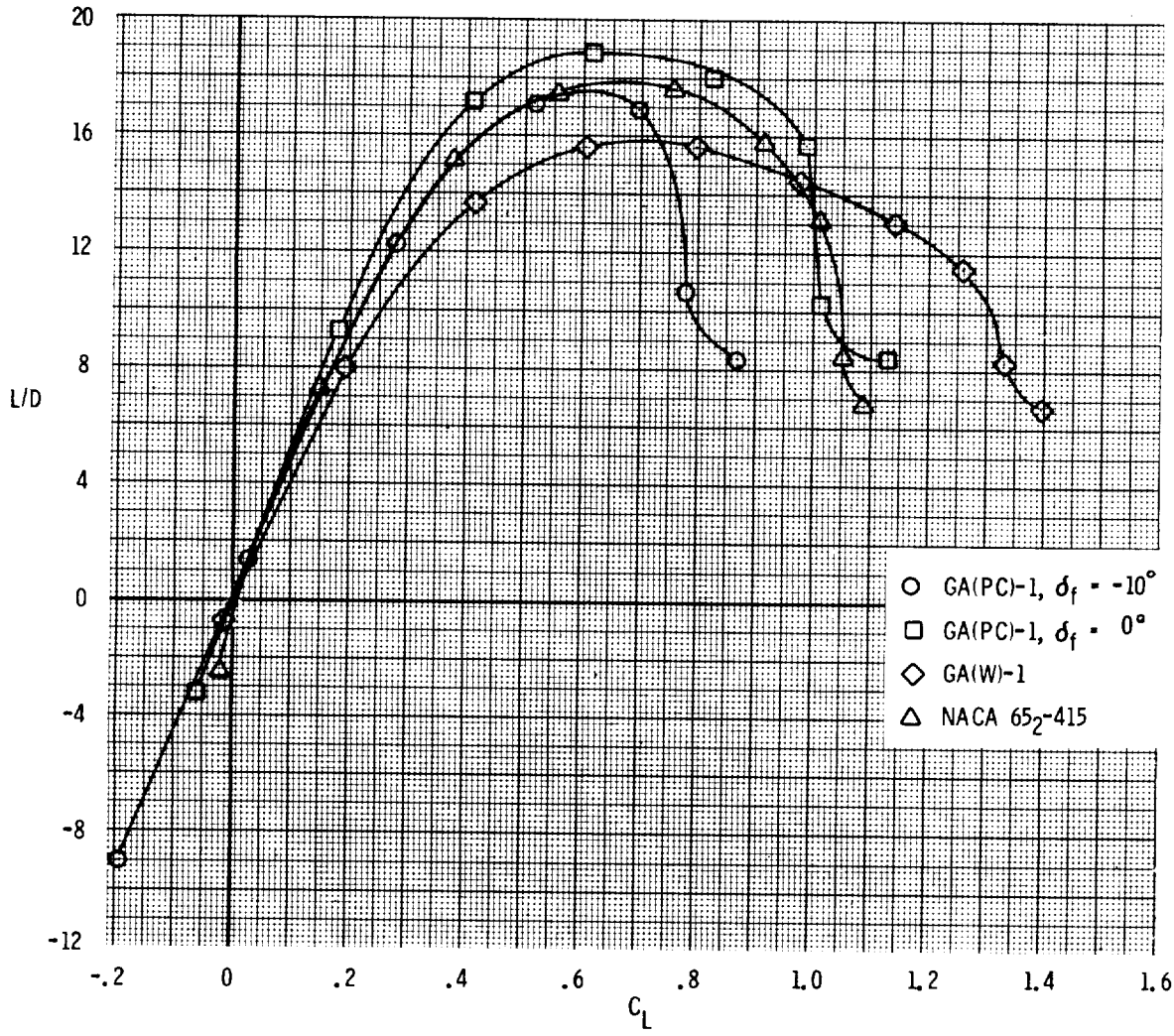

Figure 25.- Lift/drag as a function of C_L for three configurations.

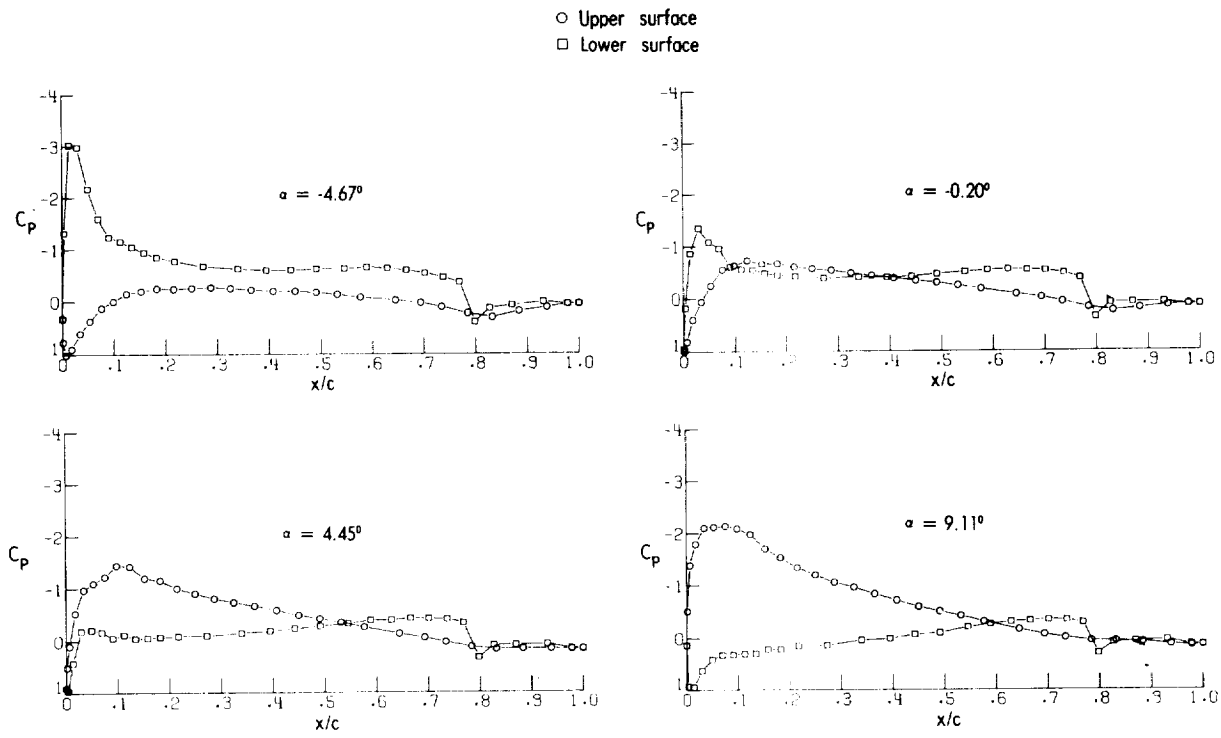

(a) Surface-pressure distributions, $\delta_f = -10^o$.

Figure 26.- Section surface-pressure distributions and wake total-pressure profiles for NASA GA(PC)-1 wing with various flap deflections. ($R = 1.72 \times 10^6$.)

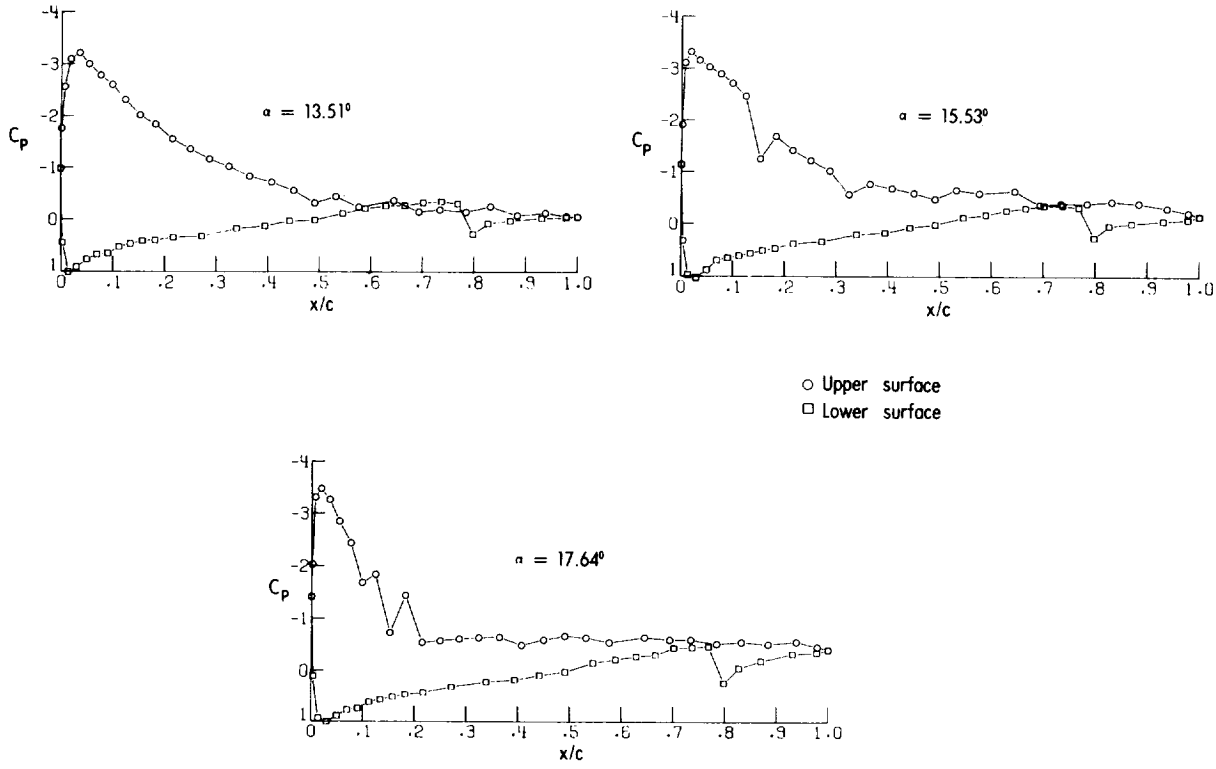

(a) Concluded.

Figure 26.- Continued.

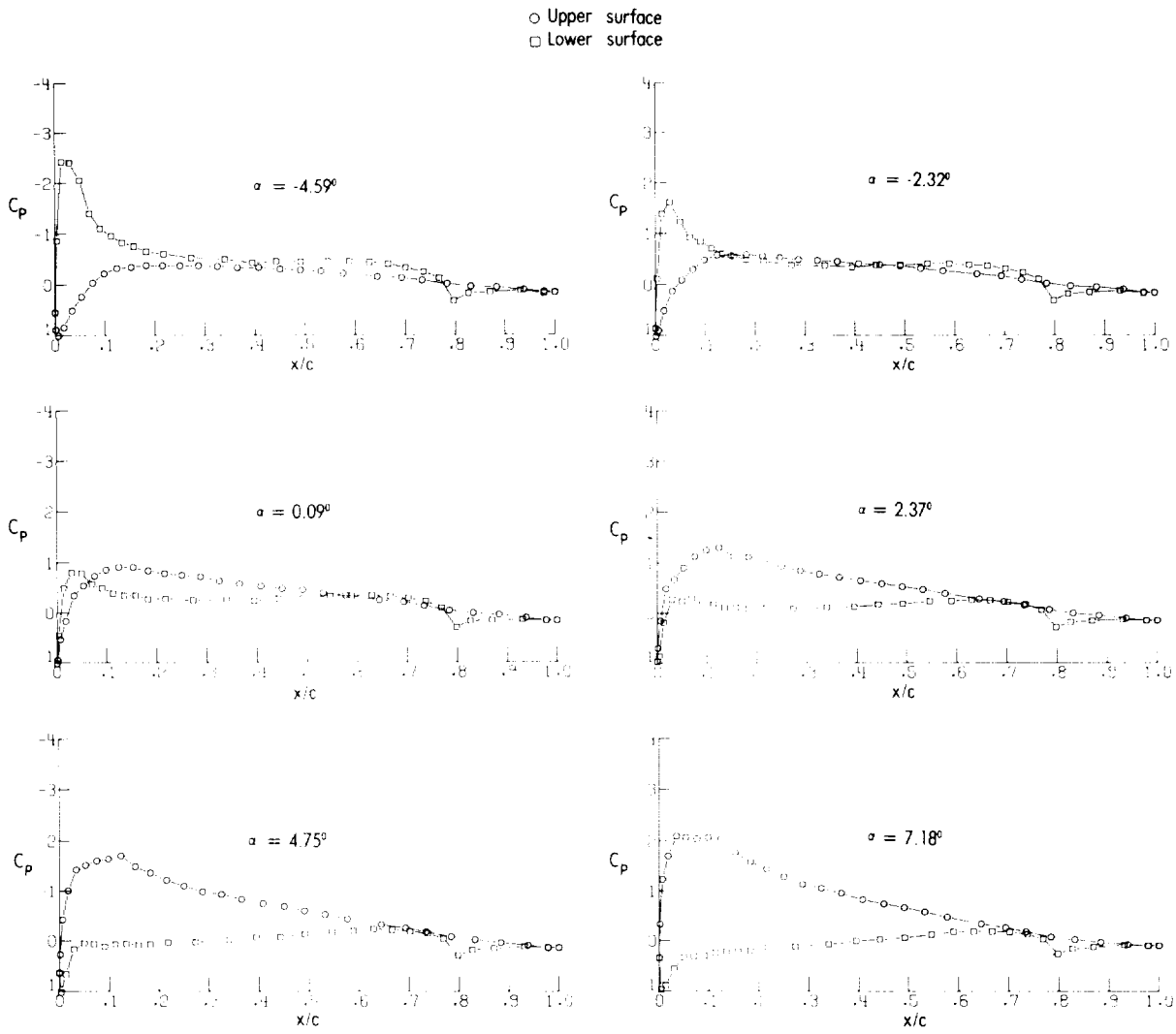

(b) Surface-pressure distributions, $\delta_f = 0^o$.

Figure 26.- Continued.

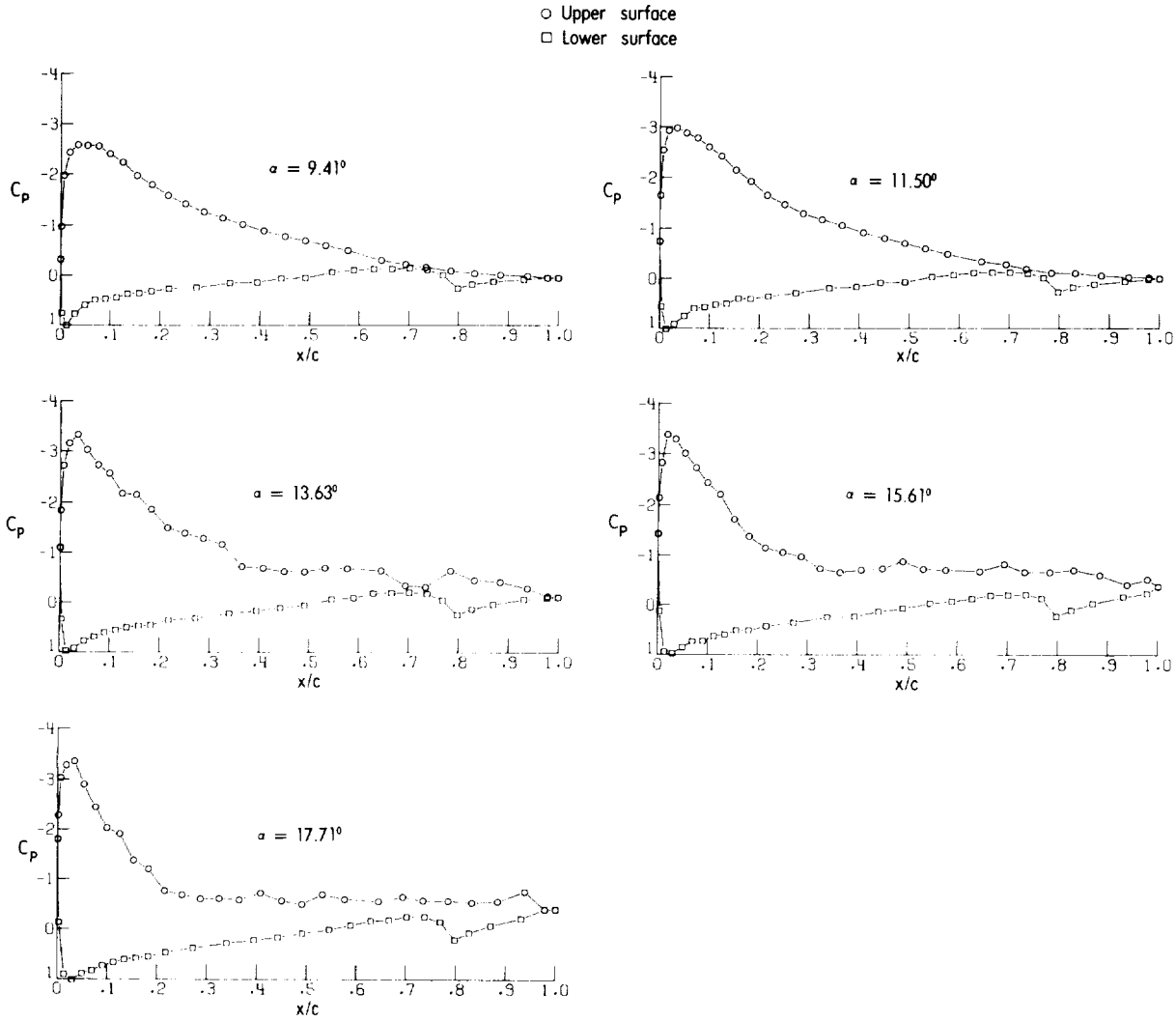

(b) Concluded.

Figure 26.- Continued.

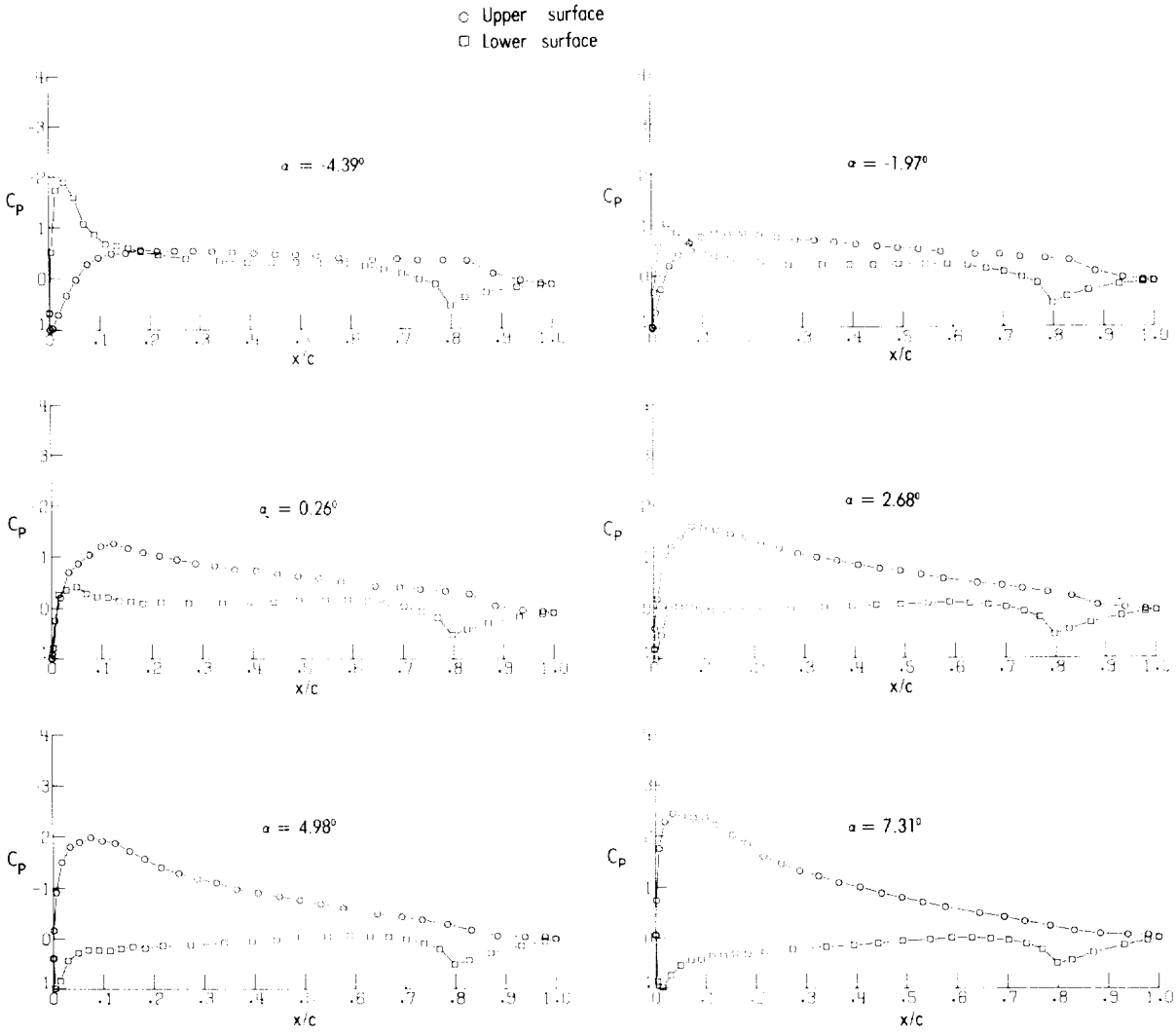

(c) Surface-pressure distributions, $\delta_f = 10^o$.

Figure 26.- Continued.

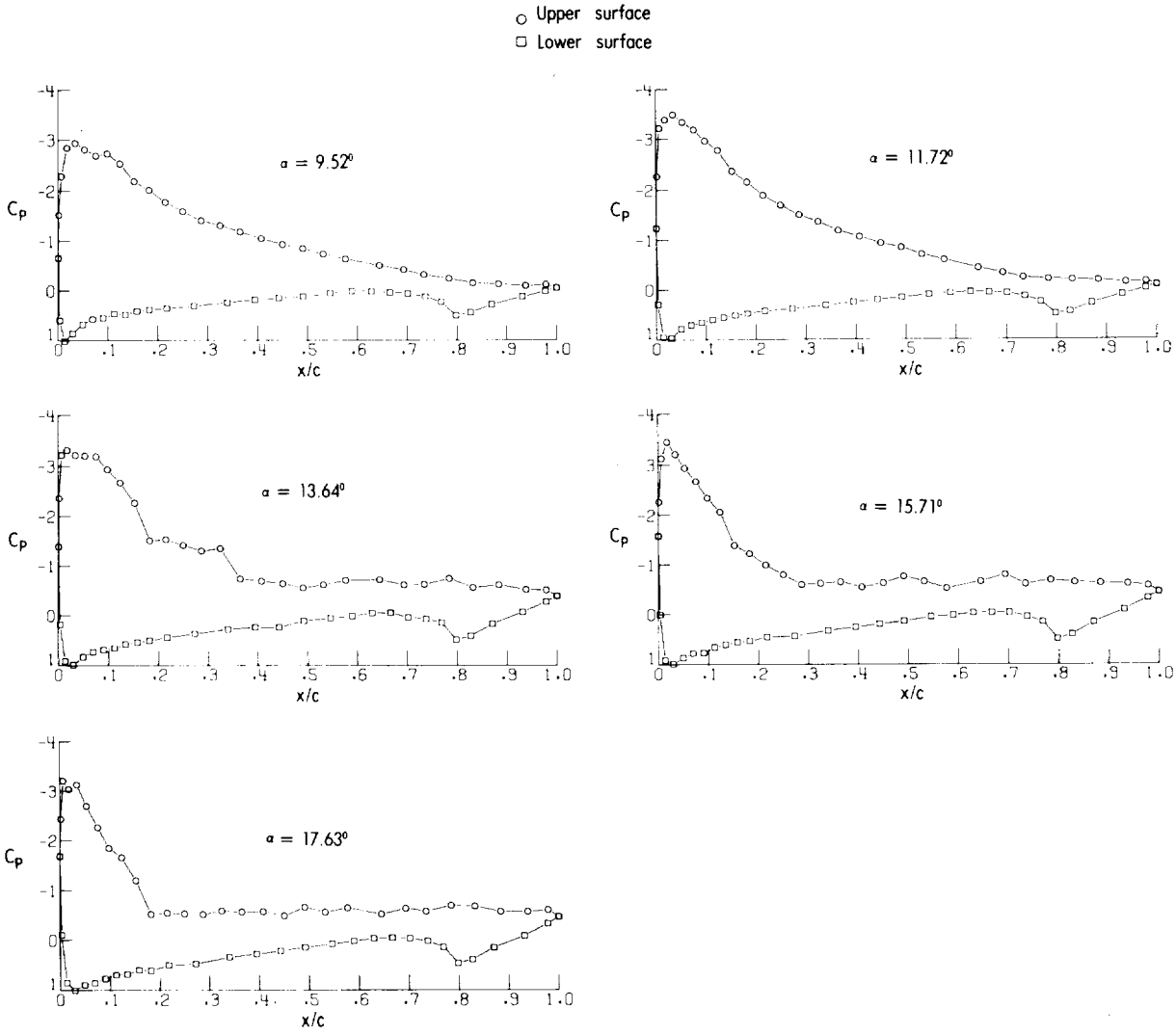

(c) Concluded.

Figure 26.- Concluded.

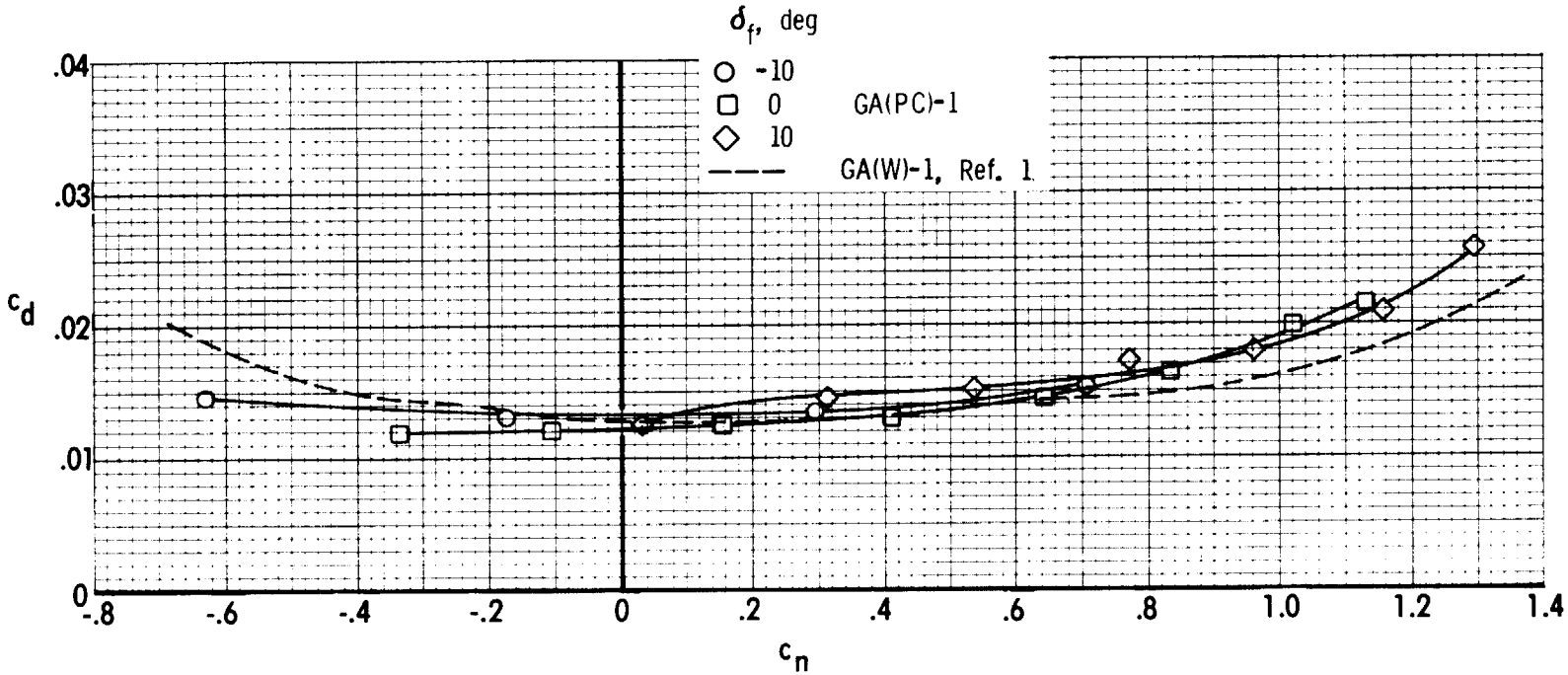

Figure 27.- Section drag and normal-force coefficients determined from experimental wake total-pressure profiles and surface-pressure distributions of NASA GA(PC)-1 airfoil. ($R = 1.72 \times 10^6$.)

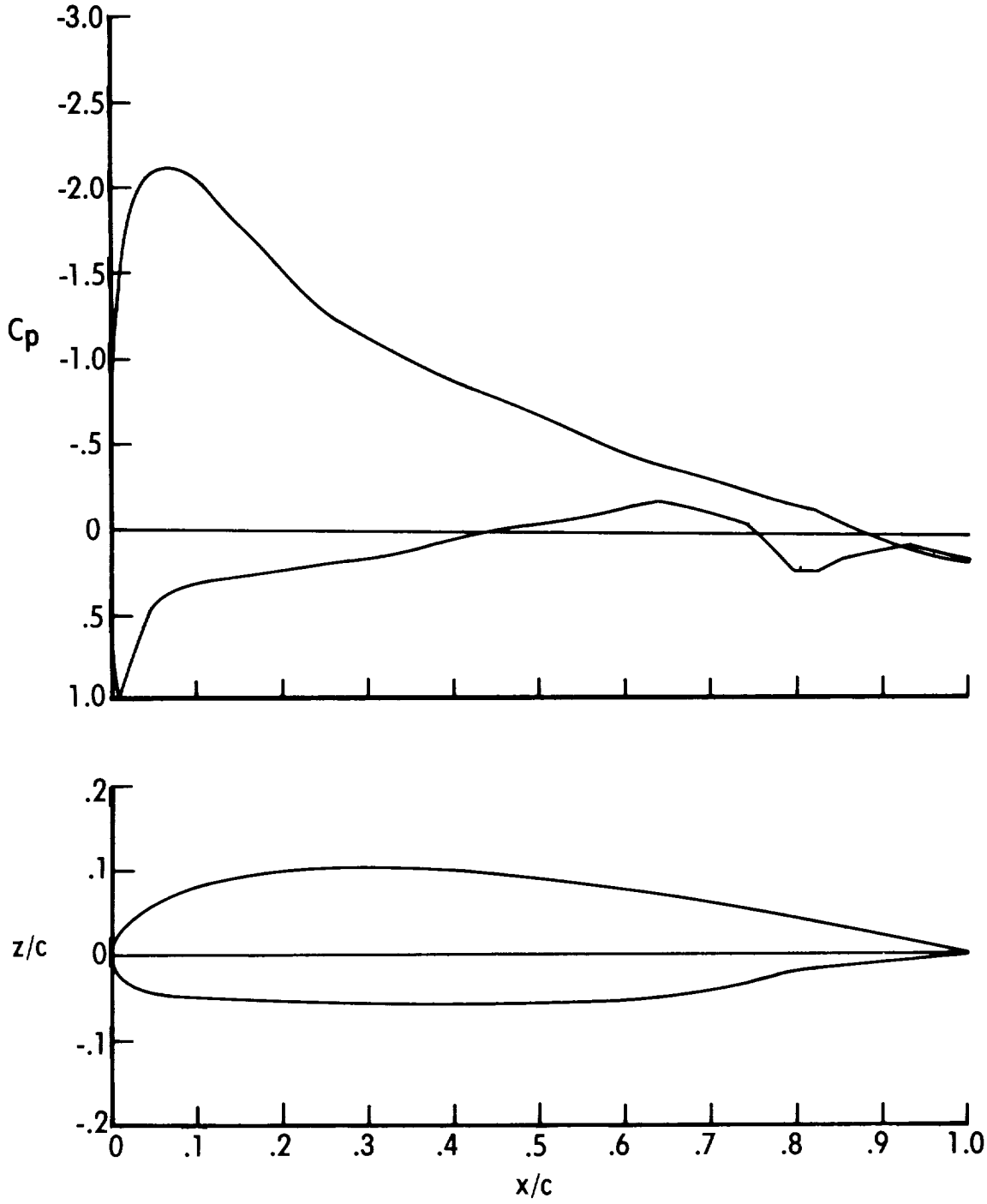

Figure 28.- Pressure distributions for NASA GA(PC)-1 airfoil at design condition of $C_L = 0.9$, $\delta_f = 0^o$.